

Copyright
by
Jacqueline Leslie Stair
2006

**The Dissertation Committee for Jacqueline Leslie Stair Certifies that this is the
approved version of the following dissertation:**

**SYNTHESIS AND CHARACTERIZATION OF SHORT-CHAIN
PEPTIDES FOR USE IN METAL REMEDIATION AND
PRECONCENTRATION**

Committee:

James A. Holcombe, Supervisor

Jennifer S. Brodbelt

John T. McDevitt

Keith J. Stevenson

Lynn E. Katz

**SYNTHESIS AND CHARACTERIZATION OF SHORT-CHAIN
PEPTIDES FOR USE IN METAL REMEDIATION AND
PRECONCENTRATION**

by

Jacqueline Leslie Stair, B.S.

Dissertation

Presented to the Faculty of the Graduate School of

The University of Texas at Austin

in Partial Fulfillment

of the Requirements

for the Degree of

Doctor of Philosophy

The University of Texas at Austin

December, 2006

Dedication

I dedicate this dissertation to my four brothers Jason, Jeremy, Justin, and Jacob.

Acknowledgements

I first want to thank those who have guided me through this journey and helped shape my views of scientific research. I thank Dr. Holcombe for his guidance and the opportunity to have this insightful learning experience. Thank you to the elders, Lisa and Ashley, for showing me the ropes. I also thank Lisa for her work on the biopolymer review paper. I thank Bill for being the life of the lab and Nikhilesh for his camaraderie through our difficult classes and qualifying exams. Brianna and Adam, it was a pleasure working with you on the ETV-ICPMS bead project. I cannot forget my partners in crime, John and Carina. I have been through thick and thin with you two; I will never forget the great times we shared. I expect there will be many more to come! I also want to thank my parents for being so supportive and not asking too many times “are you going to be a student forever?” I also thank my brothers, all four of them, for coming to visit me all the way in Texas numerous time. I have a feeling Jake will be saying Hook ‘em Horns for the rest of his adult life. A special thanks to my best friends Anne, Melissa S., and Melissa B. Last but not least, I want to thank my incredibly supportive boyfriend, Ian. Thank you for your love and guidance; and giving me perspective.

SYNTHESIS AND CHARACTERIZATION OF SHORT-CHAIN PEPTIDES FOR USE IN METAL REMEDIATION AND PRECONCENTRATION

Publication No. _____

Jacqueline Leslie Stair, Ph.D.

The University of Texas at Austin, 2006

Supervisor: James A. Holcombe

Designing materials for metal remediation and preconcentration based on naturally occurring metal binding proteins has become of growing interest due to their inherent selective and strong binding, ease of synthesis and available amino acid building blocks, and environmental innocuity. One approach is through the use of immobilized synthetic biohomopolymers which can provide the selectivity based on the amino acid side chain moiety with strong binding, easy on-demand release, and reusability.

An attempt to increase metal binding selectivity of these biohomopolymers was done through cross-linking at specific locations as to effectively “lock” in place the preferential binding cavity for a particular metal. The cross-linking of these materials resulted in decreased metal capacities with little to no increases in the targeted metal selectivity. This was likely due to the loss of bound metal during cross-linking and to a lack of rigidity in the overall cross-linked polymer.

Short composite peptides synthesized on a commercially available resin, TentaGel were also examined as a means to increase metal selectivity. These peptides showed surprisingly high metal binding capacities, strong binding, and residue per metal binding ratios which were an order of magnitude better than results previously reported for longer chain poly-amino acids (50 – 70 residues) attached to porous glass supports. Metal binding selectivity's were altered by changing only one amino acid and metal release under acidic conditions was surprisingly rapid for these shorter peptides. As a result of these findings, the metal binding and conformational changes between TentaGel immobilized short and long peptide chains during metal binding and release were monitored using Raman microscopy. These results indicated that metal release occurred via conformational changes in addition to proton displacement.

Lastly, a method to screen multi-metal binding capabilities of combinatorial peptide libraries was developed using electrothermal vaporization inductively coupled plasma mass spectrometry (ETV-ICP-MS). With the exception of metals that are bound tightly to the peptide, acid stripping of the metals in a single bead into a small volume appears as a viable quantitative analytical approach when using this method with instrumental precisions of better than $\pm 10\%$ for most metals when larger polymer beads ($\sim 250\ \mu\text{m}$) were employed.

Table of Contents

List of Tables	xii
List of Figures	xiv
Chapter 1: Introduction	1
Chapter 2: Immobilized Peptides/Amino Acids on Solid Supports for Metal Remediation	4
2.1. Introduction	4
2.2. Single Amino Acids	8
2.3. Immobilized Poly-Amino Acids on Silica and Carbon Supports	10
2.4. Membrane Immobilized Poly-Amino Acids	14
2.5. Immobilized Peptides	17
2.6. Immobilized Amino Acid for use in Ion-Exchange Chromatography	18
2.7. Immobilized Amino Acid/Peptide for Cd ²⁺ Removal from Human Plasma	21
2.8. Related Studies	22
2.9. Conclusions	23
2.10. Literature cited	24
Chapter 3: Efforts in Templating for Transition Metals Using Short-Chain Polymers and Peptides	30
3.1. Introduction	30
3.2. Materials and Methods	31
3.2.1. Chemicals	31
3.2.2. Apparatus	32
3.2.3. Synthesis and Cross-Linking Experiments	32
3.2.3.1. Cross-Linking PolyAcrylic Acid Using a Bifunctional Linker	32
3.2.3.2. Cross-Linking Copolymer (Glu, Lys)(6:4)	34
3.3. Results and Discussion	35
3.3.1. Cross-Linking PolyAcrylic Acid (PAA) Using Bifunctional Linkers	35

3.3.2.	Cross-Linking Copolymer (Glu, Lys) (6:4)	41
3.4.	Conclusions.....	48
3.5.	Literature cited	49
Chapter 4: Metal Remediation and Preconcentration Using Immobilized Short-Chain Peptides Composed of Aspartic Acid and Cysteine		
4.1.	Introduction.....	50
4.2.	Materials and Methods.....	52
4.2.1.	Chemicals.....	52
4.2.2.	Apparatus	53
4.2.3.	Peptide synthesis.....	54
4.2.4.	Peptide characterization	55
4.2.5.	Metal binding studies	55
4.2.5.1.	Single and multi-metal binding studies.....	55
4.2.5.2.	Equilibrium Studies	57
4.2.5.3.	Determination of Conditional Stability Constants.....	57
4.2.5.4.	Oxidation Studies.....	58
4.2.5.5.	Preconcentration and Recovery of Ni^{2+} and Cd^{2+} in artificial seawater.....	58
4.2.5.6.	Efforts in Metal Templating using Disulfide Bonds.....	59
4.3.	Results and Discussion	60
4.3.1.	Peptide sequences examined.....	60
4.3.2.	Peptide characterization	61
4.3.3.	Single metal binding studies	63
4.3.4.	Selected, multi-metal binding studies	70
4.3.5.	Determination of Conditional Stability Constants	76
4.3.6.	Effects of Cysteine oxidation.....	77
4.3.7.	Preconcentration of Ni^{2+} and Cd^{2+} in artificial seawater: Accuracy and recovery	79
4.3.8.	Efforts in Metal Templating using Disulfide Bonds.....	82
4.4.	Conclusions.....	85
4.5.	Literature cited	86

Chapter 5: Metal Binding Characterization and Conformational Studies Using Raman Microscopy of Resin Bound Polyaspartic Acid	90
5.1. Introduction.....	90
5.2. Methods and Materials.....	92
5.2.1. Chemicals.....	92
5.2.2. Peptide synthesis and characterization.....	93
5.2.3. Atomic absorption and metal binding experiments	93
5.2.4. Determination of conditional stability constants	95
5.2.5. Raman microscopy and peptide conformational studies ...	96
5.3. Results and Discussion	97
5.3.1. Peptide sequences examined.....	97
5.3.2. Metal binding studies	99
5.3.3. Determination of conditional stability constants	102
5.3.4. Peptide conformational studies using Raman Microscopy	104
5.3.4.1. Amide I Region.....	105
5.3.4.2. Amide II Region	109
5.3.4.3. C-C Region	111
5.4. Conclusions.....	115
5.5. Literature cited.....	117
Chapter 6: Quantitative Determination of Single Bead Metal Content from a Peptide Combinatorial Library Using ETV-ICP-MS	120
6.1. Introduction.....	120
6.2. Materials and Methods.....	122
6.2.1. Chemicals.....	122
6.2.2. Metal Binding and Extraction.....	123
6.2.3. Stereoscope measurements	124
6.2.4. ETV-ICP-MS	125
6.3. Results and Discussion	127
6.3.1. Metal determination from beads with immobilized PLAsp	127

6.3.2.	Metal determination from the combinatorial library beads	133
6.4.	Conclusions.....	136
6.5.	Literature cited	138
Chapter 7:	Conclusions and Future Work.....	140
7.1.	Conclusions.....	140
7.2.	Future Work	145
7.2.1.	Templating	145
7.2.2.	Peptide Combinatorial Libraries For Selective Metal Binders	146
7.2.3.	Multicolumn Analysis Using Automated System	147
Vita	148

List of Tables

Table 3.1.	Flow-through reaction sequence and conditions for cross-linking PAA with bifunctional linkers using EDC/NHS.	34
Table 3.2.	Flow-through reaction sequence and conditions for cross-linking CoPoly-CPG using EDC/NHS for both a 1- and 2-Step reaction.....	35
Table 3.3.	Metal capacities of PAA-CPG before and after cross-linking experiments.	40
Table 3.4.	Metal binding capacities of Co^{2+} , Ni^{2+} , and Cd^{2+} to CPG-APS-Glu and CPG-APS-Glu-CoPoly. Metal capacities were determined from the strip analysis and verified using the breakthrough analysis ($n = 3$).....	42
Table 4.1.	Multi-metal binding capacities (μmole of metal / g of resin) of various peptide sequences on TentaGel resin	70
Table 4.2.	Metal capacities (μmole of metal / g of T_{GD_6}) using 500 mL of multi-metal solutions flowing at 1 mL/min (i.e., ca 8 h)	75
Table 4.3.	Conditional stability constants and site density ($\mu\text{mole/g}$ of resin) of T_{GD_6} with four metals.....	77
Table 4.4.	Cadmium capacity (μmole of Cd / g of resin) on immobilized peptides treated with oxidizing agents	78
Table 4.5.	Analytical accuracy and analyte recovery when preconcentrating Ni^{2+} and Cd^{2+} from artificial seawater	80
Table 5.1.	Metal binding capacities of Mg^{2+} , Co^{2+} , Cd^{2+} , and Ni^{2+} to PLAsP on TentaGel resin.....	99
Table 5.2.	Conditional stability constants and total number of sites ($\mu\text{mole/g}$ of resin) of T_{D_6} , $\text{T}_{\text{D}_{20}}$, and $\text{T}_{\text{D}_{30}}$ with four metals.	103

Table 6.1.	ICP Operating Parameters.....	125
Table 6.2.	ETV heating program	126
Table 6.3.	Bead-to-bead variation in metal extract before and after adjusting for bead volume. Poly-L-aspartate (n=20) was immobilized on the beads.	129

List of Figures

Figure 1.1.	Number of publications per year in the area of immobilized amino acids and peptides used for metal remediation and preconcentration (Data was gathered using the search engines Scifinder and Web of Science with approximately 40 search terms).	1
Figure 2.1.	Selected set of amino acids that have been used by various researchers as immobilized chelators of metals.....	7
Figure 2.2.	Schematic representation of an immobilized peptide under binding ready (A), metal binding (B), and metal release (C) conditions. M^{2+} represents a divalent metal species.	11
Figure 3.1.	Activation of carboxylate functionalities using EDC.	36
Figure 3.2.	pH requirements for each process during metal templating reactions. The bottom arrows depict the ideal conditions for a 1- and 2-step reaction.....	37
Figure 3.3.	Breakthrough curve analysis of PAA using $10\ \mu\text{g mL}^{-1}\ \text{Co}^{2+}$ (HEPES buffer pH 7) after 30 min treatments of pH 7, 8, 9, and 10 HEPES buffer.....	38
Figure 3.4.	Breakthrough curve analysis of PAA using $10\ \mu\text{g mL}^{-1}\ \text{Co}^{2+}$ in HEPES buffer at pH 7 before reaction (solid line), immediately after adding EDC/NHS (square dotted line), and thereafter (circle dotted lines).	39
Figure 3.5.	Breakthrough curve analysis of the copolymer using $10\ \mu\text{g mL}^{-1}\ \text{Co}^{2+}$ (HEPES buffer pH 7) after 30 min treatments of $0.02\ \text{mol L}^{-1}$ HEPES buffer at pH 7, 8, 9, and 10.	41

Figure 3.6.	Breakthrough curve analysis of the copolymer using $10 \mu\text{g mL}^{-1} \text{Co}^{2+}$ (HEPES buffer pH 7) before and after 2-step cross-linking.	43
Figure 3.7.	Cobalt absorbance from the column effluent during metal binding of the hard binding sites (0-10 min) and then introduction of neutral solutions of $20 \text{ mmol L}^{-1} \text{MES}/60 \text{ mmol L}^{-1} \text{NHS}$, $20 \text{ mmol L}^{-1} \text{MES}$, and $20 \text{ mmol L}^{-1} \text{HEPES buffer}$	45
Figure 3.8.	Effluent Co^{2+} concentration from Copoly-CPG column during metal binding of hard sites and then the introduction of an EDC cross-linking solution.	46
Figure 3.9.	Effluent Co^{2+} concentration from Copoly-CPG column during metal binding of hard sites and then the introduction $40 \text{ mmol L}^{-1} \text{EDC pH 8.0}$ cross-linking reaction.	47
Figure 4.1.	Pictorial representation of the flow through system used analysis of material packed into microcolumns.	54
Figure 4.2.	Single metal capacities of various peptides synthesized on TentaGel (T) resin and controlled pore glass (CPG). Peptide composition is denoted by G = Gly, D=Asp, C=Cys, and Trt = Trityl (thiol blocking group). Solutions containing $20 \mu\text{g mL}^{-1}$ of a metal in $0.02 \text{ mol L}^{-1} \text{HEPES buffer (pH 7)}$ were passed through the columns until breakthrough was observed. Capacities reported are an average of both breakthrough ($n = 3$) and strip analysis ($n = 3$) values.	63

Figure 4.3.	Cd stripped off TGD ₂ CD ₂ C, CPGGD ₂ CD ₂ C, and CPGPolyCys into AAS. The metal was loaded on the peptide using 15 mL of a 250 ppb Cd solution, rinsed for 1 min with 0.02 mol L ⁻¹ Hepes buffer, and stripped into the spectrometer with a 0.1 mol L ⁻¹ solution of nitric acid.	69
Figure 4.4.	Ratios of metal capacities from multi-metal experiments of four select peptides. Peptide composition is denoted by G = Gly, D=Asp and C=Cys. A solution containing 20 µg mL ⁻¹ of Ni ²⁺ , Cd ²⁺ , Co ²⁺ , and Mg ²⁺ in 0.02 mol L ⁻¹ HEPES buffer (pH 7) was run until breakthrough of each metal was observed via AAS. Capacities reported are from strip analysis only.....	71
Figure 4.5.	TGD ₆ breakthrough analysis of Co ²⁺ , Cd ²⁺ , Mg ²⁺ , and Ni ²⁺ overlaid. Each metal was monitored separately via FIA-FAAS while a multi-metal solution (20 µg mL ⁻¹ in all metals) was passed through the column.....	72
Figure 4.6.	Signal broadening due to dispersion in the FIA system and mixing in the FAAS mixing chamber. Ni absorbance after a 20 µg mL ⁻¹ Ni ²⁺ solution was aspirated into the instrument via a peristaltic pump and then cleared using 0.1 mol L ⁻¹ HNO ₃ . This process was repeated 3X.....	81
Figure 4.7.	Pictorial representation of the reversible cross-linking procedure. ..	82
Figure 4.8.	Metal capacities of TGD ₅ C, TGD ₂ CD ₂ C, and TGD ₄ C ₂ after exposure to templating conditions with no metal (A), templating conditions after binding Mg ²⁺ (B), and templating conditions after binding Ni ²⁺ (C). The metal capacities of Mg ²⁺ , Ni ²⁺ , and Cd ²⁺ are reported before templating (white box), after templating with metal and iodosobenzoate (striped box), and after reduction with DTT (grey box).	83

Figure 5.1.	Raman Spectra of dry TentaGel resin from manufacturer (bottom) and after solvent exposure (top). Two spectra of each sample type were collected and each spectrum was collected on a new bead.....	105
Figure 5.2.	Raman spectra (amide I region) of PLAs synthesized on TentaGel resin for TD ₆ , TD ₂₀ , and TD ₃₀ . The solution conditions in each set are pH 7 HEPES buffer (bottom spectrum), 20 $\mu\text{g mL}^{-1}$ Cd in HEPES buffer (middle spectrum), and 0.1 mol L ⁻¹ HNO ₃ (top spectrum). TD ₆ , TD ₂₀ , and TD ₃₀ have different intensity scales. The dotted line is positioned to assist in viewing the relative peak positions. The secondary structure locations from left to right (1700 -1600 cm ⁻¹) are β -turns, β -sheets, random chain, and α -helices.....	107
Figure 5.3.	Raman spectra (amide II region) of PLAs synthesized on TentaGel resin. (See caption from Figure 2) The secondary structure locations from left to right (1335 -1225 cm ⁻¹) are β -turns, β -sheets, random chain, and α -helices.....	110
Figure 5.4.	Raman spectra (C-C region) of PLAs synthesized on TentaGel resin. (See caption from Figure 2). The secondary structure locations from left to right (1000 -880 cm ⁻¹) are β -turns, β -sheets, random chain, and α -helices.	112

Figure 5.5. Raman spectra (C-C region) of TD30 after exposure to 0.1 mol L ⁻¹ HNO ₃ , 20 µg mL ⁻¹ Ni ²⁺ , Cd ²⁺ , Co ²⁺ , or Mg ²⁺ in HEPES, and pH 7 HEPES buffer. The TentaGel resin spectrum was subtracted from each spectrum. Two spectra of each sample type were collected and each spectrum was collected on a new bead. In this figure, the spectra Ni ²⁺ , Cd ²⁺ , Co ²⁺ , and Mg ²⁺ bound to the peptide is identical to that seen for TD6 and TD20.	114
Figure 6.1. Stereoscope image of PLAsp-Tentagel beads after metal complexation.	127
Figure 6.2. Concentration of metal extracted from single TentaGel-PLAsp beads and calculated bead volumes (right axis). The error bars represent ± 1 σ (n = 3) based on error propagated using the analysis error of the sample, blank, and calibration solutions. (Two beads were present in Well #5.)	128
Figure 6.3. Single bead metal extract concentrations of TentaGel-PLAsp normalized to the individual bead volumes. The error bars represent ± 1 σ (n = 3) based on error propagated using the analysis error of the sample, blank, and calibration solutions. (Two beads were present in Well #5.)..	130
Figure 6.4. Stereoscope image of the peptide library beads after metal complexation.	133
Figure 6.5. Single bead metal extract concentrations of the peptide combinatorial library normalized to the individual bead volumes. The error bars represent ± 1 σ (n = 3) based on error propagated using the analysis error of the sample, blank, and calibration solutions. Mg concentration in well B, C, E, and J were negligible. (<0.6 ug/mm ³)	135

Chapter 1: Introduction

This dissertation focuses on improving the metal binding properties of immobilized peptides for metal remediation and preconcentration. Firstly, two studies undertaken to enhance the metal-binding selectivity of immobilized peptides are presented. Next, the secondary structure formed during metal binding of a long biohomopolymer attached to a polymer support is investigated. Lastly, a new method to analyze single beads from peptide combinatorial libraries as a facility to determine selective metal binding sequences is presented.

A thorough review of peptides and amino acids immobilized onto solid supports for metal remediation and preconcentration is presented in Chapter 2. Figure 1.1. shows the number of publications in this area per year found when preparing this review.

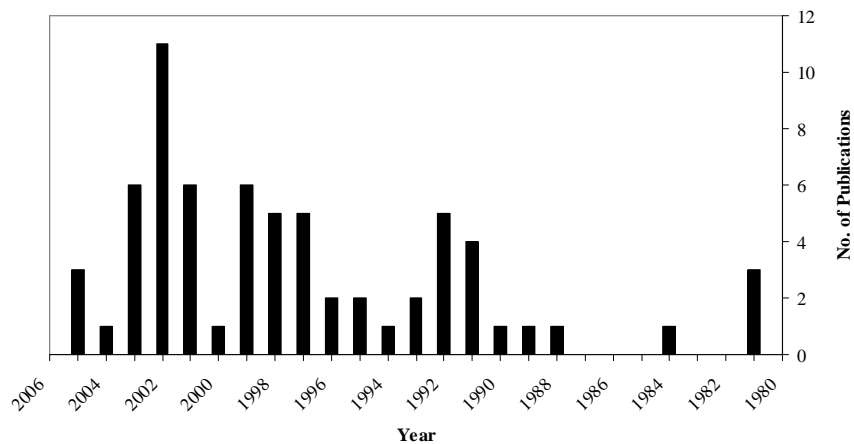


Figure 1.1. Number of publications per year in the area of immobilized amino acids and peptides used for metal remediation and preconcentration (Data was gathered using the search engines Scifinder and Web of Science with approximately 40 search terms).

The number of publications retrieved from a literature search shows steady interest in this area from 1988 until present, with a peak in 2002. The larger number of publications in 2002 originates from various research groups and the subsequent fall may be a result of diminished research funding for environmental studies. Much of published work focuses on the attachment of single amino acids or homopeptides to solid supports with little modification. As a result, many metal binding residues have been thoroughly characterized for their metal binding selectivities and capacities. Continued interest in this field is required to improve the selectivity of these materials and to design peptide chelators in a more intelligent manner based on metal binding protein sequences; in addition to the use of peptide combinatorial libraries.

Chapters 3 and 4 propose two different methods for increasing the metal selectivity of these peptide materials. Chapter 3 focuses on efforts to metal template through the cross-linking of simple homopeptides immobilized to solid supports. Chapter 4 demonstrates the use of composite short-chain peptides to control selectivity. These studies also demonstrate the use of a common solid phase peptide synthesis (SPPS) resin for not only peptide synthesis but also for subsequent use as an ion-exchange resin.

Chapter 5 examines the secondary structure of a commonly used peptide, polyaspartic acid (PLAsp), during metal binding and release. This study also shows the unique metal binding properties in relation to peptide length on polymeric (SPPS) supports.

Chapter 6 demonstrates the utility of electrothermal vaporization inductively coupled mass spectrometry (ETV-ICPMS) for the determination of single bead metal content from peptide combinatorial libraries. This study also examines the precision from bead-to-bead during sample preparations and instrumental detection.

These studies as a whole contribute to the improvement of metal selective immobilized peptides. The knowledge of peptide secondary structure on supports in addition to the synthesis and modification of “intelligently designed” peptides, will aid in the development of new materials to be used for current and future metal remediation needs.

Chapter 2: Immobilized Peptides/Amino Acids on Solid Supports for Metal Remediation

2.1. INTRODUCTION

Heavy metals are introduced into the environment through a number of industrial processes.¹ Depending on the chemical form and exposure level; heavy metals can potentially be very harmful to humans and have a negative impact on the environment. Unlike organic pollutants, metal contamination is exacerbated by the fact that metals are a non-degradable, recirculating contaminant and accumulate in the environment.^{2,3} As a direct result of this fact, it is necessary to remediate heavily contaminated sites. This can only be accomplished by isolation and recovery of heavy metals since degradation is not an option. As a first attempt at remediation, bulk techniques, such as simple filtration or precipitation are often utilized.^{3,4} Although these techniques are useful in removing a significant fraction of the contaminant, they are unable to reduce the contaminant levels to meet environmental agency regulations for many of the more toxic metals. As a result, a polishing or finishing step must be employed. This finishing step is often in the form of a chemical extraction. The ideal metal extraction and reclamation technique must have the following attributes:

1. Selectivity – binding only to the metal of interest, thus allowing for separation from metals that are harmless or beneficial that could overwhelm the available binding sites and significantly reduce the efficiency or capacity of the extracting media.
2. Strong binding – necessary if effective removal from contaminated areas to an allowable level is to be realized.
3. Easy release – allowing for efficient preconcentration of the contaminant and rejuvenation or reuse of the media.

4. Environmental innocuity – preventing further contamination when the media is ultimately discarded.
5. Stability – ability to be reused with an extended lifetime, ensuring cost effectiveness.

In many instances, the attributes sited for remediation are identical to those desired if preconcentration methodologies are sought as a means of assisting analytical detection methods. With the need to establish concentration levels in the low to sub-ppb levels, validation of the remediation procedure requires sensitive analytical tools. While techniques exist for all regulated contaminant levels, many labs must resort to less sensitive instrumental capabilities and must employ preconcentration tools to detect regulatory levels.

Currently, the most common chemical modes of metal removal include ion exchangers or removal by chelation with synthetic crown ethers or other macrocyclic cage molecules.⁵⁻⁸ The most significant drawback associated with typical ion exchangers is the lack of selectivity in metal binding and/or weak binding characteristics. While crown ethers are both selective and strong binders, due to polydentate chelation within a sized cavity, they often exhibit slow release kinetics⁵. This is a potential problem when metal reclamation is required. In addition, many crown ethers are also very toxic, so using them may simply add to the problem of contamination.

As a result of the inherent problems with most of the current metal remediation strategies, researchers are now turning toward natural systems. For the purposes of limiting the scope of this review, the vast body of research in phytoremediation will not be covered, although it remains a very active and effective approach to remediation for both natural waters and soils. Similarly, the use of immobilized unicellular algae and other micro-organisms in metals preconcentration and remediation has a long history

with encouraging results but lies outside the scope of this review. However, the likely source of binding in these unicellular material are the chemicals that make up the organism, one could consider a more focused effort at isolation of these particular biocompounds and direct utilization of only those cellular components that are directly involved in metal binding. While these can range in character from simple cellulose to more elaborate proteins, this review will focus on the potential utility of amino acids, peptides, and proteins that have been immobilized on a substrate for general use in column applications.

A well known class of metal binding proteins, the metallothioneins, is an example of such biomolecules that are characterized as having a high degree of metal binding specificity and have been isolated in a wide variety of organisms(e.g., ⁹⁻¹²). Their strong binding characteristics and selectivity seem to fit the criteria of the ideal metal chelator. Upon immobilization these proteins seemed to lose their metal binding capabilities outside of the pristine cellular environment where they typically function in nature ¹³. In this particular instance, closer examination of several metallothioneins showed that their sequences contained a significantly high percentage of cysteine residues and that sulfhydryl groups present on these residues are primarily responsible for metal binding.^{10,11} This suggests the possibility of using simpler amino acid chains or synthetic peptides (e.g., poly-amino acids) as metal binding alternatives to natural peptides. Considering only the natural set of amino acids, one can readily recognize a variety of functionalities that could serve as coordination sites for metal chelation. Using amino acids as building blocks with their various side chains and recognizing that peptides are simple polymers of these units using a common amide linkage, a wide variety of interesting chelators could be envisioned. More specifically, these chelators may exhibit

the desired characteristics of specificity and have the added side benefit of being non-toxic when discarded.

This review will focus on studies directed at metal binding by immobilized amino acids (Figure 2.1) as well as short chain polypeptides. In some instances the incorporation of amino acids into short polymeric chains or evaluation of anionic compounds are also included.

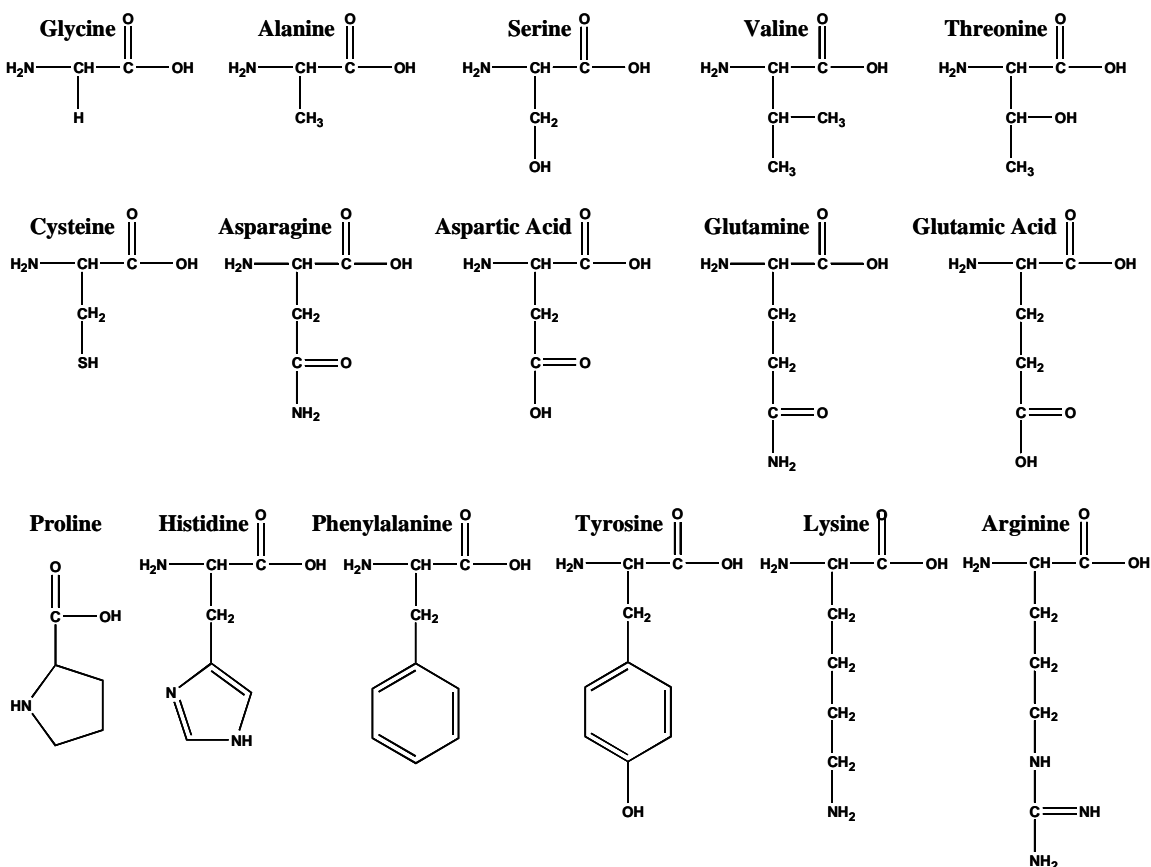


Figure 2.1. Selected set of amino acids that have been used by various researchers as immobilized chelators of metals.

2.2. SINGLE AMINO ACIDS

As mentioned previously, cysteine (Cys) is a major component of a group of metal binding proteins, called metallothioneins.¹¹ As a result, researchers have investigated Cys immobilized onto a solid support for use as a metal chelator. Elmahadi and Greenway utilized Cys immobilized onto silanized controlled pore glass (CPG) through a gluteraldehyde linker for preconcentration of Cd^{2+} , Co^{2+} , Cu^{2+} , Hg^{2+} , Pb^{2+} , and Zn^{2+} .¹⁴ Capacities for these metals were determined through breakthrough curve analysis and calculated at 12.48, 5.50, 7.86, 6.06, 11.66, and 7.88 mmol of metal/g of dry resin, respectively.

Denizli and coworkers^{15,16} and Disbudak et al.¹⁷ also utilized immobilized Cys for metal preconcentration and remediation. In each of these studies 2-methacryloylamindocysteine (MAC) was allowed to react with 2-hydroxyethylmethacrylate (HEMA) in an aqueous medium. The product was spherical beads, with an average size of 150 – 200 μm , of poly(2-hydroxyethylmethacrylate – methacryloylamidocysteine), (p(HEMA-MAC)). The beads were characterized according to their swelling ratio, FTIR analysis, and elemental analysis. The spectroscopic studies were conducted in the absence of metal to characterize the beads and confirm the incorporation of MAC, not to study the metal binding characteristics. In separate studies, binding characteristics were determined for As^{3+} , Cd^{2+} , Cr^{3+} , Cu^{2+} , Hg^{2+} , and Pb^{2+} ; and it was shown that while the pHEMA beads exhibited negligible Cd^{2+} binding, p(HEMA-MAC) beads exhibited significant Cd^{2+} capacity. The microbeads can be regenerated with an acidic solution. Several studies have been conducted using glycine (Gly) residues supported on various crosslinked resins. George and coworkers,¹⁸ and Vinodkumar and Matthew¹⁹ studied the metal binding capabilities and the effects of the degree of crosslinking on metal uptake on polyacrylamide crosslinked with N,N'-

methylene-bis-acrylamide (NNMBA) with supported Gly. Gly was incorporated into the resin by transamidation using a solution containing an excess of the sodium salt of glycine. The metals studied include Co^{2+} , Cu^{2+} , Fe^{2+} , Fe^{3+} , Ni^{2+} , and Zn^{2+} . Metal binding increased with an increase in crosslinking, until 8% crosslinking and then decreased. Interestingly, the metal desorbed resins showed specificity toward the previously desorbed metal over other metals. This was attributed to “pockets” left by the desorbed metal or the “memory” of the ligand for the metal.

George et al. also studied the metal binding ability of divinylbenzene (DVB)-crosslinked polyacrylamide supported Gly toward Co^{2+} , Cu^{2+} , Ni^{2+} , and Zn^{2+} .²⁰ Once again, Gly residues were introduced through transamidation with Gly. Interestingly, as the degree of crosslinking increases from 2-20%, the metal complexation decreases due to a decrease in the available carboxylate ligands for metal binding with an increase in DVB content. The resin does show enhanced specificity toward the desorbed metal over other metals in subsequent runs, and the time for rebinding of the desorbed metal is significantly less for rebinding than it is for initial binding as seen with the NNMBA crosslinked resin.

Finally, George et al. directly compared the metal-ion complexation characteristics between Gly functionalities supported on DVB-crosslinked polyacrylamide and NNMBA-crosslinked polyacrylamide toward Co^{2+} , Cu^{2+} , Ni^{2+} , and Zn^{2+} .²¹ DVB was chosen because it is more rigid and hydrophobic than NNMBA. The NNMBA-crosslinked polyacrylamide was shown to be more effective at metal complexation than the DVB-crosslinked resin while DVB showed increased selectivity over NNMBA. Again, metal rebinding is much faster and more specific than initial binding on both resins. Each of these resins can be regenerated by acid washing and reused.

In a procedure similar to that described previously by Denizli^{15,16} and Disbudak,¹⁷ Say et al. prepared poly(hydroxyethyl methacrylate-co-methacrylamidohistidine) p(HEMA-co-MAH) beads for metal complexation.²² Again, these beads were fully characterized without metals bound by swelling studies, FTIR, and elemental analysis of the bead. In additional experiments, the metal binding affinity was demonstrated to be $\text{Cu}^{2+} > \text{Cr}^{3+} > \text{Hg}^{2+} > \text{Pb}^{2+} > \text{Cd}^{2+}$ and the beads could be easily regenerated with 0.1M HNO_3 .

In an attempt to prepare a novel molecular imprinted adsorbent to remove heavy metals, Say et al. synthesized Cu^{2+} – imprinted poly(ethylene glycol dimethacrylate-methacryloylamidohistidine/ Cu^{2+}) (poly(EGDMA-MAH/ Cu^{2+})) microbeads by dispersion polymerization of EGDMA and MAH/ Cu^{2+} .²³ After removal of the Cu^{2+} , these beads exhibited a maximum Cu^{2+} capacity of 48 mg of Cu^{2+} /g of support and excellent selectivity of Cu^{2+} over Zn^{2+} , Ni^{2+} , and Co^{2+} . Metal binding exhibited a strong dependence on pH, with increased binding at increased pH. Cu^{2+} was easily desorbed with EDTA and the beads were reusable without a significant loss in capacity.

Phenylalanine (Phe) has also been immobilized onto spherical macroreticular styrene-divinylbenzene beads to create a chelating resin.²⁴ This resin was capable of separating Cu^{2+} from Co^{2+} and Ni^{2+} . Co^{2+} and Ni^{2+} are not retained on the column at pH 3 while copper is and can be eluted with 1 M HCl. The beads are also capable of removing Cu^{2+} from seawater.

2.3. IMMOBILIZED POLY-AMINO ACIDS ON SILICA AND CARBON SUPPORTS

In addition to single amino acids, poly-amino acids and peptides have been immobilized onto solid supports for use in metal chelating systems. Jurbergs and Holcombe attached poly-L-Cysteine (PLCys) (n~50 residues) to CPG via a procedure

described by Masoom and Townshend²⁵ and characterized it according to its Cd^{2+} binding capabilities²⁶. Using breakthrough analysis, it was determined that PLCys was an effective chelator for Cd^{2+} . Through competitive binding studies using ethylenediaminetetraacetic acid (EDTA) and ethylenediamine dihydrochloride (en) as competing ligands, conditional stability constants were calculated at 10^{13} for the very strong binding sites, $10^9 - 10^{11}$ for the strong binding sites and 10^6 for the intermediate sites. Although there is very strong binding, the metal can be quantitatively recovered using 0.1M HNO_3 , making the column fully regenerable and reusable (Figure 2.2.).

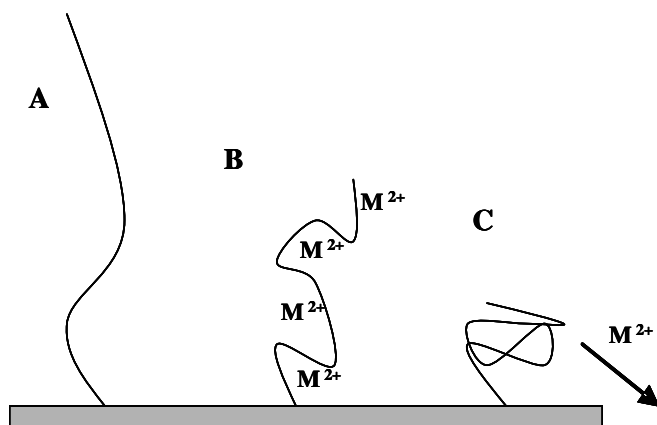


Figure 2.2. Schematic representation of an immobilized peptide under binding ready (A), metal binding (B), and metal release (C) conditions. M^{2+} represents a divalent metal species.

A study of Cd^{2+} capacity at various pH's revealed that the affinity of PLCys for Cd^{2+} had a significant dependence on pH. There was very little binding in acidic pHs and binding increased as pH increased. They postulated that at elevated pHs the PLCys is more hydrophilic due to the sulfhydryl groups being deprotonated. As a result, the peptide chain would be unfolded due to an increased hydration from ion-dipole

interactions and the side chains may be more accessible in an unfolded peptide, thus leading to an increase in metal capacity. They were also able to determine that the metal binding of PLCys may be mass transport limited since they observed the Cd^{2+} capacity increase as the solution flow rate was decreased. Various concentrations of hard acid metals in the influent stream (e.g., alkali and alkaline earth metals, Co^{2+} and Ni^{2+}) had very little effect on PLCys - Cd^{2+} binding.

Later, a comparison of the metal binding capabilities of PLCys (n~50 residues) and 8-hydroxyquinoline (8HQ), both immobilized onto CPG, was conducted.²⁷ Once again using breakthrough analysis in metal capacity determination, PLCys showed more selectivity against harder acid metals than 8HQ. While 8HQ strongly complexes a broad range of metals (Cd^{2+} , Co^{2+} , Cu^{2+} , Ni^{2+} , and Pb^{2+}), PLCys isolated soft acid metals such as Cd^{2+} and Pb^{2+} and had very little affinity for Co^{2+} or Ni^{2+} . Thus, they reasoned that PLCys should be efficient in isolating many of the heavy metals from complex matrices containing hard acid metals. The conditional stability constants, again determined through competitive binding studies with EDTA and en, agreed with the previously reported values reported by Jurbergs and Holcombe.²⁶

In the process of studying various supports, Miller and Holcombe evaluated Cys immobilized on porous carbon, a more inexpensive support.²⁸ Both PLCys (n~50 residues) and the Cys monomer were tethered to Carbopack™-X, a commercially available porous carbon, by derivitizing the carbon with carboxylate functionalities by acid activation and linking the PLCys or Cys through the use of 1-ethyl-3-[3-(dimethylamino)propyl]carbodiimide (EDC). Breakthrough analysis and competitive binding studies demonstrated that porous carbon is an effective support for immobilized ligands. In fact, the capacities for all metals tested were consistently higher on the porous carbon than on CPG. It is suggested that this may be due to the immobilization

efficiency. The immobilization procedure is much simpler for porous carbon than for CPG, possibility resulting in greater coverage of the polymer onto the support. Conditional stability constants were in good agreement with previous work done on CPG. Wildgoose et al. attached PLCys to graphite powder for metal remediation.²⁹ The peptide was attached through “building block” chemistry with 4-nitrophenyl moieties and was characterized using electrochemical and X-ray photoelectron spectroscopic (XPS) techniques. Increased metal capacities over convention solid state supports were attributed to higher surface coverages on the graphite support.

Johnson and Holcombe not only attached PLCys to an electrode composed of glassy carbon, but also used the electrode potential to control metal binding and release.³⁰ An applied potential was used to oxidize and reduce the disulfide bonds on the peptide. Reduction to thiols prepared the peptide for metal binding. Oxidation of the available thiol moieties to disulfide bonds after metal binding resulted in a zipper effect disrupting the binding cavity and gradually reduced the charged binding sites.

Gutierrez et al. used the same approach as Jurbergs and Holcombe²⁶ by attaching poly-L-aspartic acid (PLAsp) (n~50 residues) to CPG to test its metal binding capabilities.³¹ The binding affinity of PLAsp is $\text{Cu}^{2+} > \text{La}^{3+} \approx \text{Ce}^{3+} \approx \text{Eu}^{3+} > \text{Pb}^{2+} > \text{Cd}^{2+} > \text{Ni}^{2+} > \text{Co}^{2+} > \text{Mn}^{2+} > \text{Ca}^{2+} > \text{Na}^{2+}$, which is somewhat complimentary to PLCys and consistent with carboxylate functionality complexing. A further study comparing the metal binding characteristics of PLAsp and poly-L-glutamic acid (PLGlu) on CPG was done by Malachowski and Holcombe.³² In this study, it was determined that metal binding capacities and conditional stability constants of these two peptides were the same. The presence of an additional methylene group was shown not to alter the metal binding properties of these materials.

In an attempt to find a cheaper alternative to PLAsp, Miller et al. compared immobilized PLAsp to immobilized poly-acrylic acid (PAA), a synthetic polymer.³³ The results for PLAsp-CPG are similar to those reported above. Additionally, metal binding was measured as a function of pH and capacity again decreased with a decrease in pH due to protonation of the carboxylates and possible conformational changes at low pH (ca. <pH=4) for PLAsp-CPG. Stability studies show that PLAsp-CPG exhibited minimal loss of capacity upon exposure to 0.05M ammonium acetate buffer, 5% H₂O₂, and elevated temperature (60°C).

Miller and Holcombe also studied gold as a support for PLAsp.³⁴ Gold was chosen because it acts as an inert surface, acting only as an anchor for the polymer and remaining unreactive toward the metals in solution. The gold used initially was in the form of gold transmission electron microscopy (TEM) grids that were stacked in a microcolumn with thin PTFE spacers between each grid to promote mixing and flow. The immobilization of the polymer was conducted on-line with an FI system, using a modification of a procedure described by Leggett.³⁵ The metal binding trend remained the same as for PLAsp on CPG but the capacities were considerable higher for the PLAsp on gold for all of the metals studied; Al³⁺, Ce³⁺, Cu²⁺, Eu³⁺, Fe³⁺, and La³⁺. This is possibly due to a more efficient immobilization procedure. The same authors also attempted to employ gold coated CPG substrates for immobilization prepared by electroless coating techniques, but the results were not encouraging due to patchy gold coverage and possible pore blockage by the deposited gold.³⁶

2.4. MEMBRANE IMMOBILIZED POLY-AMINO ACIDS

In addition to silica, gold and carbon, poly-amino acids have also been immobilized onto membranes. Membrane technology is very well developed in the area

of separations and remediation (e.g., ³⁷⁻³⁹). Often used in the passive separation of contaminants from solution, popular membrane technologies include reverse osmosis, nanofiltration and ultrafiltration. In heavy metal sorption the membrane is often functionalized with a metal chelating group such as iminodiacetate, amidoxime, phosphoric acid or sulfonic/carboxylic groups to facilitate metal removal.⁴⁰⁻⁴⁷ Thus, the membrane serves as a support for the metal binding material and with the attachment of these groups the membrane can be tuned to exclude specific solutes.

Recently, researchers have investigated the attachment of amino acids and poly-amino acids to membrane surfaces for metal extraction purposes. For example, Bhattacharyya and coworkers attached poly-L-glutamic (PLGlu) (n~93 residues) acid to several different microfiltration membranes (both silica and cellulose-based) to study the heavy metal sorption characteristics.⁴⁸ The polymer was attached to the membranes through an aldehyde functional group on the surface of the membrane. It was shown that the PLGlu functionalized membrane is capable of binding heavy metals with the affinity following the order of $Pb^{2+} \geq Cu^{2+} > Ni^{2+} \approx Cd^{2+}$. The membrane also exhibited preferential binding of Pb^{2+} and Ni^{2+} over Ca^{2+} . The binding characteristics were dependant upon the type of membrane used, the degree of PLGlu functionalization, pH, and metals present.

Poly-D-aspartic acid (PDAsp) and poly-L-aspartic acid (PLAsp) have also been successfully immobilized onto both cellulose and silica based microfiltration membranes.⁴⁹ These functionalized membranes show capacities for Cu^{2+} , Cd^{2+} , and Pb^{2+} that are consistently higher than conventional ion exchange and chelation resins, in the range of mmol of metal/g of sorbant. Not unexpectedly, little difference was seen in the performance in PDAsp and PLAsp. Ritchie and coworkers outlined the three primary mechanisms for metal sorption to include ion exchange, chelation, and electrostatic

interactions.⁴⁹ Due to the polymeric nature of these ligands attached to a membrane, electrostatic interactions take the form of counterion condensation. Condensation zone binding is an important factor in the increase in binding capacity of functionalized membranes over conventional ion exchange systems due to the high charge density within the membrane pores.

In similar studies, Hestekin et al. show the differences that result from PLGlu and PLAsp bound to either pure cellulose or cellulose acetate based membranes.⁵⁰ Counterion condensation was more closely evaluated and a continuous flow system was employed with the membrane system. Results indicate that pure cellulose membranes with a higher surface area provide more aldehyde linkage groups for greater polymer attachment and that counterion condensation is an important mechanism for metal ion sorption in membrane systems.

Denizli et al. synthesized a poly (2-hydroxyethylmethacrylate-co-methacrylamindophenylalanine) membrane for copper adsorption.^{51,52} The membranes were prepared through UV-initiated photopolymerization of 2-methacrylamidophenylalanine (MAPA) and 2-hydroxyethylmethacrylate (HEMA) with azobisisobutyronitrile present as an initiator. Characterization of this membrane revealed the order of metal affinity to be $\text{Hg}^{2+} > \text{Ni}^{2+} > \text{Cu}^{2+}$, with metal adsorption increasing with increased pH, leveling off at pH 5.0. The capacities of these membranes were reported as mmol of metal/m² of membrane. The membranes can be regenerated with 0.1M HNO₃ and reused without significant loss of capacity.

Researchers have also attached Phe to a polyethylene membrane, in the form of a hollow fiber, through radiation-induced graft polymerization.⁵³ The attachment of the polymer was conducted using two different reaction schemes in an effort to determine which method would produce the highest density of functional groups. The first method

involved grafting glycidyl methacrylate (GMA) to the fiber and then coupling the Phe to the GMA. The second method involved attaching the Phe to the GMA first and then grafting the Phe-GMA to the fiber. Although the fiber was not fully characterized for metal binding capacity, the Cu^{2+} binding along the cross section was monitored and a uniform distribution of Cu^{2+} through the fiber was found. This demonstrated a homogeneous distribution of Phe through the fiber. It was also concluded that the second reaction scheme (grafting the Phe-GMA complex to the fiber) occurred at a rate 180-fold less than grafting the GMA alone. The preliminary results from this study indicate that with further investigation, this technology may be applicable to heavy metal remediation.

2.5. IMMOBILIZED PEPTIDES

Peptides and short chains of amino acids have also been immobilized for metal extraction. Terashima et al. immobilized a fusion protein synthesized from maltose binding protein (pmal) and human metallothionein (MT) onto Chitopearl resin.⁵⁴ This resin was evaluated for its Cd^{2+} and Ga^{2+} binding capabilities. Interestingly, the optimal pH for Cd^{2+} binding was determined to be 5.2 while for Ga^{2+} it was 6.5. Based on the hard and soft acid-base theory and the analysis of the adsorption isotherms of these metals, the results indicate that the cysteine residues of the MT moiety of the immobilized protein are responsible for Cd^{2+} binding. Other negatively charged residues such as Asp, Glu, lysine (Lys), serine (Ser), threonine (Thr), glutamine (Gln), and asparagines (Asn) bind Ga^{2+} . As a result of this strong metal binding dependence on pH, this system can distinguish between these two metals.

Another class of metal binding proteins, synthetic phytochelatins, has shown improved Cd^{2+} binding over metallothioneins.⁵⁵ Xu, et al used a novel approach by attaching a cellulose-binding domain (CBD) to a synthetic phytochelatin (EC20). The

CBD attached itself to a cellulose support thus immobilizing the phytochelatin.⁵⁶ Upon addition of Cd^{2+} the CBD-EC20 membrane bound the metal at a ratio of $\sim 10 \text{ Cd}^{2+}/$ immobilized CBD-EC20 while the membrane with only the CBD attached did not bind any Cd^{2+} . Upon addition of EDTA, Cd^{2+} was removed and the membrane capacity was restored.

The binding domains of cysteine-containing transport proteins known as *merT* and *merP* have also been studied by Huang et al.⁵⁷ These peptides were synthesized and immobilized onto chemically modified diatomaceous earth (Celite 545). In these studies, the metal binding capacity of Cu^{2+} , Cd^{2+} , and Pb^{2+} to these materials was determined and it was suggested that MerP bound an increased amount of metal due to adjoining cysteine groups positioned in the peptide.

Another interesting study was that conducted by Sayed, Saleh, and Hasan where they extracted metal binding amino acids from surplus chicken feathers.⁵⁸ The chicken feathers were treated with alkali solutions of 0.95 N NaOH and 0.6 N NaOCl to extract the amino acids from the bulk feather material. The amino acid composition was determined and the amino acids were immobilized onto silica. These materials were used to remove Ca^{2+} , Mg^{2+} , Fe^{2+} , and Mn^{2+} from industrial wastewater.

2.6. IMMOBILIZED AMINO ACID FOR USE IN ION-EXCHANGE CHROMATOGRAPHY

In contrast to remediation applications where it is desirable to have extremely strong binding, other applications have interest in moderate binding so that the substrate can be used in chromatographic separations via partitioning. Single amino acids immobilized onto silica surfaces have been used extensively for ligand-exchange,⁵⁹ metal chelation⁶⁰ and affinity chromatography⁶¹. The use of these materials for ion-exchange chromatography has not been as widely explored. Amino acids by nature are

zwitterions meaning they possess both positively and negatively charged sites. Zwitterion-exchangers are of particular interest as new stationary phases for high performance liquid chromatography (HPLC) as they may separate both anionic and cationic species in a single solution. These materials also show increases in mass transport and ion selectivity. Attachment of amino acids to silica is a simple way to achieve a variety of zwitterionic stationary materials.

In the last decade, research in this area has been advanced by Nesterenko⁶² who initially explored L-hydroxyproline (Hypro) bonded silica as an anion-exchange material. The amino acid was attached to silica particles through the secondary amine via 3-glycidoxypentyltriethoxysilane. Separation of nine anions (SCN^- , ClO_4^- , I^- , NO_3^- , Br^- , Cl^- , IO_3^- , H_2PO_4^- , and NO_2^-) was observed at pH 3.13 with citric acid as the eluent. Significant changes in retention times were observed for different eluents and small adjustments in pH.

Nesterenko expanded his investigations using L-arginine (Arg), L-valine (Val), L-tyrosine (Tyr), L-proline (Pro), and Hypro.⁶³⁻⁶⁵ Amino acids were again attached to the silica through the N-terminus and the ligands acid-base properties were used to tune ion interactions. Cation and anion-exchange properties of each amino acid were determined in addition to varying effects of carboxylic acid eluent concentration and pH. Immobilized Pro and Hypro successfully separated 6-8 various anions in a single solution under acidic conditions. Immobilized Val and Tyr were characterized as pure cation exchangers as the secondary amine interactions with surface silanol groups make anion-ligand interactions negligible. Surprisingly, Arg was also characterized as a cation exchanger with poor separation of anions. The amine functionalities of Arg are also hindered as a result of interactions with surface silanol groups. Interactions between surface silanol groups and charged sites of the amino acid in these systems tend to dictate

ion selectivity. It was postulated that the basicity of the amino groups enhances charge localization due to a change in the multilayer structure at the silica surface and ultimately establish the exchange properties of the attached amino acid. Asp and Glu, amino acids possessing additional carboxylate functionalities, were also studied.⁶⁶ Various solutes such as alkali and alkaline earth metal cations were used in the study along with six benzene derivatives for sorbent evaluation. Asp and Glu were shown to be efficient cation exchangers.

Investigations of bound amino acid-metal cation interactions (i.e., complex forming or ion-exchange) were done using Glu.⁶⁷ Glu was chosen because of the relatively stable complexes it forms with metal cations and was evaluated using alkali, alkaline earth and transition metals. Conditions such as pH, ionic strength, organic solvent, and temperature were varied. An increase in the non-polar and also the proton accepting character of organic solvents showed marked increases in capacities and changes in the metal binding character. Also, at both high ionic strength and pH, the chelate effect was shown to prevail over ion-exchange mechanisms.

In recent studies, Kiseleva et al. examine the zwitterionic-exchange properties of commercially available silica bound poly-aspartic acid (PAsp).⁶⁸ PAsp is attached to surface amine groups through the carboxylate functionalities and thus aligns parallel to the silica surface. The stationary phase contains neutral amide groups along with residual aminopropyl and unreacted carboxylate groups. The poly-amino acid was able to simultaneously separate anions and alkali and alkaline earth metal cations showing the utility of using zwitterionic-exchange column for both cation and anion separations. The optimal pH range for PAsp bound silica is 3.0-3.5 due to the zwitterionic character of the various surface groups.

Additionally, Liu and Sun have shown that Cys immobilized onto a polyacrylonitrile-divinylbenzene resin has a significant affinity for Ag^+ , Hg^{2+} , Au^{3+} , Pt^{4+} with capacities in the range of 0.39 – 1.22 mmol of metal/g of resin.⁶⁹ It was also shown that the immobilized Cys resin is capable of separating these metals chromatographically. In a mixed solution Pt^{4+} , Hg^{2+} , and Ag^+ were eluted sequentially and Au^{3+} was retained by the column and eluted off with 0.1% thiourea in 0.1 M hydrochloric acid.

These researchers also conducted a comparison of the ability of three chelating ion-exchange resins to separate Mo^{6+} and W^{6+} .⁷⁰ The three functionalities immobilized onto the polyacrylonitrile-divinylbenzene resins were thioglycollic acid linked by 1,6-hexanediol, thioglycollic acid linked by ethylene glycol, and Cys linked by 1,6-hexanediol. After the initial run of Mo^{6+} and W^{6+} , which was unsuccessful in the separation, the Cys resin was not investigated further

2.7. IMMOBILIZED AMINO ACID/PEPTIDE FOR Cd^{2+} REMOVAL FROM HUMAN PLASMA

Removal of heavy metals from water is certainly a significant environmental problem. If water supplies were contaminant free, heavy metal poisoning would not be a concern. Unfortunately, this is not the case and there is currently no specific affinity adsorbent treatment for Cd^{2+} poisoning.⁷¹ Bektas and co workers immobilized cysteine onto poly(2-hydroxyethylmethacrylate) (PHEMA) microspheres. The PHEMA microspheres were synthesized from a suspension of HEMA and EGDMA.⁷² They demonstrated that these microspheres were capable of binding 0.065 mmol Cd^{2+} /g of support from human plasma. Additionally, they can be reused without significant loss of capacity.

In another attempt to develop a method for removal of Cd^{2+} from human plasma Denizli et al. immobilized cysteinylhexapeptide (CysHP) to poly(2-hydroxyethyl methacrylate) beads.⁷¹ The sequence of the hexapeptide was Lys-Cys-Thr-Cys-Cys-Ala (alanine) and it was immobilized to the beads through a monochlorotriazinyl dye ligand, Cibacron Blue F3GA. The maximum Cd^{2+} bound from human plasma onto these beads in a packed-bed column-based system was determined to be 11.8 mg of Cd^{2+} /g of support.

2.8. RELATED STUDIES

Several researchers have focused on more in depth studies pertaining to the metal binding capabilities of these systems. These include the effects of oxidation on Cys chelation and preconcentration,⁷³ the effects of temperature on Lys and Glu retention of cations,⁷⁴ and the effects of heats of adsorption on PLAsp cation binding⁷⁵. Additionally, a study was conducted in which atomic force microscopy was used to examine conformational changes in immobilized PLCys in various environments.³³ By measuring the height of immobilized PLCys from the surface of a glass slide, it was confirmed that in neutral solutions the polymer chain was generally oriented perpendicular to the surface. With the addition of a metal, the height decreased ca. 15 nm. The addition of acid decreased the height another 10-15 nm, thus supporting the idea that a significant tertiary structure change had occurred. At low pHs the PLCys likely exists as a tight random coil on the surface. Raising the pH returned the structure to its original form.

2.9. CONCLUSIONS

Research involving the use of immobilized amino acids, peptides and proteins for metal remediation and similar purposes has shown great promise. Amino acids are ideal building blocks for metal chelation systems. They provide a wide range of binding functionalities and are attached to one another through simple amide linkages. These novel binders are easily attached to silica, carbon, gold and polymeric particles; silica and cellulose based membranes; and incorporated into polymerized resins. The amino acid of interest can be immobilized through either the amine or carboxylate terminus or modified to provide other possible linkage chemistries. Studies show that immobilized amino acids, peptides, and proteins are all capable of metal capacities in the $\mu\text{mole} - \text{mmole} / \text{g}$ of resin range. Much research involving the use of amino acids as zwitterion-exchange materials has also proved fruitful. In addition, metal selectivity and specificity can be achieved by altering the amino acid functionalities and/or immobilization procedures used. There are still many directions continuing research in this area could head, including the use of peptide libraries and increased metal-template studies.

2.10. LITERATURE CITED

1. Forstner, U.; Wittmann, G. T. W. *Metal Pollution in the Aquatic Environment*; Springer-Verlag: New York, 1981.
2. Vernet, J. P. *Impact of Heavy Metals on the Environment*; Elsevier: New York, 1992.
3. Ireland, M. P. *Biological Monitoring of Heavy Metals*; Wiley: New York, 1991.
4. Friber, L.; Nordberg, G. F.; Vouk, B., Eds. *Handbook on the Toxicology of Metals*; Elsevier: Amsterdam, 1979.
5. Chen, L. H.; Chung, C. S. *Inorganic Chemistry* **1988**, 27, 1880-1883.
6. Franklin, S. J.; Raymond, K. N. *Inorganic Chemistry* **1994**, 33, 5794-5804.
7. Hou, Z.; Raymond, K. N.; O'Sullivan, B.; Esker, T. W.; Nishio, T. *Inorganic Chemistry* **1998**, 37, 6630-6637.
8. Hou, Z.; Sunderland, C. J.; Nishio, T.; Raymond, K. N. *Journal of the American Chemical Society* **1996**, 118, 5148-5149.
9. Harrison, P. M. *Metalloproteins*; Verlag Chemie: Weinheim, 1985.
10. Suzuki, K. T.; Imura, N.; Kimura, A. *Metallothionein Iii: Biological Roles and Medical Implication*; Birkhauser Verlag: Boston, 1993.
11. Stillman, M. J.; Shaw, C. F.; Suzuki, K. T., Eds. *Metallothioneins, Synthesis, Structure and Properties of Metallothioneins, Phytochelatins, and Metal-Thiolate Complexes*; VCH: New York, 1992.
12. Sigel, H.; Sigel, A. *Metal Ions in Biological Systems*; Marcel Dekker: New York, 1989.
13. Anderson, B. R. Dissertation, Univ. of Texas, Austin, 1994.
14. Elmahadi, H. A. M.; Greenway, G. M. *Journal of Analytical Atomic Spectrometry* **1993**, 8, 1009-1014.

15. Denizli, A.; Garipcan, B.; Karabakan, A.; Say, R.; Emir, S.; Patir, S. *Separation and Purification Technology* **2003**, 30, 3-10.
16. Denizli, A.; Garipcan, B.; Emir, S.; Patir, S.; Say, R. *Adsorption Science & Technology* **2002**, 20, 607-617.
17. Disbudak, A.; Bektas, S.; Patir, S.; Genc, O.; Denizli, A. *Separation and Purification Technology* **2002**, 26, 273-281.
18. George, B.; Pillai, V. N. R.; Mathew, B. *Journal of Macromolecular Science, Pure and Applied Chemistry* **1998**, A35, 495-510.
19. Vinodkumar, G. S.; Mathew, B. *Chemistry- A European Journal* **1998**, 34, 1185-1190.
20. George, B.; Mathew, B. *J. Macromol. Sci., Pure Appl. Chem.* **2001**, A38, 429-449.
21. George, B.; Pillai, V. N. R.; Mathew, B. *Journal of Applied Polymer Science* **1999**, 74, 3432-3444.
22. Say, R.; Garipcan, B.; Emir, S.; Patir, S.; Denizli, A. *Macromolecular Materials and Engineering* **2002**, 287, 539-545.
23. Say, R.; Birlik, E.; Ersoz, A.; Yilmaz, F.; Gedikbey, T.; Denizli, A. *Analytica Chimica Acta* **2003**, 480, 251-258.
24. Sugii, A.; Ogawa, N.; Iinuma, Y.; Yamamura, H. *Talanta* **1981**, 28, 551-556.
25. Masoom, M.; Townshend, A. *Analytica Chimica Acta* **1984**, 166, 111-118.
26. Jurbergs, H. A.; Holcombe, J. A. *Analytical Chemistry* **1997**, 69, 1893-1898.
27. Howard, M.; Jurbergs, H. A.; Holcombe, J. A. *Journal of Analytical Atomic Spectrometry* **1999**, 14, 1209-1214.
28. Miller, T. C.; Holcombe, J. A. *Analytica Chimica Acta* **2002**, 455, 233-244.

29. Wildgoose, G. G.; Leventis, H. C.; Davies, I. J.; Crossley, A.; Lawrence, N. S.; Jiang, L.; Jones, T. G. J.; Compton, R. G. *Journal of Materials Chemistry* **2005**, *15*, 2375-2382.
30. Johnson, A. M.; Holcombe, J. A. *Analytical Chemistry* **2005**, *77*, 30-35.
31. Gutierrez, E.; Miller, T. C.; Gonzalez-Redondo, J. R.; Holcombe, J. A. *Environmental Science and Technology* **1999**, *33*, 1664-1670.
32. Malachowski, L.; Holcombe, J. A. *Analytica Chimica Acta* **2004**, *517*, 187-193.
33. Miller, T. C.; Holcombe, J. A. *Journal of hazardous materials* **2001**, *83*, 219-236.
34. Miller, T. C.; Holcombe, J. A. *Analytical Chemistry* **1999**, *71*, 2667-2671.
35. Leggett, G. J.; Roberts, C. J.; Williams, P. M.; Davies, M. C.; Jackson, D. E.; Tendler, S. J. B. *Langmuir* **1993**, *9*, 2356-2362.
36. Miller, T. C.; Holcombe, J. A. *Analytica Chimica Acta* **2002**, *454*, 37-44.
37. Bhattacharyya, D.; Mangum, W. C.; Williams, M. E. *Reverse Osmosis*, 4th ed.; Wiley: New York, 1997.
38. Ho, W. S. W.; Sirkar, K. K., Eds. *Membrane Handbook*; Chapman and Hall: New York, 1992.
39. Noble, R. D.; Stern, S. A., Eds. *Membrane Separations Technology: Principles and Applications*; Elsevier: New York, 1995.
40. Konishi, S.; Saito, K.; Furusaki, S.; Sugo, T. *Industrial & Engineering Chemistry Research* **1992**, *31*, 2722-2727.
41. Konishi, S.; Saito, K.; Furusaki, S.; Sugo, T. *Journal of Membrane Science* **1996**, *111*, 1-6.
42. Li, G.-Q.; Konishi, S.; Saito, K.; Sugo, T. *Journal of Membrane Science* **1994**, *95*, 63-69.

43. Tsuneda, S.; Saito, K.; Furusaki, S.; Sugo, T.; Okamoto, J. *Journal of Membrane Science* **1991**, 58, 221-234.
44. Iwata, H.; Saito, K.; Furusaki, S.; Sugo, T.; Okamoto, J. *Biotechnology Progress* **1991**, 7, 412-418.
45. Sugiyama, S.; Tsuneda, S.; Saito, K.; Furusaki, S.; Sugo, T.; Makuuchi, K. *Reactive Polymers* **1993**, 21, 187-191.
46. Yamagishi, H.; Saito, K.; Furusaki, S.; Sugo, T.; Ishigaki, I. *Industrial & Engineering Chemistry Research* **1991**, 30, 2234-2237.
47. Saito, K.; Ito, M.; Yamagishi, H.; Furusaki, S.; Sugo, T.; Okamoto, J. *Industrial & Engineering Chemistry Research* **1989**, 28, 1808-1812.
48. Bhattacharyya, D.; Hestekin, J. A.; Brushaber, P.; Cullen, L.; Bachas, L. G.; Sikdar, S. K. *Journal of Membrane Science* **1998**, 141, 121-135.
49. Ritchie, S. M. C.; Bachas, L. G.; Olin, T.; Sikdar, S. K.; Bhattacharyya, D. *Langmuir* **1999**, 15, 6346-6357.
50. Hestekin, J. A.; Bachas, L. G.; Bhattacharyya, D. *Industrial & Engineering Chemistry Research* **2001**, 40, 2668-2678.
51. Denizli, A.; Say, R.; Patir, S.; Arica, Y. *Reactive & Functional Polymers* **2000**, 46, 157-164.
52. Denizli, A.; Say, R.; Patir, S.; Arica, Y. *Separation Science and Technology* **2001**, 36, 2213-2231.
53. Kiyohara, S.; Sasaki, M.; Saito, K.; Sugita, K.; Sugo, T. *Reactive & Functional Polymers* **1996**, 31, 103-110.
54. Terashima, M.; Oka, N.; Sei, T.; Yoshida, H. *Biotechnology Progress* **2002**, 18, 1318-1323.

55. Bae, W.; Chen, W.; Mulchandani, A.; Mehra, R. K. *Biotechnology and bioengineering* **2000**, 70, 518-524.
56. Xu, Z.; Bae, W.; Mulchandani, A.; Mehra, R. K.; Chen, W. *Biomacromolecules* **2002**, 3, 462-465.
57. Huang, C.-C.; Su, C.-C.; Hsieh, J.-L.; Tseng, C.-P.; Lin, P.-J.; Chang, J.-S. *Enzyme and Microbial Technology* **2003**, 33, 379-385.
58. Sayed, S. A.; Saleh, S. M.; Hasan, E. E. *Mansoura Science Bulletin, A: Chemistry* **2005**, 32, 1-19.
59. Gubitz, G.; Jellenz, W.; Santi, W. *Journal of Chromatography* **1981**, 203, 377.
60. Bacold, M. D.; Rassi, X. E. *Journal of Chromatography* **1990**, 512, 237.
61. Gaida, A. V.; Monastyrskii, V. A.; Magerovskii, Y. V.; Staroverov, S. M.; Lisichkin, G. V. *Journal of Chromatography* **1988**, 424, 385-391.
62. Nesterenko, P. N. *Journal of High Resolution Chromatography* **1991**, 14, 767-768.
63. Nesterenko, P. N. *Journal of Chromatography* **1992**, 605, 199-204.
64. Nesterenko, P. N.; Kopylov, R. V.; Tarasenko, D. A.; Shpigun, O. A.; Zolotov, Y. A. *Doklady Akademii Nauk* **1992**, 326, 838-841.
65. Nesterenko, P. N.; Shpigun, O. A.; Zolotov, Y. A. *Doklady Akademii Nauk* **1992**, 324, 107-110.
66. Nesterenko, P. N.; Elefterov, A. I.; Tarasenko, D. A.; Shpigun, O. A. *Journal of Chromatography, A* **1995**, 706, 59-68.
67. Elefterov, A. I.; Kolpachnikova, M. G.; Nesterenko, P. N.; Shpigun, O. A. *Journal of Chromatography A* **1997**, 769, 179-188.
68. Kiseleva, M. G.; Kebets, P. A.; Nesterenko, P. N. *Analyst (Cambridge, United Kingdom)* **2001**, 126, 2119-2123.

69. Liu, C. Y.; Sun, P. J. *Analytica Chimica Acta* **1981**, 132, 187-193.
70. Liu, C. Y.; Sun, P. J. *Talanta* **1984**, 31, 353-356.
71. Denizli, A.; Yavuz, H.; Arpa, C.; Bektas, S.; Genc, O. *Separation Science and Technology* **2003**, 38, 1869-1881.
72. Bektas, S.; Disbudak, A.; Denizli, A.; Genc, O. *Trace Elements and Electrolytes* **2002**, 19, 26-32.
73. Howard, M.; Jurbergs, H. A.; Holcombe, J. A. *Analytical Chemistry* **1998**, 70, 1604-1609.
74. Kolpachnikova, M. G.; Penner, N. A.; Nesterenko, P. N. *Journal of Chromatography, A* **1998**, 826, 15-23.
75. Kebets, P. A.; Kuz'mina, K. A.; Nesterenko, P. N. *Zhurnal Fizicheskoi Khimii* **2002**, 76, 1639-1642.

Chapter 3: Efforts in Templating for Transition Metals Using Short-Chain Polymers and Peptides

3.1. INTRODUCTION

Constructing chemical formations that bind or have affinity towards specific molecules (i.e., molecular recognition) has been widely explored in recent years, while trace metal recognition research has received less attention. Creating templates for metal ions allow for more selective preconcentration and extraction processes over current ion-exchange methods. This is extremely valuable for environmental clean-up or industrial recovery purposes.

Template formation relies heavily on choice and stereochemistry of binding functionalities. One class of compounds that demonstrate high selectivity based on cavity size is the crown ethers. These structures are usually two dimensional with strong binding, and often require harsh chemicals to remove the metal from the preformed cavity. A wider variety of molecular templates for metal binding were synthesized by Raymond and coworkers, where they constructed three dimensional cavities for various metals.¹ Previous attempts to synthesize selective resin beads used bi or tri-dentate chelators to bind the metal and then used emulsion polymerization to create the polymer bead around the metal-complex, effectively templating for a metal species of interest.^{2,3} Although this method does result in selective metal uptake in some cases, metal removal is, again, difficult due to the strong, rigid complexes immobilized into the polymer beads.

A class of short-chain peptides, biohomopolymers,⁴ have been shown to have strong binding, yet easy release due to the peptide changing its tertiary structure during these processes. Forming templates could occur by sparingly cross-linking these polymers while the metal is complexed. Ideally, if templated, the polymer would retain

the specific metal-binding conformation after release of the metal and the binding pH is again imposed.

In this study, the use of poly(acrylic acid) and a random copolymer (Glutamic Acid (Glu):Lysine (Lys)) (6:4) covalently attached to glass supports and packed into micro-columns was used to perform specific functional chemistry in order to induce metal template formation. The objective is to limit our reaction cross-linking yields, so that cavities are retained while maintaining flexibility in the polymer to permit tertiary structure change for on-demand metal release by changes. These studies are the first attempts at “on-line”, metal templating.

3.2. MATERIALS AND METHODS

3.2.1. Chemicals

All chemicals were reagent grade unless noted, and deionized distilled water was used to prepare solutions. All glassware was soaked overnight in 4 mol L⁻¹ HNO₃ prior to use. The controlled pore glass (CPG) (Sigma, PG240-120) had a mean pore diameter of 22.6 nm (80-120 mesh). Stock solutions of 1000 µg mL⁻¹ Cd²⁺ (Anderson Laboratories) and Ni²⁺ (SCP Science) atomic absorption standards in 4% HNO₃ were used to prepare the loading solutions for the various metal binding experiments. For Co²⁺ (J.T. Baker), the loading solution was prepared from standardized solutions of the reagent grade nitrate salt in 1% (v/v) HNO₃ and 1% (v/v) HCl. A 0.2 mol L⁻¹ (N-[Hydroxyethyl]piperazine-N'-[2-ethanesulfonic acid]) (HEPES) (Aldrich) buffer and a 0.2 mol L⁻¹ (2-(N-Morpholino)ethanesulfonic acid) (MES) (Sigma) buffer was prepared and purified by passing the buffer through a 100-200 mesh Chelex 100 (Bio-Rad) ion exchange column. Poly(acrylic acid) (50 wt%) (Acros) and a random copolymer (Glutamic Acid

(Glu):Lysine (Lys)) (6:4) (MW 20,000-50,000) were purchased from Aldrich. Other reagents used included nitric acid, N-(3-Dimethylaminopropyl)-N'-ethylcarbodiimide (EDC), o-iodosobenzoic acid (Sigma); ninhydrin reagent, potassium cyanide (Acros); N-hydroxysuccinimide (NHS), (Fisher); ethylene diamine (EN), and diamino octane (ON), Gluteraldehyde, piperidine (99%), and 3-aminopropyltriethoxysilane (98%) (Aldrich).

3.2.2. Apparatus

A Varian FAAS (model AA-875) with an acetylene/air flame was used for all metal determinations. Hollow cathode lamps were operated at the manufacturer recommended current for Co, Ni, and Cd of 7, 3.5, and 3.5 mA. Wavelengths for Co, Ni, and Cd were 240.7, 232.0, and 228.8 nm, respectively, and were used in conjunction with a monochromator bandpass of 0.2 nm for Co and Ni, and 0.5 nm for Cd.

Solution reached the FAAS using an eight-roller peristaltic pump (Manostat Carter 4/8 cassette pump); 0.76 mm i.d. PTFE tubing and connectors, and columns (3 mm x 25 mm fitted with 100 μ m PTFE frits) (Omnifit). A Kel-F tee was placed after the column and immediately in front of the nebulizer to minimize the noise level by providing air compensation for the “solution starved” nebulizer. Approximately 0.05 g of dry resin was packed into the columns, filling approximately 50% of the column. The remaining dead space was loosely packed with glass wool which had no discernable metal binding capacity for the metals used in this study.

3.2.3. Synthesis and Cross-Linking Experiments

3.2.3.1. Cross-Linking PolyAcrylic Acid Using a Bifunctional Linker

Polyacrylic acid (PAA) was immobilized onto CPG using a previous method.⁵ PAA-CPG, before and after cross-linking, was characterized by comparing metal capacities determined by breakthrough and strip analysis. A 10 μ g mL⁻¹ solution of a

particular metal (Ni^{2+} , Cd^{2+} , or Co^{2+}) in 0.02 mol L^{-1} HEPES buffer (pH 7.0) was passed through each column at 1 or 2 mL min^{-1} until breakthrough was reached (i.e., when the FAAS absorbance signal became constant and indicated that the effluent concentration had reached the influent concentration). After breakthrough, HEPES buffer was passed through the columns at 1 mL min^{-1} for ~ 1 min to remove metal-containing solution from the column dead volume and line tubing. A slower flow rate was used to inhibit removal of metal bound to weak sites. A 0.1 mol L^{-1} HNO_3 solution was then passed through the column at 2 mL min^{-1} to strip the metal from the column. In some cases, the metal extract was collected in an appropriate volumetric flask for subsequent “strip analysis” via FAAS.

The stability at high pHs of the covalent attachment of PAA to CPG was examined by monitoring the Co^{2+} metal capacity before and after exposure to 30 min of a pH 7, 8, 9, and 10 0.02 mol L^{-1} HEPES buffer solution. A solution of 40 mmol L^{-1} EDC and 60 mmol L^{-1} NHS in 0.02 mol L^{-1} HEPES buffer was used to demonstrate the reversibility of the EDC/NHS reaction. The solution was passed at 2 mL min^{-1} through the column for 30 min. Breakthrough curve and strip analysis using $10 \mu\text{g mL}^{-1}$ Co^{2+} were collected sequentially until no further change in the metal capacity was observed. For cross-linking experiments, two diamines, ethylene diamine and diamino octane, were used as bifunctional linkers and EDC/NHS was used to activate the carboxylate functionalities. Cross-linking solutions were passed through columns packed with CPG-PAA and further characterized. Table 3.1. shows the reaction sequence and conditions.

Table 3.1. Flow-through reaction sequence and conditions for cross-linking PAA with bifunctional linkers using EDC/NHS.

Cross-Linking Reaction (2 mL/min)	
2 min	0.1 mol L ⁻¹ HNO ₃ Acid
2 min	0.02 mol L ⁻¹ HEPES buffer (pH 7.0)
30 min	40 mmol L ⁻¹ EDC 60 mmol L ⁻¹ NHS in MES pH 5.5
10 min	125 mmol L ⁻¹ EN&ON (pH 8.0)
60 min	10 µg mL ⁻¹ Co ²⁺ in HEPES ramping pH from 8.0 to 10.0

3.2.3.2. Cross-Linking Copolymer (Glu, Lys)(6:4)

A random copolymer (Glu:Lys) (6:4) (MW 20,000-50,000) was attached to CPG through the amine functionalities using a procedure previously described for polyaspartic acid attachment to CPG.⁶ All metal capacity measurements were made using breakthrough and strip analysis as described in the previous section. The stability at high pHs of the copolymer to CPG was also examined using a 10 µg mL⁻¹ Co²⁺ solution in 0.02 HEPES buffer and breakthrough analysis. To determine if metal was extracted from CoPoly-CPG during cross-linking experiments, columns loaded with Co²⁺ hard sites were exposed neutral solutions of 60 mmol L⁻¹ NHS and 20 mmol L⁻¹ MES, 20 mmol L⁻¹ MES, 20 mmol L⁻¹ HEPES buffer, and 4 mmol L⁻¹ of EDC in HEPES buffer at pH 6, 7,

and 8. Both the 1- and 2-step cross-linking experimental parameters are described in Table 3.2.

Table 3.2. Flow-through reaction sequence and conditions for cross-linking CoPoly-CPG using EDC/NHS for both a 1- and 2-Step reaction.

Cross-linking 1-Step Reaction		Cross-linking 2-Step Reaction	
2 min	0.1 mol L ⁻¹ HNO ₃ Acid	2 min	0.1 mol L ⁻¹ HNO ₃ Acid
2 min	0.02 mol L ⁻¹ HEPES buffer (pH 7.0)	2 min	0.02 mol L ⁻¹ HEPES buffer (pH 7.0)
3 min	10 ug mL ⁻¹ Co ²⁺ HEPES (pH 7.0)	15 min	4 mmol L ⁻¹ EDC 15 mmol L ⁻¹ NHS MES (pH 4.5)
15 min	40 mmol L ⁻¹ EDC HEPES (pH 8.0)	30 min	20 ug mL ⁻¹ Co ²⁺ HEPES raise from pH 7.0 to pH 10.0
2 min	Acid	2 min	Acid

3.3. RESULTS AND DISCUSSION

3.3.1. Cross-Linking PolyAcrylic Acid (PAA) Using Bifunctional Linkers

Aqueous cross-linking of PAA using EDC/NHS carboxylate activation and diamines as bifunctional linkers, was used as a means to template for transition metals. EDC is a carbodiimide that undergoes the reaction shown in Figure 3.1 to produce activated carboxylate groups that can form amide bonds upon attack by a lone pair from a primary amine.

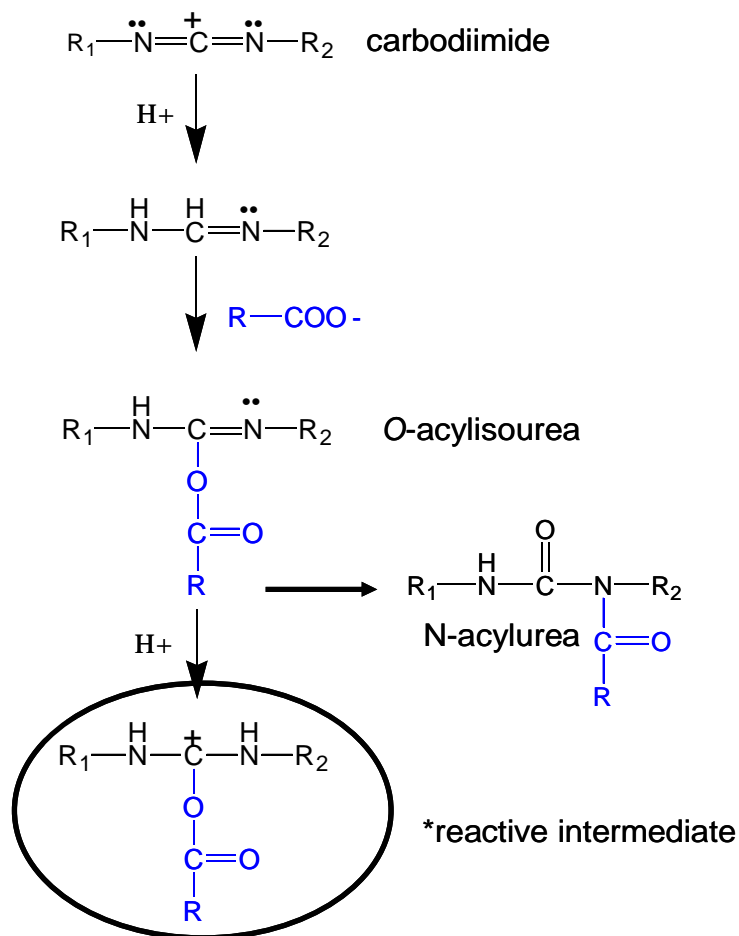


Figure 3.1. Activation of carboxylate functionalities using EDC.

Once formed, the *O*-acylisourea can undergo rearrangement to form the undesirable N-acylurea side product if it is shielded or is in a hydrophobic environment. NHS is another activating molecule that can be added to EDC and will displace the *O*-

acylisourea keeping the carboxylate functionality reactive for a longer periods of time and also prevents the formation of the N-acylurea.

The conditions for metal binding, carboxylate activation, and amine bond formation, all require a unique pH range. Figure 3.2. illustrates the pH requirements for these reactions and also shows the pH range used in the studies discussed in this chapter for both 1-step reactions where activation and cross-linking occur after metal is bound, and 2-step reactions where initially the carboxylates are activated and then the metal is introduced while the pH is raised.

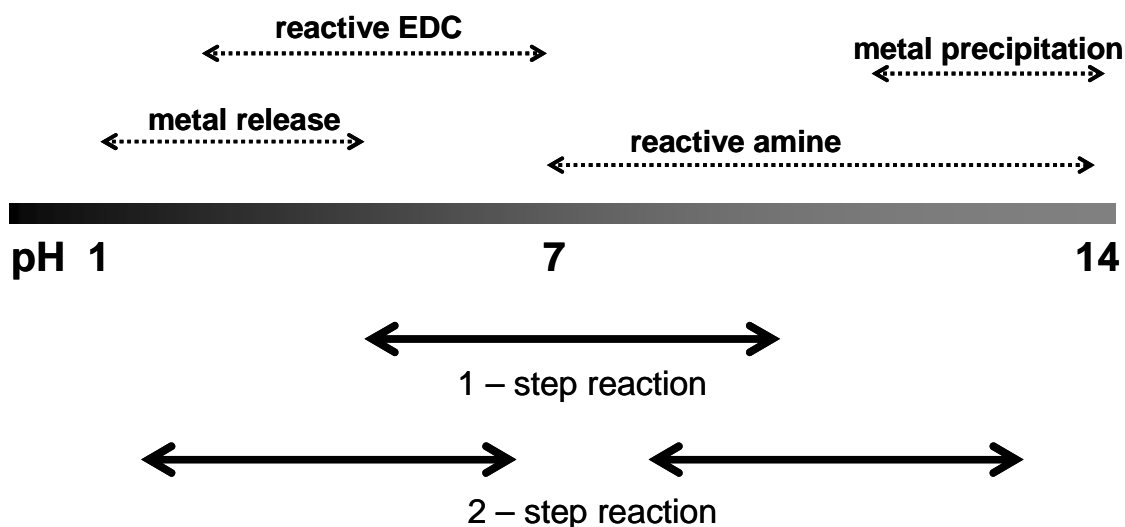


Figure 3.2. pH requirements for each process during metal templating reactions. The bottom arrows depict the ideal conditions for a 1- and 2-step reaction.

Due to the high pHs necessary for efficient amide bond formation (i.e., reactive amine groups), the stability of the siloxane bonds that covalently attach PAA to CPG was evaluated by exposing the column to solutions of increasing pHs (pH 7-10) (Figure 3.3.). The breakthrough capacity remained at approximately 12 ug Co^{2+} /g of CPG and no capacity was lost due to the exposure. This indicates that no capacity loss during cross-linking experiments should occur as a result of the high pH conditions imposed during cross-linking experiments.

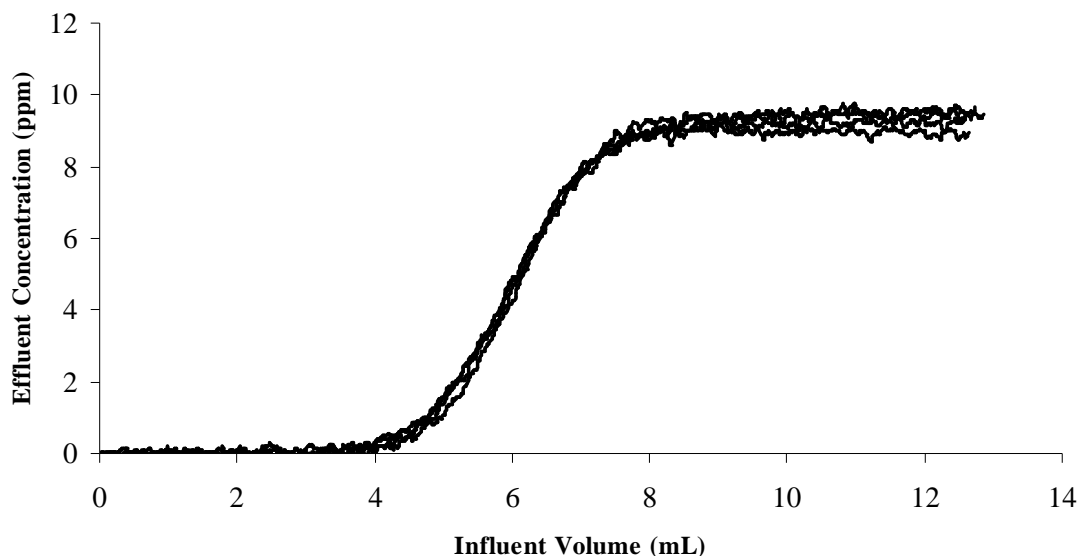


Figure 3.3. Breakthrough curve analysis of PAA using $10 \mu\text{g mL}^{-1} \text{Co}^{2+}$ (HEPES buffer pH 7) after 30 min treatments of pH 7, 8, 9, and 10 HEPES buffer.

When cross-linking with EDC/NHS, available carboxylates are activated, however, if amide bonds are not formed at those sites water will, in most cases, regenerate the carboxylate group. To determine the extent of EDC/NHS reversibility, PAA was exposed to a solution of EDC/NHS and the Co^{2+} capacity was monitored over

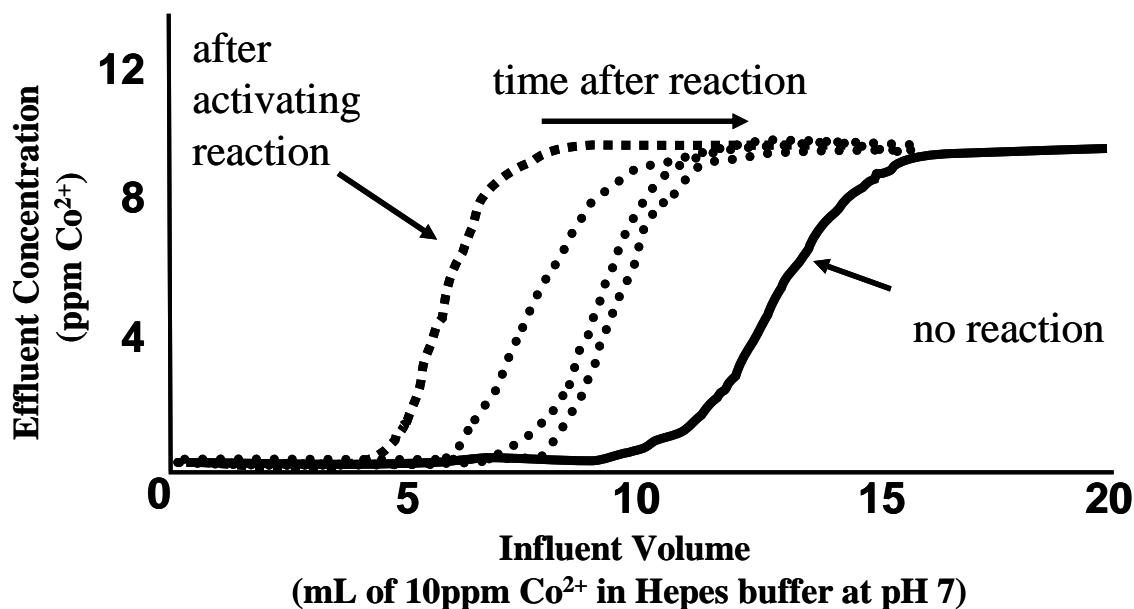


Figure 3.4. Breakthrough curve analysis of PAA using $10 \mu\text{g mL}^{-1} \text{Co}^{2+}$ in HEPES buffer at pH 7 before reaction (solid line), immediately after adding EDC/NHS (square dotted line), and thereafter (circle dotted lines).

time using breakthrough analysis. Figure 3.4. shows the capacity decrease after exposure to the EDC/NHS solution due to modification of some of the carboxylate functionalities with EDC. The NHS can replace EDC, prolonging carboxylate activation eventually returning to the carboxylate functionality if no amide formation occurs. In contrast, EDC may undergo rearrangement to form the N-acylurea which is irreversible, permanently altering those carboxylate functionalities. The activation of groups is a little more than 50%. This control will enable us to activate some, but not all of the carboxylate functionalities in hopes of lightly cross-linking the material.

The results indicated that although 2X excess of NHS is added, there is still some irreversible N-acylurea formation from the EDC coupling. This makes characterization of these materials more difficult. A decrease in metal capacity may not purely indicate the presence of cross-links between the peptide, but may also include the formation of N-

acylurea. Monitoring the relative metal binding capacities of a few metals was used to indicate if templating (i.e., cross-linking) occurs.

With this in mind, PAA was templated for Co^{2+} . Results for the cross-linking of PAA using a continuous flow reaction are shown in Table 3.3.

Table 3.3. Metal capacities of PAA-CPG before and after cross-linking experiments.

Metal	Initial Capacity ($\mu\text{mole/g CPG}$)	Capacity after Cross-linking #1 ($\mu\text{mole/g CPG}$)	Capacity after Cross-linking #2 ($\mu\text{mole/g CPG}$)
Co^{2+}	27 ± 3	13 ± 3	7 ± 4
Ni^{2+}	25 ± 2	12 ± 3	10 ± 3
Cd^{2+}	74 ± 5	28 ± 4	16 ± 3

After the first Cross-linking reaction, all metal capacities decreased with the Cd^{2+} capacity decreasing at a fast rate than Co^{2+} and Ni^{2+} . The capacity decreased more than that of just with EDC/NHS when no diamines were added (Figure 3.4). This indicated that the diamines are attaching either at one end or both ends. A second attempt to cross-link this column was made to increase the number of cross-links and to fully link amines that were only attached at one end. The capacities further decreased with no noticeable enhancements for Co^{2+} , however, the $\text{Co}^{2+}/\text{Cd}^{2+}$ capacity ratio did increase, but was still less than one indicting a selectivity preference for Cd^{2+} . The use of bifunctional linkers made templating difficult since both ends of the linker needed to be attached at optimal positions where the carboxylates were activated. The use of a zero degree cross-linker, cross-links via functional groups on a particular peptide with no bifunctional linker, may prove to be a better choice for templating via this method.

3.3.2. Cross-Linking Copolymer (Glu, Lys) (6:4)

A copolymer composed of Glu and Lys residues was used in an attempt to form zero length cross-links between the peptide via amide linkages. In this way, no additional cross-linker would need to be added. Only EDC/NHS would be added to activate the carboxylates and the amine groups from the lysines on the peptide are available to react at the activated sites. The stability of the copolymer immobilization was also examined by exposing a column packed with the polymer to HEPES buffer at pH's 7, 8, 9, and 10 (30 min each). The results are shown in Figure 3.5.

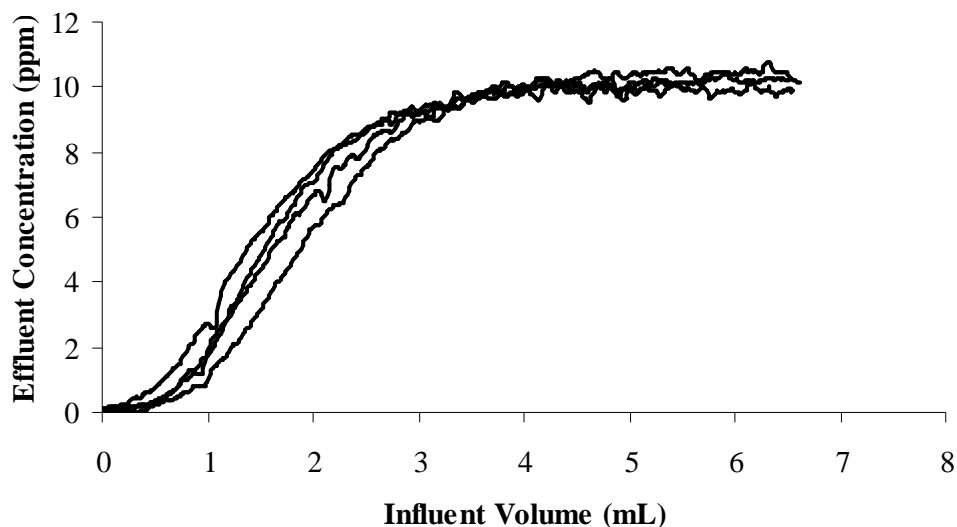


Figure 3.5. Breakthrough curve analysis of the copolymer using $10 \mu\text{g mL}^{-1} \text{Co}^{2+}$ (HEPES buffer pH 7) after 30 min treatments of 0.02 mol L^{-1} HEPES buffer at pH 7, 8, 9, and 10.

No drastic changes were observed in the Co^{2+} capacity after exposure to the different solution pHs. There was a slight increase in capacity due to some material loss from the column from unclogging procedures. As with the PAA immobilization, the siloxane

bonds are relatively stable for short exposures at high pH conditions. To our knowledge, this is the first attempt to immobilized CoPoly onto CPG. The Ni^{2+} , Cd^{2+} , and Co^{2+} capacities of CPG before (CPG-APS-Glu) and after (CPG-APS-Glu-CoPoly) CoPoly immobilization are shown in Table 3.4. This was done to verify that the CoPoly was successfully attached to CPG.

Table 3.4. Metal binding capacities of Co^{2+} , Ni^{2+} , and Cd^{2+} to CPG-APS-Glu and CPG-APS-Glu-CoPoly. Metal capacities were determined from the strip analysis and verified using the breakthrough analysis (n = 3).

Metal	CPG-APS-Glu ($\mu\text{mole/g CPG}$)		CPG-APS-Glu-CoPoly ($\mu\text{mole/g CPG}$)	
	pH 7.0	pH 8.0	pH 7.0	pH 8.0
Co^{2+}	5 ± 1	$11 \pm <1$	18 ± 1	27 ± 1
Ni^{2+}	$2 \pm <1$	11 ± 1	$12 \pm <1$	27 ± 1
Cd^{2+}	$3 \pm <1$	$11 \pm <1$	23 ± 1	45 ± 1

The increase in capacity after the attachment of CoPoly does indicate that some polymer was immobilized. The metal binding sites also increase when the pH is increased from pH 7.0 to 8.0. For metal templating purposes, it is important to have free amine groups that can still participate in cross-linking via the formation of amide bonds. The number of free amines present before and after CoPoly immobilization was determined using the Ninhydrin test.^{7,8} An amine coverage of $3 \pm 2 \mu\text{mol NH}_3/\text{g}$ of CPG on CPG-APS-Glu and $16 \pm 1 \mu\text{mol NH}_3/\text{g}$ of CPG on CPG-APS-Glu-CoPoly was calculated. This provides evidence of successful immobilization; in addition to the presence of free amines that can take part in cross-linking.

The 2-step reaction was used to achieve the best reaction conditions for both activation and cross-linking. The activation solution was optimized to activate half of the

carboxylate groups as indicated by a 50% decrease in the Co^{2+} capacity after activation. The 2-step cross-linking reaction involved the activation of the carboxylates at low pH, loading of Co^{2+} to the remaining metal-binding sites, and then raising the pH for optimally positioned amine groups to react. Figure 3.6. represent the results observed for these experiments. The overall capacity change for Co^{2+} did not change. Since we are activating 50% of the carboxylate functionalities, we would expect some capacity decrease if any cross-linking did occur. EDC/NHS activated carboxylates may have a shorter lifetime than our overall cross-linking reaction when most of metal pockets are formed.

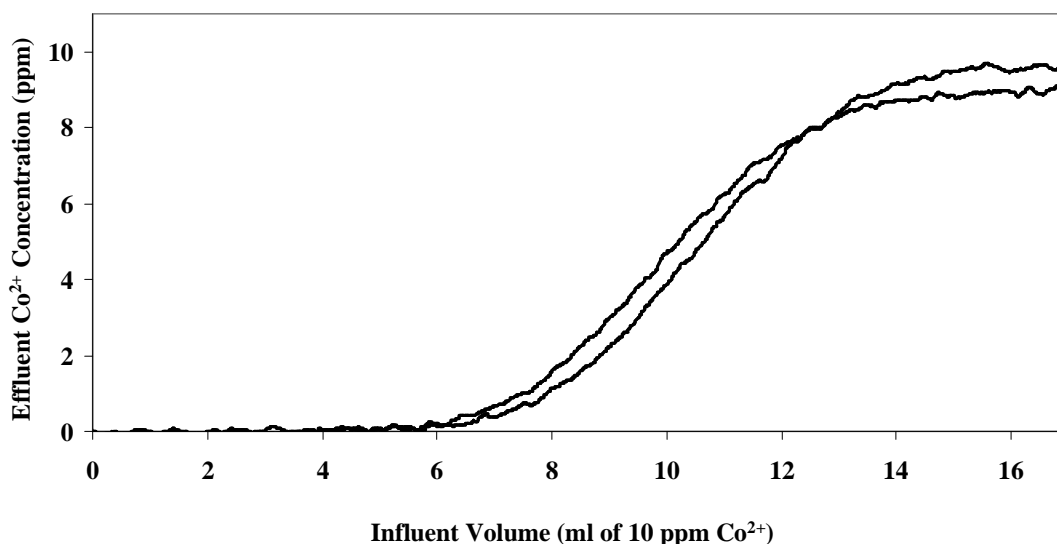


Figure 3.6. Breakthrough curve analysis of the copolymer using $10 \mu\text{g mL}^{-1} \text{Co}^{2+}$ (HEPES buffer pH 7) before and after 2-step cross-linking.

In an attempt to cross-link the binding cavity *after* the metal is introduced, a 1-step reaction was used. A higher concentration of activating solution was used as to ensure the cross-linking of the available functional groups that were not participating in binding and to increase amide bond formation. Monitoring the metal effluent during the 1-step cross-linking reaction using EDC/NHS in MES buffer showed that much of the metal was stripped off during this process (not shown), yet no capacity changes were observed. Before additional attempts were made to metal template, the cross-linking agents were passed through a metal bound column, to determine if metal is extracted by EDC, NHS, or MES. Figure 3.7. shows Co^{2+} hard sites being filled and then neutral solutions of MES/NHS, MES, and HEPES passed through the column. EDC was left out of these reactions to ensure no cross-linking would occur which also may force metal out of the peptide binding cavities. When MES/NHS or MES was added after metal was bound, much of the metal was extracted from the CoPoly binding sites. For a 1-step reaction where the reaction solution is passed through the column with metal bound, the use of NHS and MES would be prohibitive to the formation of cavities around a metal.

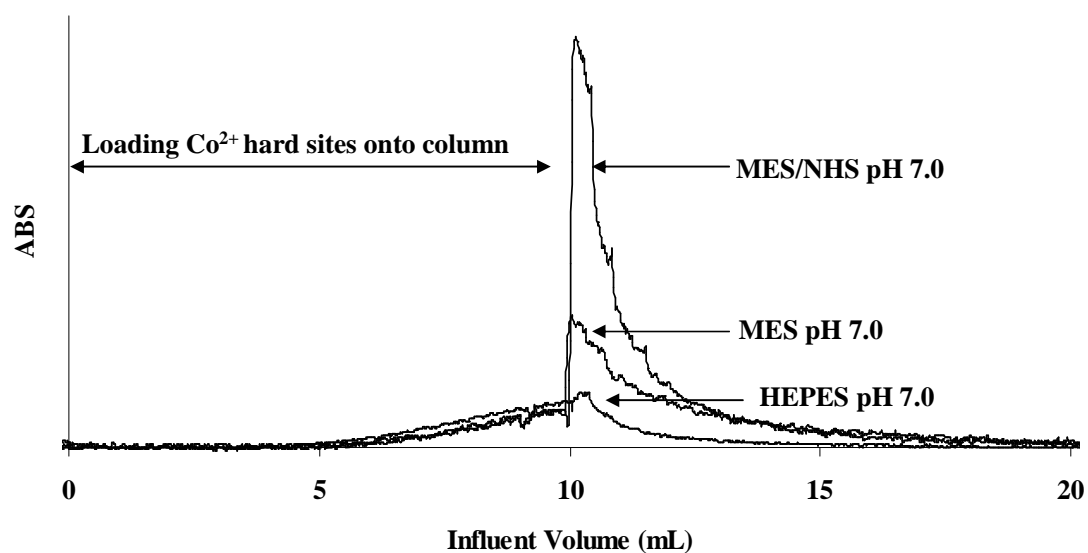


Figure 3.7. Cobalt absorbance from the column effluent during metal binding of the hard binding sites (0-10 min) and then introduction of neutral solutions of 20 mmol L^{-1} MES/ 60 mmol L^{-1} NHS, 20 mmol L^{-1} MES, and 20 mmol L^{-1} HEPES buffer.

The metal extracted when introducing only EDC was also examined at pH 6, 7, and 8 (Figure 3.8.).

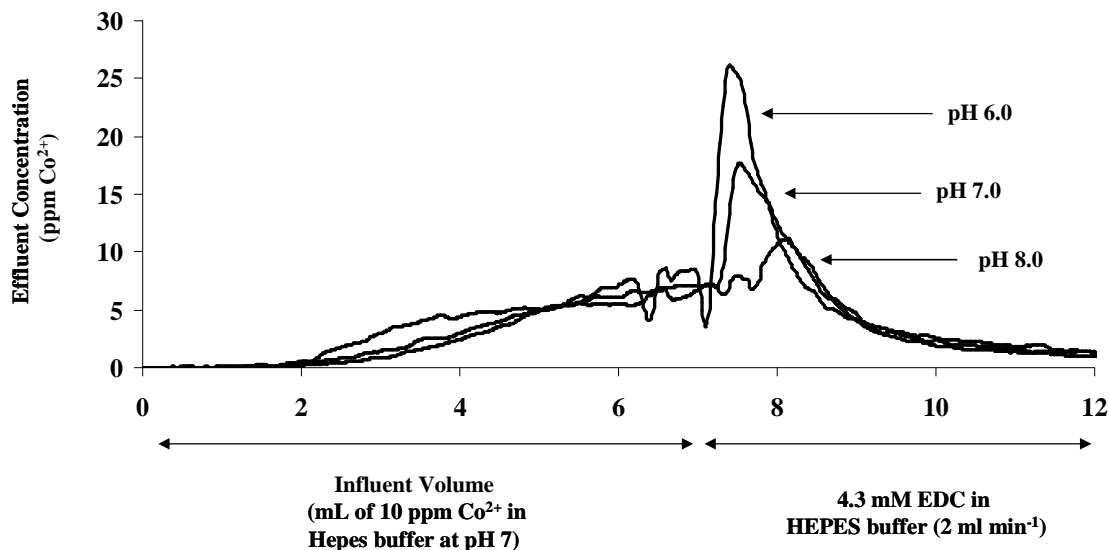


Figure 3.8. Effluent Co^{2+} concentration from Copoly-CPG column during metal binding of hard sites and then the introduction of an EDC cross-linking solution.

The hard sites were initially loaded with Co^{2+} , and then the EDC cross-linking solution was added at pH 6.0, 7.0, and 8.0. In slightly acid condition, pH 6.0, most of the metal was extracted likely due to some protonation of the carboxylate side chains.

For the actual one-step cross-linking reaction, EDC only was used at a pH of 8 which should increase amine reactivity and limit metal extracted from the peptide. Figure 3.9. shows the transient Co^{2+} of the metal effluent during metal binding and cross-linking. Initially, Co^{2+} was bound to the CoPoly hard sites and then EDC was added to cross-link free carboxylates with free amines. The EDC solution did extract some of the metal from the column. This amount was greater than that seen in Figure 3.7. due to a 10 fold increased in EDC concentration used, yet still less than that seen with NHS (Figure 3.7.). The acid strip after the reactions indicated that metal was still bound to the column during these reaction conditions.

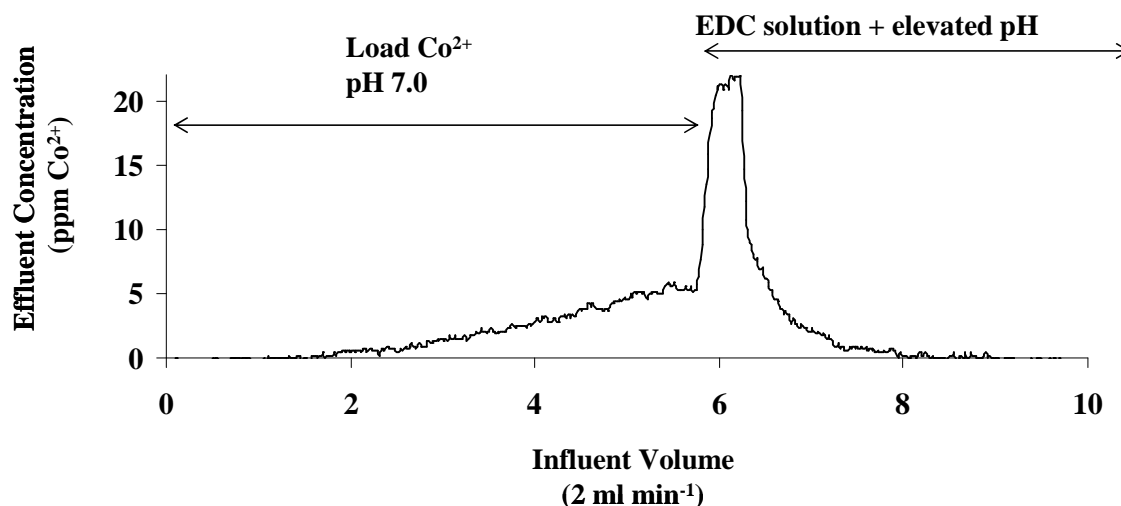


Figure 3.9. Effluent Co^{2+} concentration from Copoly-CPG column during metal binding of hard sites and then the introduction 40 mmol L^{-1} EDC pH 8.0 cross-linking reaction.

For these reactions, we did not see any indication of cross-linking based on the metal capacities that remained unchanged. The one step reaction was repeated at higher pHs and also showed no evidence of cross-linking. The positioning and activation of

both the carboxylates and amine groups may not be optimal for cross-linking and making quasi-rigid structures in this way. Due to the large size of the CoPoly, the low surface coverage may have also contributed to the difficulty in cross-linking these materials.

3.4. CONCLUSIONS

Cross-linking was explored to improve the metal selectivity of PAA and a copolymer composed of Glu and Lys through templating. Reactions with PAA required a bifunctional linker to cross-link the polymer at various locations after metal was bound. Cross-linking in this manner resulted in a decrease in the metal capacity likely due to a combination of carboxylates forming the N-acylurea side product, linking one end of a diamine, or both ends of a diamine. Although much of the capacity decreased from N-acylurea formation with some possible cross-links, the formation of possible cross-links did not increase the metal capacity for Co^{2+} . Slight selectivity changes were observed, but were likely the result of a decrease in carboxylate functionalities. Similar results were observed for the copolymer, however, no indication of amide linkages were observed due to the column returning to its pre-cross-linking state as noted by no changes in the metal capacity. The difficulty with using these methods is the need for the metal to remain bound to the peptide with minimal change in the preferential binding cavity during cross-linking. Aqueous cross-linking, especially with EDC, was a challenge due to the pH condition requirements of the cross-linkers and the groups cross-linked; in addition to the need to avoid low pHs that would release the bound metal. Analysis of multi-metal solutions may have proved a better analysis tool for determining the metal selectivity. In addition, the use of a packed, highly dense peptide environment may prove to be better templating material using similar zero cross-linkers.

3.5. LITERATURE CITED

1. McMurry, T. J.; Raymond, K. N.; Smith, P. H. *Science* **1989**, *244*, 938-943.
2. Kido, H.; Miyajima, T.; Tsukagoshi, K.; Maeda, M.; Takagi, M. *Analytical Sciences* **1992**, *8*, 749-753.
3. Uezu, K.; Nakamura, H.; Goto, M.; Murata, M.; Maeda, M.; Takagi, M.; Nakashio, F. *Journal of Chemical Engineering of Japan* **1994**, *27*, 436-438.
4. Malachowski, L.; Stair, J. L.; Holcombe, J. A. *Pure and Applied Chemistry* **2004**, *76*, 777-787.
5. Miller, T. C.; Holcombe, J. A. *Journal of hazardous materials* **2001**, *83*, 219-236.
6. Gutierrez, E.; Miller, T. C.; Gonzalez-Redondo, J. R.; Holcombe, J. A. *Environmental Science and Technology* **1999**, *33*, 1664-1670.
7. Sarin, V. K.; Kent, S. B. H.; Tam, J. P.; Merrifield, R. B. *Analytical Biochemistry* **1981**, *117*, 147-157.
8. Atherton, E.; Sheppard, R. C. *Solid Phase Peptide Synthesis-a Practical Approach*; IRL Press: Oxford, 1989.

Chapter 4: Metal Remediation and Preconcentration Using Immobilized Short-Chain Peptides Composed of Aspartic Acid and Cysteine

4.1. INTRODUCTION

Novel materials for metal preconcentration and remediation are of considerable interest in areas of environmental and materials science. One growing area in metal remediation and extraction involving the use of immobilized amino acids and peptides has been recently reviewed¹ and was also covered in chapter 2. By determining the amino acids responsible for metal interactions in metal binding proteins,^{2,3} such as the metallothioneins,⁴ a synthetic route to producing chelators with preferred selectivity and optimal capacity may be feasible. By constructing new ion-exchange materials consisting of amino acid building blocks, unique systems can be made due to the variety of amino acids that can be used and sequentially attached through amide linkages.

Previously, commercially available single amino acids and biohomopolymers consisting of a single type of amino acid were attached to solid supports for use in metal binding studies.¹ These studies indicated that immobilized amino acids and peptides have high capacities and frequently exhibit selectivities in the metals that they bind. These selectivities are based primarily on the side group functionality of the amino acid. For example, Cys⁵ and poly-L-cysteine (PLCys)⁶⁻⁸ bind soft metal acids such as Cd²⁺ and Pb²⁺ to a greater extent than hard metal acids such as Ni²⁺ and Co²⁺ while poly-L-aspartic (PLAsp)^{9,10} acid shows an increased affinity for Ni²⁺ and Co²⁺. Anionic species such as the chromates and arsenates have also been shown to bind to immobilized poly-L-histidine (PLHis), which contains a positively charged imidazole side chain in acidic solutions.¹¹

On-demand, metal release has also been an advantage of immobilized amino acids and peptides allowing them to be easily reused. Usually, introduction of an acid will cause the metal to be displaced by protons and/or facilitate a tertiary structure change, as in the case of biohomopolymers. Atomic force microscopy (AFM) was used to confirm these various structural changes of PLCys when exposed to buffer, metal and acidic solutions.¹² The binding character of redox active peptides can also be controlled electrochemically as shown recently by Johnson and Holcombe,¹³ where oxidation and reduction of PLCys immobilized on a carbon disk electrode was used to control metal binding and release.

Although a number of studies have explored using combinatorial peptide libraries for use in catalysis by metal complexes,¹⁴⁻¹⁶ immobilized peptides containing more than one type of amino acid have rarely been explored for their use in metal preconcentration and remediation.^{1,17} A recent paper explored the metal binding characteristics of two similar homopolymers, poly-L-glutamate (PLGlu) (40 – 70 residues) and PLAsp (50 – 80 residues).¹⁰ In spite of the extra methylene in the side chain of the glutamates, there was no noticeable difference in the binding characteristics for the metals tested. Short chain peptides containing more than one residue type may give greater control over selectivity and binding capacity than the simpler systems explored thus far. Shibata and coworkers, for example, in an attempt to mimic the binding selectivity and the catalytic activity of isopenicillin N synthase (IPNS), synthesized a peptide library (8-11 residues) on TentaGel resin by altering a linking peptide (1-3 residues) joining sequences of IPNS.¹⁸ Changes in bead color when exposed to metal solutions indicated selective metal uptake by some beads in the library from changing only 1-3 residues. Measurable changes in metal binding selectivities by changing only one amino acid in a backbone modified peptide were shown by Ye and coworkers.¹⁹

In order to examine the metal binding properties of small peptides consisting of varying amino acids, fluorenylmethoxycarbonyl (Fmoc)-solid phase peptide synthesis (SPPS)^{20,21} has been employed in the present study to create customized peptides (2 and 7 residues) on TentaGel resin beads. Three amino acids (Gly, Asp, and Cys) were chosen for the metal binding studies based on their side chain functionalities.^{1,22,23} Unlike typical SPPS where the peptides of interest are created and then cleaved off the resin, the peptides were left attached to the resins. The resins were then packed into microcolumns and the binding properties of Ni^{2+} , Cd^{2+} , Co^{2+} and Mg^{2+} were characterized by analysis of breakthrough curves, where flame atomic absorption spectrophotometry (FAAS) detection was employed.

4.2. MATERIALS AND METHODS

4.2.1. Chemicals

All chemicals were reagent grade unless noted, and deionized distilled water was used to prepare solutions. All glassware was soaked overnight in 4 mol L⁻¹ HNO₃ prior to use. Peptide synthesis reagents NovaSyn TG (TentaGel) resin (170 mesh; 0.30 mmol/g), glycine (Fmoc-Gly-OH), aspartic acid (Fmoc-Asp(t. butyl ester (OtBu))-OH), cysteine (Fmoc-Cys(trityl (Trt))-OH), 2-(1H-Benzotriazole-1-yl)-1,1,3,3-tetramethyluronium tetrafluoroborate (TBTU), and 1-Hydroxybenzotriazole (98%) (HOBt) were used as received from Novabiochem. The controlled pore glass (CPG) (Sigma, PG240-120) had a mean pore diameter of 22.6 nm (80-120 mesh). Stock solutions of 1000 µg mL⁻¹ Cd²⁺ (Anderson Laboratories) and Ni²⁺ (SCP Science) atomic absorption standards in 4% HNO₃ were used to prepare the loading solutions for the various metal binding experiments. For Co²⁺ and Mg²⁺ (J.T. Baker), the loading solutions were prepared from

standardized solutions of the reagent grade nitrate salt in 1% (v/v) HNO₃ and 1% (v/v) HCl. A 0.2 mol L⁻¹ (N-[Hydroxyethyl]piperazine-N'-[2-ethanesulfonic acid]) (HEPES) (Aldrich) buffer was prepared and purified by passing the buffer through a 100-200 mesh Chelex 100 (Bio-Rad) ion exchange column. The artificial seawater was prepared using sodium chloride, potassium bicarbonate, magnesium sulfate (Fisher); and calcium carbonate (Acros).⁶ Other reagents used included nitric acid o-iodosobenzoic acid(Sigma); ninhydrin reagent, potassium cyanide, DL-1,4-dithiothreitol (99%) (DTT), trifluoroacetic acid (99%), triethylsilane (99%), N,N-dimethylformamide (DMF) (Acros); stannous chloride (Matheson, Coleman & Bell); ethyl alcohol (Aaper Alcohol and Chemical Co.); pyridine, methanol, dichloromethane (DCM), N-methylmorpholine (NMM) (Fisher); piperidine (99%), and 3-aminopropyltriethoxysilane (98%) (Aldrich).

4.2.2. Apparatus

A Varian FAAS (model AA-875) with an acetylene/air flame was used for all metal determinations. Hollow cathode lamps were operated at the manufacturer recommended current for Co, Ni, Cd, and Mg of 7, 3.5, 3.5, and 3.5 mA. Wavelengths for Co, Ni, Cd and Mg were 240.7, 232.0, 228.8 and 285.2 nm, respectively, and were used in conjunction with a monochromator bandpass of 0.2 nm for Co and Ni, and 0.5 nm for Cd and Mg.

As shown in Figure 4.1, solution reached the FAAS using an eight-roller peristaltic pump (Manostat Carter 4/8 cassette pump); 0.76 mm i.d. PTFE tubing and connectors, and columns (3 mm x 25 mm fitted with 100 µm PTFE frits) (Omnifit). A Kel-F tee was placed after the column and immediately in front of the nebulizer to minimize the noise level by providing air compensation for the “solution starved” nebulizer. Approximately 0.02 g of dry resin was packed into the columns, filling approximately 20% of the column. The remaining dead space was loosely packed with

glass wool. The glass wool had no discernable metal binding capacity for the metals used in this study.

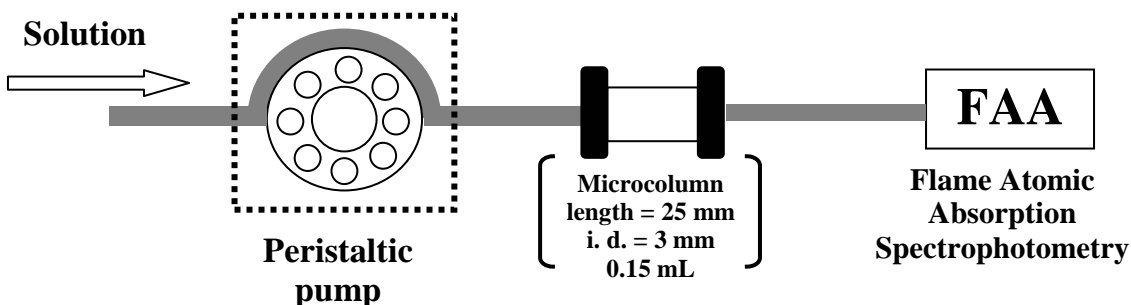


Figure 4.1. Pictorial representation of the flow through system used analysis of material packed into microcolumns.

4.2.3. Peptide synthesis

All immobilized peptides consisting of seven amino acids were synthesized by Fmoc-solid phase peptide synthesis (SPPS) using a Ranin Symphony Quartet automated peptide synthesizer. The CPG used was activated using nitric acid and 3-aminopropyltriethoxysilane²⁴ before attaching the peptide in a similar manner. Peptides synthesized on TentaGel were double coupled (each amino acid coupling reaction was performed twice) while the peptide synthesized on CPG was triple coupled due to poor reaction efficiencies. TentaGel is an ideal resin when using it for both peptide synthesis and continuous flow studies because it swells minimally in various solvents, yet has good transport through its cross-linked interior.

All immobilized peptides consisting of two amino acids were synthesized manually by the batch method. Coupling was done by combining 10 mL of 0.1 mol L⁻¹

amino acid in DMF with 10 mL of 0.1 mol L⁻¹ TBTU and 0.4 mol L⁻¹ NMM in DMF and then mixing with the resin. Once each amino acid addition was complete (ninhydrin analysis), the Fmoc group was cleaved using 0.5 mol L⁻¹ HOBt in a piperidine/DMF (20/80) solution. At the end of the synthesis, the protecting groups on each amino acid were cleaved using 0.5 mL of triethylsilane and 0.5 mL of DI water in 20 mL TFA. The resulting resin was rinsed with DMF, methanol and DCM; then dried (3 h) using a speed vac concentrator (Savant) connected to a cold trap (Heto) (-115°C) that was held under vacuum.

4.2.4. Peptide characterization

Peptide sequence verification and purity evaluation was determined by Edman degradation (ABI Procise 49X cLC protein sequencer) in conjunction with the ninhydrin test. A quantitative ninhydrin test^{20,25} using a HP8453 UV-visible spectrophotometer determined the number of amine functionalities on the TentaGel surface that did not react with the first amino acid coupling. A %C elemental analysis was conducted in duplicate (MHW Laboratories; Phoenix, AZ) on CPG_{GD₂CD₂C} and CPG with silanization agents to determine the peptide surface coverage.

4.2.5. Metal binding studies

4.2.5.1. Single and multi-metal binding studies

The previously described analysis system was utilized in the metal binding studies after a 15 min warm-up of pumps, tubing and lamps. Before binding experiments were performed, the columns were conditioned by passing 20 mL of 0.1 mol L⁻¹ HNO₃ followed by 4 mL of 0.02 mol L⁻¹ HEPES buffer (pH 7.0). For resins containing Cys, all solutions were deaerated with N₂ gas for 20 min, and 40 mL of 0.02 mol L⁻¹ of DTT was passed through each column before introducing the buffer. This was done to ensure

reduction of disulfide groups. Metal solutions were then passed through the columns and monitored by FAAS. For the single metal studies, a $20 \mu\text{g mL}^{-1}$ solution of a particular metal (Ni^{2+} , Cd^{2+} , Co^{2+} or Mg^{2+}) in 0.02 mol L^{-1} HEPES buffer (pH 7.0) was passed through each column at 2 mL min^{-1} (or a linear velocity of $11 \pm 2 \text{ cm/s}$) until breakthrough was reached (i.e., when the FAAS absorbance signal became constant and indicated that the effluent concentration had reached the influent concentration). For the multi-metal studies, a $20 \mu\text{g mL}^{-1}$ solution of Ni^{2+} , Cd^{2+} , Co^{2+} and Mg^{2+} in 0.02 mol L^{-1} HEPES buffer (pH 7.0) was passed through the columns (2 mL min^{-1}) until breakthrough was reached for all metals in solution, which required approximately 30 min.

After breakthrough, HEPES buffer was passed through the columns at 1 mL min^{-1} for ~ 1 min to remove metal-containing solution from the column dead volume and line tubing. A slower flow rate was used to inhibit removal of metal bound to weak sites. A 0.1 mol L^{-1} HNO_3 solution was then passed through the column at 2 mL min^{-1} to strip the metal from the column. The solution was collected in an appropriate volumetric flask for subsequent “strip analysis” via FAAS. Acidified standards, which were not retained by the column, were passed through the system to construct a calibration curve. Capacity values for the single metal studies were determined using both breakthrough and strip data, while only the strip values were used for the multi-metal studies.

Transient Cd^{2+} strip profiles were also examined. Columns were loaded with 15 mL of a $0.25 \mu\text{g mL}^{-1}$ Cd^{2+} solution, exposed to HEPES buffer for 1 min to remove excess metal solution in the dead volume, and then stripped with 0.1 mol L^{-1} nitric acid into the FAAS. These experiments were carried out using a flow rate of 1 mL min^{-1} to minimize the impact of mass transport and better reflect differences in equilibrium governed rates of release.

4.2.5.2. Equilibrium Studies

A multi-metal solution (500 mL of 20 $\mu\text{g mL}^{-1}$ Ni^{2+} , Cd^{2+} , Co^{2+} , and Mg^{2+} in 0.02 mol L^{-1} HEPES buffer) was passed continuously through the column at 1 mL min^{-1} , which required ca. 8h. By comparing capacities after this extended period of time with data from the breakthrough curve, which required ca. 30 min; it could be postulated whether equilibrium was established in the TentaGel resin column during breakthrough.

Before running the multi-metal solutions, columns were treated in one of the following ways: metal-free HEPES buffer pretreatment; preloading with 50 mL of 20 $\mu\text{g mL}^{-1}$ Cd^{2+} solution (1 mL min^{-1}); or preloading with 50 mL of 20 $\mu\text{g mL}^{-1}$ Ni^{2+} solution (1 mL min^{-1}). Preloading with Cd^{2+} or Ni^{2+} before multi-metal introduction was done to determine if the column reaches an equilibrium state in spite of initially filling sites with a particular metal. At the end of the experiment, the metal bound to each column was determined by strip analysis using FAAS.

4.2.5.3. Determination of Conditional Stability Constants

Regularized regression analysis was used to determine conditional stability constants. The QUASI program²⁶ was used to perform calculations on the binding isotherms created from the single metal breakthrough curves. The breakthrough curve data were smoothed using Savitzky-Golay least squares smoothing routine with a 50 point window (Origin). While data was collected at 2.0 Hz, yielding ca. 4000 data points from start to breakthrough, that data was sampled in Excel to give 150-200 points for use in the QUASI program. A smoothness regularizing function was employed with a regularization parameter of 0.01. The borders for the spectral window of log K were set automatically. The log K grid spacing was set to 0.1 and an absolute weighting was used. A constant and a linear isotherm were allowed to account for strong and weak sites, respectively, outside the spectral window. Since large values of K can produce metal

concentrations in the effluent that are below detectability, the upper limit for log K were determined from S/N considerations and detection limit (3σ) for the particular metals studied using FAAS detection.

4.2.5.4. Oxidation Studies

A 1×10^{-3} mol L⁻¹ solution of o-iodosobenzoic acid in HEPES buffer at pH 7.0 and a 1% hydrogen peroxide solution were used to determine the effect of Cys oxidation on Cd²⁺ binding. For each of these studies, Cd²⁺ column capacity was determined before exposure to an oxidizer and after 10 min (at 2 mL min⁻¹) exposure to each oxidizing solution. DTT was used to return the columns to their reduced state as previously described.

4.2.5.5. Preconcentration and Recovery of Ni²⁺ and Cd²⁺ in artificial seawater

The first preconcentration experiments were done by loading the columns for 5.0 min (1.0 mL min⁻¹) with an artificial seawater solution containing 0.075 µg mL⁻¹ of Cd²⁺ and 0.30 µg mL⁻¹ of Ni²⁺. The seawater matrix contained 10,000 µg mL⁻¹ Na⁺, 1,250 µg mL⁻¹ Mg²⁺, 400 µg mL⁻¹ K⁺, and 400 µg mL⁻¹ Ca²⁺.⁶ After loading, each metal was stripped directly into the FAAS using 0.10 mol L⁻¹ HNO₃ at 1.0 mL min⁻¹. Standard solutions were prepared in 0.020 mol L⁻¹ of HEPES buffer for both metals, loaded on the column for 5.0 min (1 mL min⁻¹), and stripped directly into the FAAS using 0.1 mol L⁻¹ HNO₃. The standard solutions used were 0.05, 0.075, and 0.1 µg mL⁻¹ of Cd²⁺ and 0.20, 0.30 and 0.40 µg mL⁻¹ of Ni²⁺. The resulting transient signals from the samples and standards were collected and peak areas were used to calculate the analytical accuracy. Enrichment factors were determined by dividing the analyte concentration before preconcentrating by the analyte concentration after preconcentration. The analyte

concentration after preconcentration was calculated using the width of the transient signal that contained 90% of the sample area to determine the preconcentrated volume.

Since reproducible but inefficient binding could still produce a high degree of analytical accuracy, a recovery study was conducted. This involved passing the 50 mL of seawater solution containing $0.05 \mu\text{g mL}^{-1} \text{Cd}^{2+}$ and 100 mL of seawater solution containing $0.05 \mu\text{g mL}^{-1} \text{Ni}^{2+}$ through the columns at an influent rate of 1.0 mL min^{-1} and pH of 7. The metals were stripped off the columns into 5 mL volumetric flasks using $0.10 \text{ mol L}^{-1} \text{HNO}_3$. By comparing the mass collected in the strip with the mass passed through the column, the binding efficiency (or recovery) could be assessed. Independent experiments confirmed that any metal bound to the column could be removed using acid with 100% efficiency.

4.2.5.6. Efforts in Metal Templating using Disulfide Bonds

For templating experiments, the columns were initially loaded with a particular metal to half of the column capacity. This was done to minimize loading of the weaker binding sites and to leave most of the thiols available for cross-linking. Making a template for Cd^{2+} was not attempted due to a high affinity of the metal for the thiol cross-linking sites. The mild oxidant o-iodosobenzoic acid (1 mmol L^{-1} , pH 8.0 in HEPES buffer) was introduced at 2 mL min^{-1} for 10 min and used to oxidize the available thiol groups to disulfide cross-links. The column was then exposed to $0.10 \text{ mol L}^{-1} \text{HNO}_3$ to remove the metal and then rinsed with 0.02 mol L^{-1} HEPES buffer. A mixed metal solution of $40 \mu\text{g mL}^{-1} \text{Mg}^{2+}$, Ni^{2+} , and Cd^{2+} was used to characterize the peptides via FAAS.

4.3. RESULTS AND DISCUSSION

4.3.1. Peptide sequences examined

Six peptides each composed of seven residues (one Gly followed by various combinations of Cys and Asp residues to yield a total of seven residues) were chosen to look at metal capacity and selectivity changes as Cys residues are substituted for Asp residues in small peptide chains. All peptide sequences were synthesized with an initial Gly residue to ensure a complete reaction close to the resin surface and to provide some rotational movement of the finished peptide. While Cys and Asp are both potential cation binders, Cys has an affinity for soft metal acids. Unlike combinatorial studies where a possible 64 peptides could be created and monitored for metal uptake, six peptides were chosen to study extensively the quantitative metal binding preferences as subtle changes were made in the peptide.

The six peptides consisted of three homopeptides composed of only Gly, Cys and Asp along with three composite peptides consisting of primarily Asp residues with 1-2 Cys residues. Since the amino acid positioned near the free end of the peptide may have greater freedom of movement than those located closest to resin attachment, Cys positions in the peptide were chosen toward the end of the chain. This may foster more efficient redox reactions in the case of disulfide formation and improved metal binding participation. In addition to the six 7-mers, three peptides consisting of one initial Gly and one binding residue (Asp or Cys) were also synthesized for comparison. One selected peptide was also immobilized onto CPG to look at metal binding characteristics when using a substrate with different properties from TentaGel.

The immobilized amino acid sequences created are shown in Figure 4.2. The nomenclature used in Figure 1 is used throughout the text where T and CPG indicate the

support media TentaGel resin and controlled pore glass, respectively. The letters G, D, and C are used as per convention to represent Gly, Asp and Cys residues.

4.3.2. Peptide characterization

Four representative peptides (T_{G7} , $T_{GD_2CD_2C}$, T_{GC6} , and $CPG_{GD_2CD_2C}$) were evaluated for composition and purity. Each peptide on TentaGel was prepared in the same manner. Gly attachment is known to be an easy coupling while Cys residues are known for their coupling difficulty. Thus, the peptides examined were chosen based on their differing coupling behavior. The Edman degradation showed that all three peptides on TentaGel were of the correct sequence and calculated to be 93-95% pure (with error of 10% or less) using a cumulative repetitive yield analysis²⁷. A ninhydrin test performed on resins with the initial Fmoc-protected Gly attached ($T_{G(Fmoc)}$) indicated that $5 \pm 1\%$ of the TentaGel surface did not react. Since this peptide remained blocked at the N-terminus, only amines not associated with the Gly residues were observed. The TentaGel resins received from Novabiochem have 0.30 ± 0.03 mmol of amine functional groups per g of resin determined by Fmoc-alanine substitution and subsequent UV analysis of the cleaved Fmoc groups. Taking into consideration the ~5% surface that did not react and the ~7-5% of the peptides that had the improper sequence, the overall amount of desired peptide was calculated to be 0.27 ± 0.03 mmol of peptide/g of resin. This value is used to calculate metal to residue binding ratios for all TentaGel resins. Although small amounts of undesired peptides will also contribute to binding, the error in the loading capacities accounts for this discrepancy.

For a comparative study, one peptide was also synthesized on CPG ($CPG_{GD_2CD_2C}$) and analyzed. In contrast to this same sequence on TentaGel, Edman degradation analysis showed that only ~40% of peptide was the correct sequence on the CPG. Most of the error, however, occurred as a result of incomplete coupling of the final Cys residue

to the peptide as indicated by the Edman degradation analysis (not shown). Although CPG has been used as a substrate for peptide^{28,29} and oligonucleotide synthesis^{30,31}, fewer chemicals and time were needed to create a high purity peptide on the TentaGel media for use in continuous flow studies. The peptide loading capacity on CPG was estimated to be 0.10 ± 0.01 mmol of peptide/g of CPG by %C analysis and agrees with loading capacities of oligonucleotides on similar CPG³¹. By using the CPG surface area, the peptide coverage on CPG_{GD₂CD₂C} was calculated to be $6.6 (\pm 0.7) \times 10^{13}$ peptides/cm² which represents close to monolayer coverage³². The peptide loading on TentaGel was calculated to be 2.5 times more than that on CPG. Interestingly, McAlpine and Schreiber have shown that 40-60% of the loading capacity on TentaGel is located on the outer 5–10 μm rather than being uniformly distributed throughout the support as is the case for porous glass media such as CPG.³³

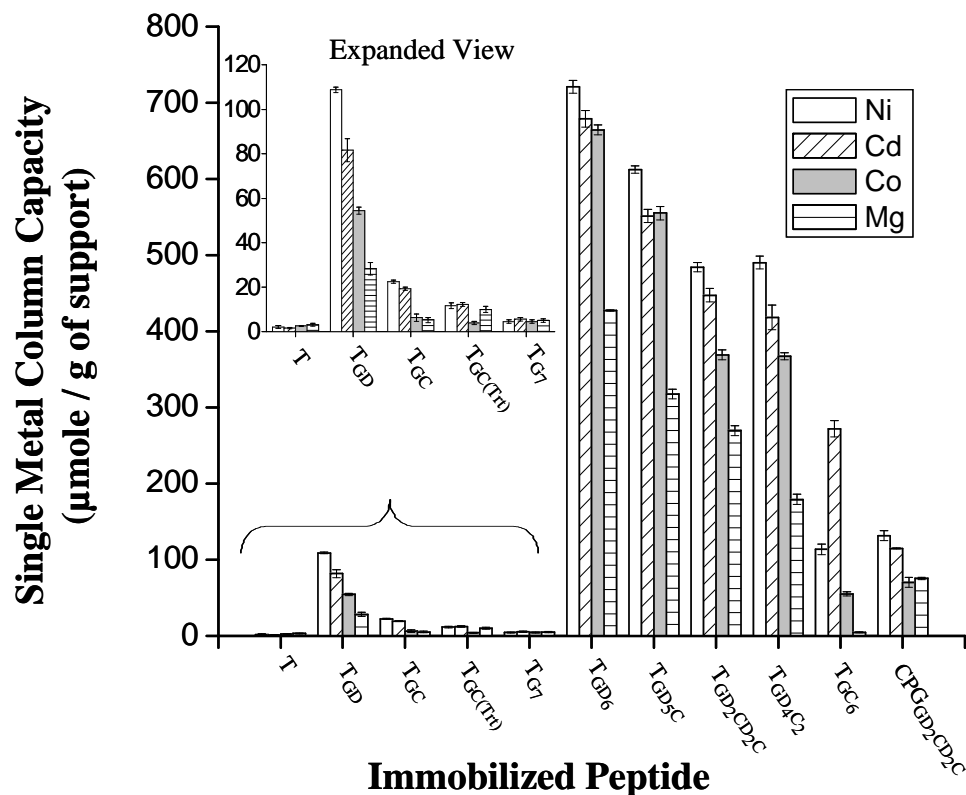


Figure 4.2. Single metal capacities of various peptides synthesized on TentaGel (T) resin and controlled pore glass (CPG). Peptide composition is denoted by G = Gly, D=Asp, C=Cys, and Trt = Trityl (thiol blocking group). Solutions containing $20 \mu\text{g mL}^{-1}$ of a metal in 0.02 mol L^{-1} HEPES buffer (pH 7) were passed through the columns until breakthrough was observed. Capacities reported are an average of both breakthrough ($n = 3$) and strip analysis ($n = 3$) values.

4.3.3. Single metal binding studies

The Ni^{2+} , Cd^{2+} , Co^{2+} and Mg^{2+} single metal capacities were determined for all peptide sequences using both breakthrough curve and strip analysis (Figure 4.2). The

TentaGel resin shows negligible binding for all of the metals tested. T_{G7} also showed minimal metal binding as glycine does not possess charged side groups and the peptide backbone apparently provides minimal binding sites in this system. This indicates that any significant metal binding by the peptides is primarily a result of charged side groups on the amino acids. Metal to residue binding ratios calculated in this study will not include the initial Gly residue due to the low metal binding capacities relative to the other residues.

With an active amino acid bound to Gly (T_{GD}, T_{GC}, and T_{GC(Trt)}), increased metal binding was observed. T_{GD} displays the highest metal binding for these two residue peptides, especially for Ni²⁺ and Cd²⁺ where the metal to Asp residue ratios are ~1:3. The metal binding trend agrees with that reported by Gulumian et al. for negative oxygen donors, such as carboxylates, in biological systems and with previous work done with immobilized Asp and Glu^{9,10,34}. T_{GC} showed greater metal preferences than T_{GD} for Ni²⁺ compared to Co²⁺ and Cd²⁺ compared to Co²⁺ and Mg²⁺. Trt blocking of the thiols, T_{GC(Trt)}, further decreased the capacity for all metals except Mg²⁺. Although the thiol groups are blocked by the Trt group, there is still appreciable binding of most metals over that of the all glycine peptide. Metal binding likely results from metal interactions with the lone pairs on sulfur atoms. An increase in Mg²⁺ binding with the Trt group may be due to interactions with delocalized pi electrons from the three benzene rings that compose the Trt group. The metal binding selectivity of T_{GC} follows trends seen in previous work evaluating PLCys⁶⁻⁸.

The remaining seven-residue peptides on TentaGel showed the expected improvement in capacities but also exhibited some unusual metal binding trends. Interestingly, columns containing only Asp and both Asp and Cys maintained a metal to Asp binding of 1:(2.2 ± 0.2) and 1:(2.5 ± 0.3) for Ni²⁺ and Cd²⁺. These ratios are also

consistent with that seen for the 2-residue peptide T_{GD} of $1:(2.5 \pm 0.3)$ and $1:(3.3 \pm 0.4)$ for Ni^{2+} and Cd^{2+} . This suggests that peptides composed of seven amino acids do not “wrap” around the metals they bind, as suggested for the longer biohomopolymers¹² that consist of 50-80 amino acid residues. Rather, the 7-mer peptides behave more like immobilized single amino acids in that they possess metal to residue binding ratios of $1:(2-3)$.³⁵⁻³⁸

Co^{2+} and Mg^{2+} capacities jump disproportionately as the peptides increase from two residues to seven residues. For example, the Co^{2+} to Asp ratio is $1:(5 \pm 0.6)$ for T_{GD} , yet it increases to $1:(2.7 \pm 0.6)$ for all seven residue peptides containing Asp. Dramatic changes are seen with Mg^{2+} where T_{GD} , $T_{GD_2CD_2C}$, $T_{GD_4C_2}$, T_{GD_5C} , and T_{GD_6} have metal to Asp ratios of $1:(10 \pm 1)$, (6 ± 1) , (4.0 ± 0.5) , (4.3 ± 0.5) and (3.8 ± 0.4) . The orientation of carboxylate groups for Co^{2+} and Mg^{2+} binding may be more easily optimized with longer peptide chains containing Asp, thus enhancing the likelihood of interchain binding. Cys groups in the composite peptides also contribute to some binding. Although T_{GD_6} has the largest capacity for any given metal, T_{GD} , which possesses five fewer Asp residues, shows more differentiation in binding capacities in the single metal studies. The longer seven residue peptides may enable weaker binding sites to form that are not created with the two residue peptides.

Overall metal capacities decrease as Asp residues are replaced with Cys residues as shown in Figure 4.2 for T_{GD_6} , T_{GD_5C} , $T_{GD_2CD_2C}$, $T_{GD_4C_2}$ and T_{GC_6} . All metals tested have binding affinity towards carboxylates, thus as less Asp residues compose the peptide certain binding sites are lost. The addition of 1-2 Cys residues, however, does not greatly affect the comparison of the different metals bound in single metal experiments. $T_{GD_2CD_2C}$ and $T_{GD_4C_2}$ appear to have similar binding capacities for Ni^{2+} , Cd^{2+} and Co^{2+} ; however, the Mg^{2+} capacity decreases when two Cys are positioned together at the end of

the peptide, viz., T_{GD4C2}. It seems evident that some Mg²⁺ binding sites are disrupted by this small change in sequence. A large decrease in Mg²⁺ binding is also seen with T_{GC6} along with a large shift in metal capacity values to Cd²⁺ over Ni²⁺ and Co²⁺. Although capacities for all metals generally decrease with the increasing number of Cys residues substituted in the peptide, it seems as though the improved selectivity for Cd²⁺ with T_{GC6} is a result of an increase in Cd²⁺ binding by the thiols and not a disproportionately larger drop in capacities for the other metals. The Cd²⁺ to Cys ratio is 1:(5.7 ± 0.7). This increase in Cd²⁺ single metal capacity is only evident with six consecutive Cys residues, not with the peptides tested possessing only one or two Cys. Previous work with PLCys also shows a binding preference of Cd²⁺ over Ni²⁺ and Co²⁺ due to the thiol groups affinity for Cd²⁺.^{6,13,39}

Although T_{GD6} binds the greatest amount of each metal tested, T_{GC6} shows more differences in metal binding capacities. For example, T_{GC6} has more than twice the overall sites for Cd²⁺ than for any of the other metals tested. Mg²⁺ binding is only 10% of the next lowest binding Co²⁺. Both hard and soft metal acids are often able to bind to hard bases, while soft bases usually show larger preferences towards soft metal acids.²³

Peptides terminating in a Cys residue also displayed an intense color change from the off-white color of the resin to a burgundy color when exposed to Ni²⁺ or Co²⁺ solutions. In the case of Ni²⁺, the metal was easily released with acid and returned to an off-white color. In the case of Co²⁺, most of the metal was released with acid, yet a small amount stayed on the column as indicated by the persistence of the burgundy color of the resins. Similar color changes have been seen with Ni²⁺ and Co²⁺ when complexed to Cys in solution.⁴⁰⁻⁴³ On the other hand, T_{GC(Trt)} did not produce a color change when the Ni²⁺ and Co²⁺ solutions were tested since the thiol functionality was blocked, indicating the color was produced through coordination with amine and thiol groups^{40,41,43,44}. Color

changes pertaining to PLCys immobilized to CPG have not been reported as the biohomopolymer is attached through the amine terminus leaving the carboxylate at the terminal end.

A combination of thiol and amine coordination from 2-3 Cys residues plus the presence of oxygen has been shown to oxidize Co^{2+} to Co^{3+} and create a burgundy colored complex.^{40,41,44} In our studies, the Co - Cys complex was not easily released with acidic solutions or chelating ligands such as EDTA. Most of the burgundy color, however, disappeared by passing a reducing solution of $0.2 \text{ mol L}^{-1} \text{ SnCl}_2$ through the column for 30 min (2 mL min^{-1}) indicating the Co^{3+} was being reduced. For future studies, peptide chains terminating in Cys should be avoided in order to sustain rapid metal release, allow disulfide formation and ensure full use of binding sites.

One sequence, $\text{GD}_2\text{CD}_2\text{C}$, was synthesized on both TentaGel resin and CPG. Metal capacities for these two supports were compared to determine if the support impacts complexation or metal capacities. Overall capacities on CPG are lower because the loading capacity is lower. The metal binding preferences and metal to residue ratios for $\text{GD}_2\text{CD}_2\text{C}$ are similar on both support media within error, and the small differences were possibly due to dissimilar immobilization chemistries, purity and/or support composition. The metal to residue ratios of Ni^{2+} and Cd^{2+} for $\text{CPG}_{\text{GD}_2\text{CD}_2\text{C}}$ are $1:(4.6 \pm 0.5)$ and $1:(5.3 \pm 0.5)$, and the ratios for $\text{T}_{\text{GD}_2\text{CD}_2\text{C}}$ are $1:(3.2 \pm 0.4)$ and $1:(3.5 \pm 0.4)$. The Co^{2+} to residue ratio on $\text{CPG}_{\text{GD}_2\text{CD}_2\text{C}}$ and $\text{T}_{\text{GD}_2\text{CD}_2\text{C}}$ are $1:(9 \pm 1)$ and $1:(4.2 \pm 0.5)$, and the Mg^{2+} to residue ratio on $\text{CPG}_{\text{GD}_2\text{CD}_2\text{C}}$ and $\text{T}_{\text{GD}_2\text{CD}_2\text{C}}$ are $1:(8 \pm 1)$ and $1:(5.8 \pm 0.7)$. The lower metal to residue values for CPG could also be a result of poor solution mass transfer and an inability to reach values close to equilibrium values as suggested by Jurbergs and Holcombe⁸.

In comparing the short peptide on CPG with longer (ca. 50 residues) homopolymers previously studied⁸⁻¹¹, one readily sees a marked improvement in metal to residue ratios for the shorter peptides. Malachowski and Holcombe have shown that Ni^{2+} to residue ratios for PLAsp and PLGlu of 1:156 and 1:159, respectively.¹⁰ In contrast, the shorter chain peptide analog of PLAsp, T_{GD_6} , has a metal to residue ratio of 1:2. This is a 50 fold increase in residue use for binding and a nearly 10 fold increase in the number of metals bound per chain. The Cd^{2+} to residue ratios for PLCys was shown to be $\sim 1:20^8$, while T_{GC_6} has a ratio of $\sim 1:6$. This indicates that the enhanced capacity values are not just a result of using a higher loading capacity resin.

In comparing the short peptides on TentaGel with the homopolymers on CPG, some differences should be noted. The length of the immobilized homopolymers have been shown to “shorten” with the introduction of metal ions indicating the formation of a three dimensional coordinating matrix.¹² The introduction of an acid caused additional shrinkage, which indicated the formation of a tight random coil that spoiled binding cavities and promoted easy release of bound metals due to a proton-induced tertiary structure change of the polymer. In the case of the small peptides (7 residues), most residues are participating in metal binding and protonation of the side chains could only occur if protons competitively displace the metal. Thus, it seems less likely that there will be significant tertiary structure changes in comparison to that seen for the larger homopolymers.

Although minimal tertiary structure changes are expected with the short 7-mer peptides, transient signals showing the release of Cd^{2+} from $\text{CPG}_{\text{GD}_2\text{CD}_2\text{C}}$ and $\text{T}_{\text{GD}_2\text{CD}_2\text{C}}$ indicate rapid release of the metal. Cd^{2+} was stripped from the 7-mers with the introduction of $0.1 \text{ mol L}^{-1} \text{ HNO}_3$ at 1 mL min^{-1} to give a $\sim 6 \text{ s}$ peak (width at half maximum) shown in Figure 4.3, which is comparable to the Cd^{2+} strip profile of the

biohomopolymer Poly-L-Cys on CPG⁶. Although biohomopolymers immobilized onto CPG have been shown to reach equilibrium *for binding* under mass transport limitations at typical flow rates of 1 mL min⁻¹⁸, the acid strip profiles are similar to the 7-mer peptides on both TentaGel and CPG. One explanation for this is that the proton concentration during the stripping process is in large excess and with the proton diffusion rate ten times that of the metals studied, solution mass transfer and lack of tertiary structure change may not limit the speed of metal release in the systems investigated.

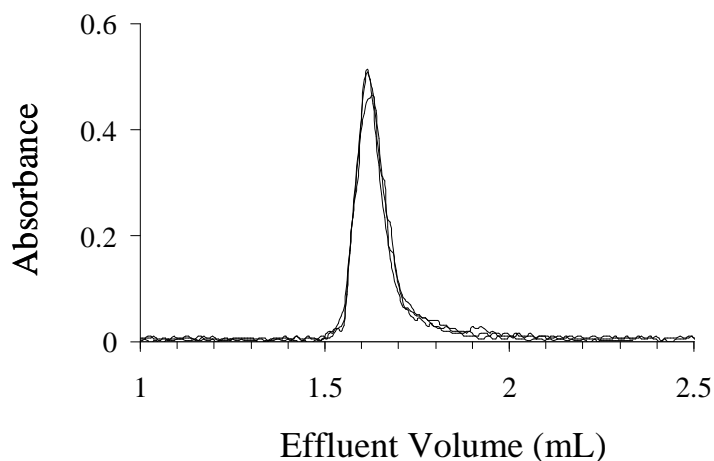


Figure 4.3. Cd stripped off T_{GD₂CD₂C}, CPG_{GD₂CD₂C}, and CPGPolyCys into AAS. The metal was loaded on the peptide using 15 mL of a 250 ppb Cd solution, rinsed for 1 min with 0.02 mol L⁻¹ Hepes buffer, and stripped into the spectrometer with a 0.1 mol L⁻¹ solution of nitric acid.

4.3.4. Selected, multi-metal binding studies

A select group of metals (Ni^{2+} , Cd^{2+} , Co^{2+} , and Mg^{2+}) were combined in a single solution to evaluate competitive metal binding for the 7-mer peptides. The capacity results are presented in Table 4.1. The metal selectivities of T_{GD6} , T_{GD5C} , T_{GD4C2} , and $\text{T}_{\text{GD2CD2C}}$ for the multi-metal studies (Figure 4.4) are more noticeable than one would predict from capacity results for the single metal studies. Co^{2+} and Mg^{2+} do not appear to compete as well for sites in the presence of Ni^{2+} and Cd^{2+} .

Table 4.1. Multi-metal binding capacities (μmole of metal / g of resin) of various peptide sequences on TentaGel resin^a

Peptide sequence	Ni^{2+}			Co^{2+}			Cd^{2+}			Mg^{2+}			Total
T_{GD6}	207	\pm	5	75	\pm	3	254	\pm	6	53	\pm	8	590 \pm 10
T_{GD5C}	200	\pm	10	71	\pm	6	250	\pm	20	57	\pm	5	580 \pm 10
T_{GD4C2}	153	\pm	10	77	\pm	4	291	\pm	7	56	\pm	4	580 \pm 20
$\text{T}_{\text{GD2CD2C}}$	137	\pm	6	72	\pm	2	199	\pm	10	70	\pm	20	470 \pm 20
T_{GC6}	57	\pm	4	26	\pm	4	111	\pm	2	<1			195 \pm 6

^aAll measurements were made in triplicate. Multi-metal solutions ($20 \mu\text{g mL}^{-1}$ Ni^{2+} , Co^{2+} , Cd^{2+} , and Mg^{2+} at pH 7) were passed through the column at 2 mL min^{-1} . T=TentaGel resin, G=glycine, D=aspartic acid, and C=cysteine.

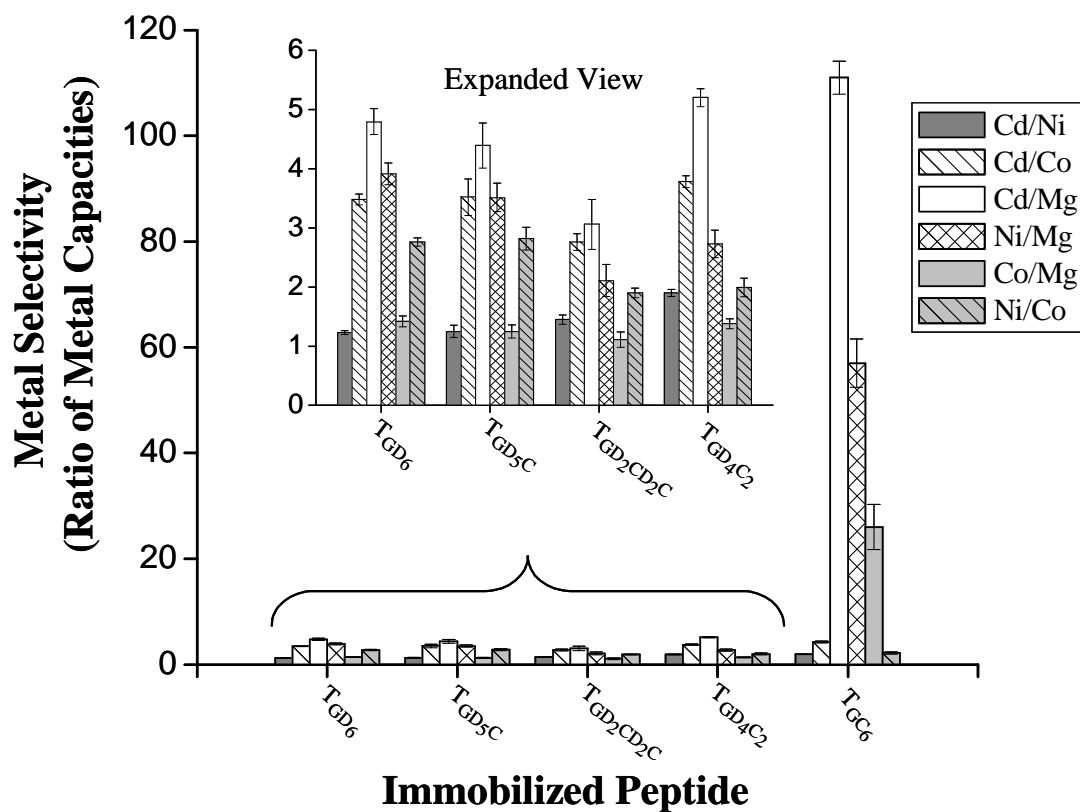


Figure 4.4. Ratios of metal capacities from multi-metal experiments of four select peptides. Peptide composition is denoted by G = Gly, D=Asp and C=Cys. A solution containing 20 $\mu\text{g mL}^{-1}$ of Ni^{2+} , Cd^{2+} , Co^{2+} , and Mg^{2+} in 0.02 mol L⁻¹ HEPES buffer (pH 7) was run until breakthrough of each metal was observed via AAS. Capacities reported are from strip analysis only.

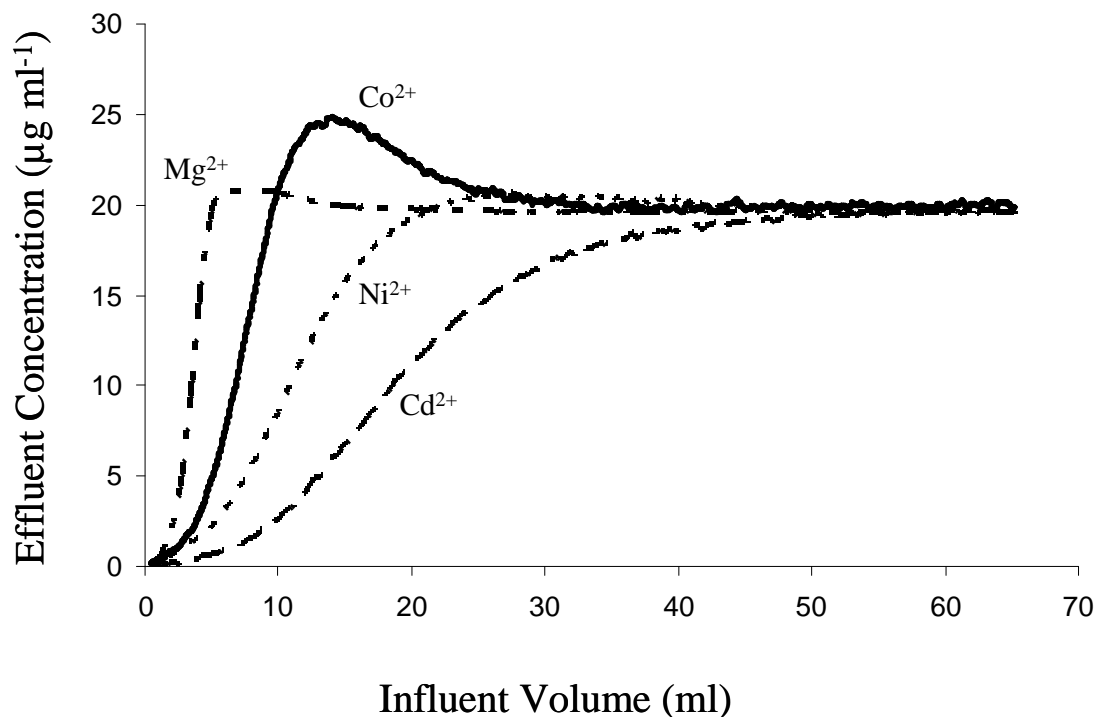


Figure 4.5. T_{GD6} breakthrough analysis of Co^{2+} , Cd^{2+} , Mg^{2+} , and Ni^{2+} overlaid. Each metal was monitored separately via FIA-FAAS while a multi-metal solution ($20 \mu g mL^{-1}$ in all metals) was passed through the column.

Figure 4.5. shows the breakthrough curves for the multi-metal solution for T_{GD6} . Small rises in effluent concentration *above* the $20 \mu g mL^{-1}$ influent concentration are seen for Mg^{2+} , Co^{2+} and to a small extent, Ni^{2+} , indicating a displacement of metals from sites by other metals. These metals are competing for either the same sites or functional groups that compose the site. Similar competitive binding behavior has also been observed with polyamino acids attached to microfiltration membranes.⁴⁵ All resin types tested show similar trends except for TGC_6 which showed no effluent concentration over $20 \mu g mL^{-1}$ (not shown). In the single metal studies, all binding sites are occupied by one metal and the set of binding equilibrium is held constant as long as cooperative binding is

not a factor, while in the multi-metal solutions metals are competing for sites or parts of sites. As more metals are bound to the resin material, the equilibrium will constantly change if metals compete for sites or functionalities composing various sites and predicting these systems can be quite difficult. Thus, it is not surprising that the total moles of metals bound from the multi-metal experiments differ from the single metal experiments. It is interesting to note, however, that the total moles of metal bound in the multi-metal studies are less than the moles bound for the metal with the highest capacity in the single metal studies. One exception is T_{GD4C2} which binds 15% more mixed metals when compared the highest single metal capacity. This increase is mainly due to Cd²⁺ binding which will be discussed further. These results suggest that metals in a single metal solution in the absence of other metals will bind to all sites possible from very strong to very weak. In the presence of competing metals, the single metal species will compete for all the sites, but bind to the strongest sites for that metal. For T_{GD6}, Cd²⁺ seems to have the largest stability constant due to the consistency of binding as other metals tested are pushed off the column. Strong sites for each metal may be different depending on size, coordination number and affinity.⁴⁶

Although small capacity differences in Ni²⁺, Co²⁺ and Cd²⁺ binding to T_{GD6}, T_{GD5C}, T_{GD2CD2C} and T_{GD4C2} were observed for the single metal binding studies, preferences in binding can be easily seen with the multi-metal solutions, thus reflecting the relative binding strength and competition for sites. Interestingly, the respective single and multi-metal binding trends for T_{GD6} were Ni²⁺ ≥ Cd²⁺ ≥ Co²⁺ > Mg²⁺ and Cd²⁺ > Ni²⁺ > Co²⁺ > Mg²⁺. Although all seven residue peptides, excluding T_{GC6}, bind more Ni²⁺ in the single metal studies, peptides with two Cys residues display large Cd²⁺ selectivities using the multi-metal solutions. On the other hand, Cd²⁺ retains its dominance on the T_{GC6} column with Cd²⁺/Ni²⁺ and Cd²⁺/Co²⁺ metal binding ratios of 2 and 4.

As denoted in Table 4.1, T_{GD4C2} exhibits nearly 50% more Cd²⁺ capacity than T_{GD2CD2C} simply as a consequence of shifting one Cys up two positions in the peptide. Cd²⁺ typically will bind to more than one Cys, thus two Cys residues together may create more binding sites for Cd.⁴⁷ This suggests that minor modifications in primary and secondary structure of short peptides may easily provide significant selectivity changes. Ni²⁺ does not seem to be influenced by the Cys shift, thus Asp is primarily responsible for Ni²⁺ capacity in these two resins. The generally accepted soft acid metal preference for thiols would suggest that T_{GC6} might exhibit significantly enhanced Cd²⁺/Ni²⁺ ratios. However, T_{GD4C2} possesses the same Cd²⁺/Ni²⁺ selectivity as T_{GC6}, yet with even greater Cd²⁺ binding capacity. Thiol functionalities of Cys residues can hydrogen bond to neighboring Asp residues, rendering the thiol groups more nucleophilic and ready to bind.⁴⁷ In addition, at pH 7 many of the thiols pertaining to T_{GC6} remain protonated (pKa ~8)⁴⁸ while those of T_{GD4C2} may be more prone to deprotonation as described above. Although similar in selectivities, the metal to residue binding ratios are higher with T_{GD4C2} than the previously explored systems using PLCys.^{6,8} T_{GC6} may be more beneficial in some instances where a large selectivity against Mg²⁺ is desired.

The multi-metal solutions were also run overnight through T_{GD6} to verify that equilibrium was reached after breakthrough (ca. 40 min), which had not been the case for earlier studies with PLCys on CPG where capacities could double with >16 h of exposure to a fixed concentration influent solution.^{6,8} This was probably as a result of slow mass transport in the CPG and not as a consequence of binding kinetics. For T_{GD6}, metal capacities for Ni²⁺, Cd²⁺ and Co²⁺ are <10% larger for

Table 4.2. Metal capacities ($\mu\text{mole of metal} / \text{g of T}_{\text{GD}_6}$) using 500 mL of multi-metal solutions flowing at 1 mL/min (i.e., ca 8 h)^a

Metal	No preloading			Cd^{2+} preloading ^b			Ni^{2+} preloading ^c		
Ni^{2+}	230	\pm	20	230	\pm	10	218	\pm	8
Cd^{2+}	274	\pm	6	283	\pm	9	282	\pm	1
Co^{2+}	105	\pm	5	100	\pm	20	110	\pm	20
Mg^{2+}	51	\pm	3	53	\pm	8	55	\pm	1

^a Metal solutions each 500 mL were passed through the column at 1 mL min⁻¹. Measurements were made in duplicate.

^b Column was preloaded with 50 mL of 20 $\mu\text{g mL}^{-1}$ Cd^{2+} in 0.02 M HEPES (pH 7) (1 mL min⁻¹).

^c Column was preloaded with 50 mL of 20 $\mu\text{g mL}^{-1}$ Ni^{2+} in 0.02 M HEPES (pH 7) (1 mL min⁻¹).

the 8 h (Table 4.2) when compared to 40 min runs (Table 4.1). Co^{2+} achieves equilibrium at a slower rate with a 30% increase in metal capacity when run for 8h. Overall, results indicate good mass transfer within the resin as well as fast binding kinetics. The ability to rapidly attain equilibrium is also supported by preloading the column with Cd^{2+} or Ni^{2+} prior to exposure to the multi-metal solution. This consistently resulted in the same binding capacities as the experiment run without preloading. This further suggests that in spite of filling “sites” with a given metal, a second metal can move freely into the resin and readily establish equilibrium conditions within the microenvironment.

4.3.5. Determination of Conditional Stability Constants

Conditional stability constants were determined for the highest capacity column, T_{GD6} and are shown in Table 4.3. In comparing the conditional stability constants and metal capacities from both the single metal and multi-metal experiments, an understanding of the binding sites may be obtained. Each “site” may represent a different number of ligands and/or a variety of coordination geometries, depending on the metal. Consequently, it’s not unexpected that the capacities and number of sites may vary with the metal cation under study.

The Cd²⁺ binding site density for the two strong sites approximately equals the experimentally determined Cd²⁺ capacity, thus indicating that most sites are occupied. The dominance of Cd²⁺ binding in the multi-metal study suggests that it dominates over the other metals, in spite of Ni²⁺ and Co²⁺ also exhibiting a significant number of strong binding sites.

Ni²⁺ has two sites at log K of 3.6 and ≥4.8, but also has site/sites that are very weak (log K < 1.1). Because only 469 μmol of sites/g of TentaGel resin is accounted for in the stronger sites, the weak sites bind 252 μmol of metal/g of TentaGel resin at this loading concentration. It appears that only the strongest sites are competitive in the multi-metal binding studies since 70% of the capacity is lost. .

The single-metal studies in Table 4.3 suggests that Co²⁺ and Mg²⁺ have a significant number of strong sites (i.e., log K values that exceed the upper limit imposed by the detection capabilities of the FAAS). However, neither is competitive in the mixed-metal study where Co²⁺ and Mg²⁺ lose 90% and 88%, respectively, of their capacities when forced to compete with Cd²⁺ and Ni²⁺.

These data point out the difficulty in predicting behavior of systems where the binding “site” takes on varying definitions depending on the ion being chelated. It

Table 4.3. Conditional stability constants and site density ($\mu\text{mole/g}$ of resin) of T_{GD_6} with four metals^a

Cd^{2+}		Ni^{2+}		Co^{2+}		Mg^{2+}	
<u>Log</u> <u>K</u>	<u>Site</u> <u>density</u>	<u>Log</u> <u>K</u>	<u>Site</u> <u>density</u> ^c	<u>Log</u> <u>K</u>	<u>Site</u> <u>density</u>	<u>Log</u> <u>K</u>	<u>Site</u> <u>density</u> ^c
4.6	396	>1.1	+ ^b	2.8	317	<1.5	+ ^b
≥ 5.5	315	3.6	173	≥ 4.7	629	3.6	173
		≥ 4.8	296			≥ 4.8	291

^aValues were calculated from binding isotherms using the QUASI program.

^bWeak sites determined by using a linear isotherm parameter could not be quantified.

^cThe total amount of Ni^{2+} and Mg^{2+} bound to T_{GD_6} is $720 \pm 9 \mu\text{mole/g}$ of resin and $427 \pm 1 \mu\text{mole/g}$ of resin.

disallows the accurate use of measured equilibrium constants and site densities in forecasting chelator behavior when competing species are in the same solution. This is in distinct contrast to, for example, a single entity chelator such as a EDTA or crown ether, where a “site” and the binding stoichiometry are relatively well defined and the same for a large number of competing cations.

4.3.6. Effects of Cysteine oxidation

The thiol groups of Cys residues can undergo oxidation to disulfides or higher oxidation states depending on spatial positioning of thiols, pH, concentration of reagents, and relative oxidation and reduction potentials.⁴⁷ Columns were treated with $1 \times 10^{-3} \text{ mol L}^{-1}$ o-iodobenzoic acid, a mild thiol-specific oxidizing agent, and 1% hydrogen peroxide, a stronger and less specific oxidizing agent. It is expected that as the thiols are oxidized to disulfides, there will be fewer sites for the metals to bind. Also, the length of the

chains, Cys positions and peptide surface density may have a large effect on oxidation kinetics.

The effect of using oxidizing agents on the peptides was determined by monitoring Cd^{2+} binding (Table 4.4). As expected, the Cd^{2+} capacity of T_{GD_6} did not change when treated with either oxidizer since it did not contain any thiols. $\text{T}_{\text{GD}_5\text{C}}$ did show a 5% and 7% decrease in capacity with o-iodosobenzoic acid and hydrogen peroxide, respectively. $\text{T}_{\text{GD}_2\text{CD}_2\text{C}}$ showed a 3% and 8% decrease in capacity with o-iodosobenzoic acid and hydrogen peroxide, respectively. The small drops in Cd^{2+} capacity suggests that most of the capacity is determined by the Asp residues in these peptides. $\text{T}_{\text{GD}_4\text{C}_2}$ showed a 5% decrease in capacity with o-iodobenzoic acid, but a 17% decrease with hydrogen peroxide. Cd^{2+} capacity is decreased by a greater extent due to

Table 4.4. Cadmium capacity (μmole of Cd / g of resin) on immobilized peptides treated with oxidizing agents^a

Peptide sequence ^b	No treatment			o-iodobenzoic acid ^c			Hydrogen peroxide ^d		
T_{GD_6}	690	±	10	700	±	10	690	±	10
$\text{T}_{\text{GD}_5\text{C}}$	551	±	8	524	±	3	513	±	5
$\text{T}_{\text{GD}_2\text{CD}_2\text{C}}$	439	±	6	423	±	1	398	±	6
$\text{T}_{\text{GD}_4\text{C}_2}$	420	±	20	396	±	7	349	±	8
T_{GC_6}	280	±	20	250	±	10	147	±	2

^aAll measurements were made in triplicate. The capacity values were determined from strip analysis.

^bT=TentaGel resin, G=glycine, D=aspartic acid, and C=cysteine

^c1 mmol L⁻¹ of o-iodosobenzoic acid passed through column at 2 mL min⁻¹ for 10 min.

^d1% hydrogen peroxide passed through column at 2 mL min⁻¹ for 10 min

sites lost where the two Cys are positioned adjacent to each other. Most of the capacity was returned (i.e., $97 \pm 10\%$) with 50 mL of 0.02 mol L^{-1} DTT (pH 8).

As expected, the peptide composed of all Cys, T_{GC6}, showed the greatest capacity decrease: a 13% capacity loss with o-iodosobenzoic acid and a 47% loss when oxidized with hydrogen peroxide. After reduction with DTT, the column capacity returned $94 \pm 7\%$ after o-iodosobenzoic acid and $83 \pm 7\%$ after H₂O₂ exposure. Previous studies with PLCys showed Cd²⁺ binding decrease by 50% when exposed to 1% hydrogen peroxide, however, total capacity returned when exposed to DTT.⁷

Along with the loss in capacity, the disappearance of the burgundy colored complex was also observed when Ni²⁺ and Co²⁺ were bound to the oxidized material and the color returned after reduction with DTT. Because color production is most likely due to the terminal Cys, this indicates that most of the terminal Cys groups are involved in disulfide formation and color formation. If the peroxide oxidized some of the thiols to sulfenites and sulfonates, these highly oxidized forms of sulfur may also take part in metal binding.⁴⁷ These current experiments indicate that short peptides containing few Cys may undergo redox reactions but do not impact the binding character of the other residues on the chain. This may be advantageous if one were to attempt to lock in a tertiary structure change by, for example, disulfide formation to improve selectivity.

4.3.7. Preconcentration of Ni²⁺ and Cd²⁺ in artificial seawater: Accuracy and recovery

While these materials could be considered for remediation, the columns could also be employed in analyte preconcentration schemes. As noted previously, reproducible but inefficient binding could still produce a high degree of analytical accuracy. Thus, in addition to determining the utility of some of these materials for

analytical preconcentration, from seawater, the binding efficiency (*viz.*, recovery) for Ni and Cd were also determined for this matrix.

Cd²⁺ and Ni²⁺ in artificial seawater were studied using T_{GD6}, T_{GD4C2}, and T_{GC6} and the results are shown in Table 4.5. As can be seen the analytical accuracies were all within the uncertainties associated with the procedure with the exception of Ni²⁺ for the Cys laden chain (T_{GC6}). The analytical error and poor recovery for Ni²⁺ on this column are not surprising since the thiols do not have a strong propensity for Ni²⁺. With the

Table 4.5. Analytical accuracy and analyte recovery when preconcentrating Ni²⁺ and Cd²⁺ from artificial seawater^a

Peptide Sequence ^b	Ni ²⁺		
	Actual conc. (μg mL ⁻¹)	Determined conc. (μg mL ⁻¹)	Recovery(%) ^c
T _{GD6}	0.30	0.30 ± 0.02	100 ± 20%
T _{GD4C2}	0.30	0.29 ± 0.02	110 ± 10%
T _{GC6}	0.30	0.23 ± 0.02	69 ± 1%
Peptide Sequence ^b	Cd ²⁺		
	Actual conc. (μg mL ⁻¹)	Determined conc. (μg mL ⁻¹)	Recovery(%) ^d
T _{GD6}	0.075	0.072 ± 0.009	95 ± 5%
T _{GD4C2}	0.075	0.073 ± 0.002	109 ± 9%
T _{GC6}	0.075	0.076 ± 0.005	110 ± 10%

^aSingle metal solutions at pH 7 were passed through the column at 1 mL min⁻¹. Measurements were made in triplicate.

^bT=TentaGel resin, G=glycine, D=aspartic acid, and C=cysteine.

^cA 100 mL 0.05 μg mL⁻¹ Ni²⁺ solution in artificial seawater was used.

^dA 50 mL 0.05 μg mL⁻¹ Cd²⁺ solution in artificial seawater was used.

exception of Ni^{2+} on T_{GC6} , the data suggests both efficient preconcentration and calibration capabilities without matching the matrix in standard preparation.

For the loading volume of 5 mL, an enrichment factor of ca. 25 was found for both Cd^{2+} and Ni^{2+} . The peak base width at 90% area of the stripped peak was 12 ± 2 s (ca. 0.2 mL) in both cases. Interesting, the inherent broadening of the signal due to dispersion in the FIA system and mixing in the FAAS mixing chamber of the burner produces a rise time of ca. 20 s (Figure 4.6) and may be the primary contributor to the width of the detected signal.

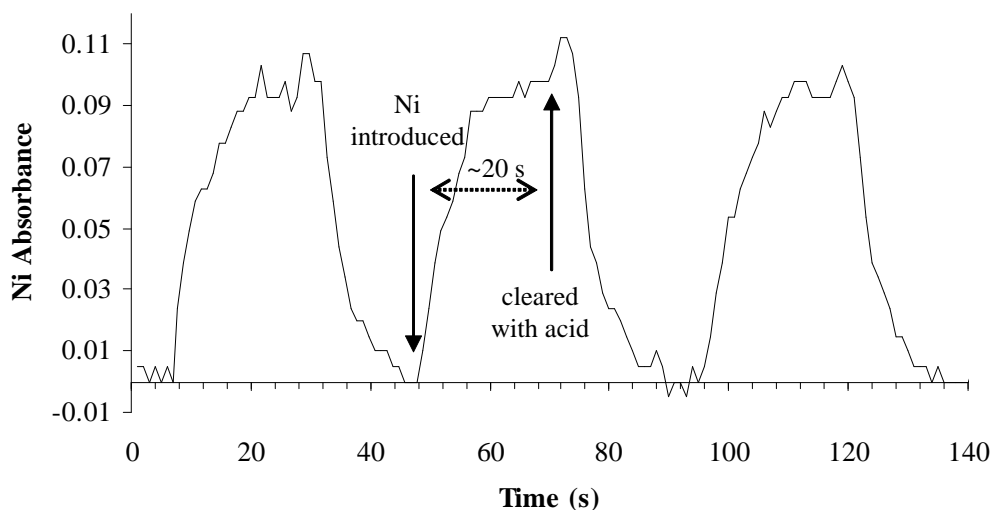


Figure 4.6. Signal broadening due to dispersion in the FIA system and mixing in the FAAS mixing chamber. Ni absorbance after a $20 \mu\text{g mL}^{-1}$ Ni^{2+} solution was aspirated into the instrument via a peristaltic pump and then cleared using $0.1 \text{ mol L}^{-1} \text{HNO}_3$. This process was repeated 3X.

4.3.8. Efforts in Metal Templating using Disulfide Bonds

Cross-linking of the peptides using a mild oxidizing agent, *o*-iodosobenzoic acid, was used to template for both Mg^{2+} and Ni^{2+} . Co^{2+} was not used in this study due to the strong red complex formed on these peptides and Cd^{2+} was not used in this study due to its strong affinity for the thiol cross-linking moieties. Figure 4.7 shows the method used for cross-linking.

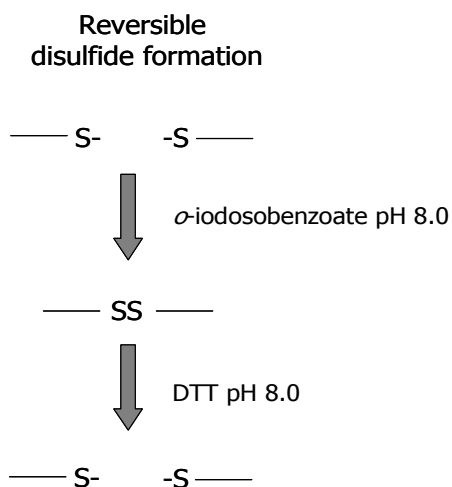


Figure 4.7. Pictorial representation of the reversible cross-linking procedure.

Three of the composite peptides were used for metal binding. Previous attempts to template using PLCys⁴⁹ were unsuccessful likely due to disulfide exchanges that can occur with many cysteine residues in close proximity.

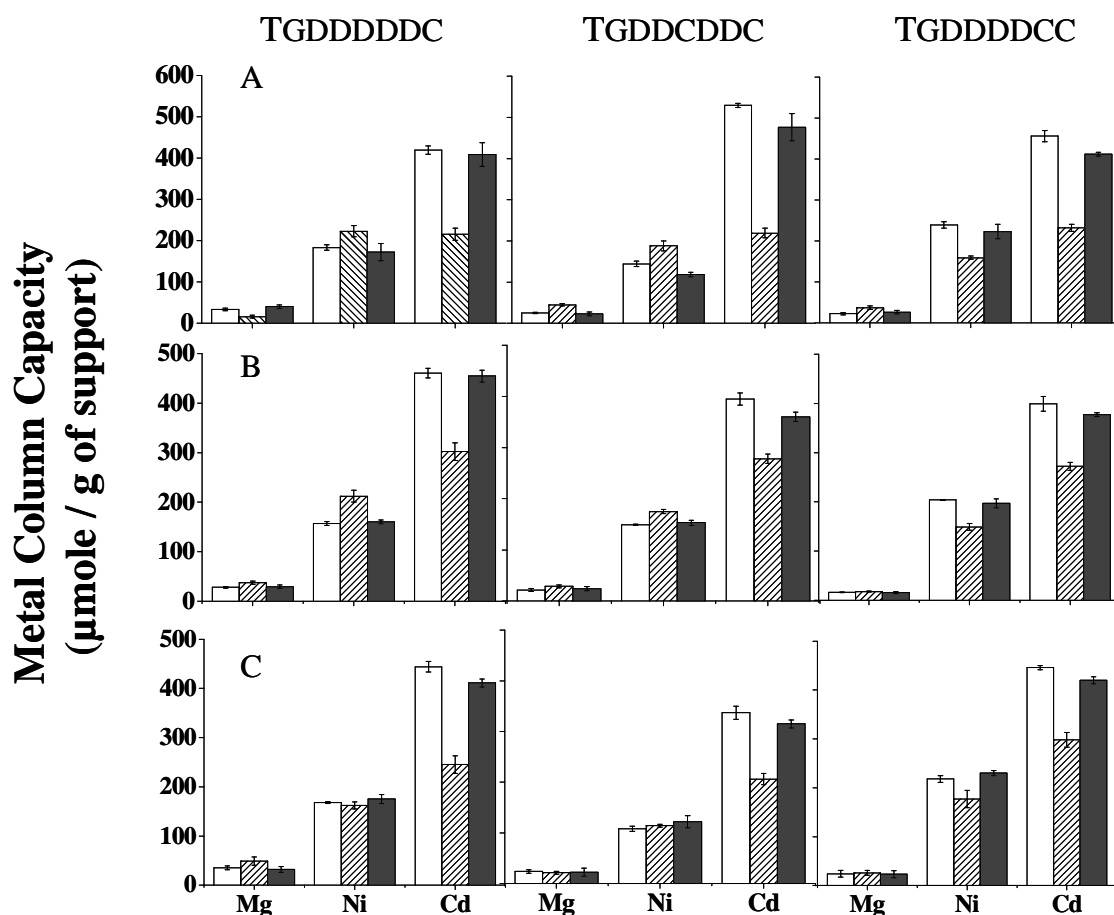


Figure 4.8. Metal capacities of T_{GD5C}, T_{GD2CD2C}, and T_{GD4C2} after exposure to templating conditions with no metal (A), templating conditions after binding Mg²⁺ (B), and templating conditions after binding Ni²⁺ (C). The metal capacities of Mg²⁺, Ni²⁺, and Cd²⁺ are reported before templating (white box), after templating with metal and iodosobenzoate (striped box), and after reduction with DTT (grey box).

Composite peptides composed of Cys with cross-linking thiol residues and Asp residues possessing an active carboxylate binding functionality were used to template for Mg²⁺ and Ni²⁺. In this way, the thiol residues were free for cross-linking and the Asp residues bind the metal species of interest. Figure 4.8. shows the results of these cross-linking experiments. The top series of bar graphs (A) show the results of the templating

experiments with no metal. The behavior of Cd^{2+} is consistent for all three columns where the capacity is dramatically reduced after cross-linking, which was expected due to less thiols available for metal binding. The high affinity of Cd^{2+} to thiol functionalities is evident and a capacity reduction indicated that approximately 50% of Cd^{2+} binding sites in these peptides involve thiol functionalities. Interestingly, the Ni^{2+} capacities tend to increase after the oxidative cross-linking of T_{GD5C} , and $\text{T}_{\text{GD2CD2C}}$. This may be a result of binding sites for Cd^{2+} composed of both thiol and carboxylate functionalities that no longer exist after oxidative cross-linking, freeing carboxylate groups and creating additional binding sites for Ni^{2+} . Less Cd^{2+} hybrid binding sites due to adjacent cysteine residues may be responsible for the decreases in Ni^{2+} capacity after the cross-linking of T_{GD4C2} ; in addition to a decrease in Ni^{2+} binding of terminal cysteines. Results for each peptide after Mg^{2+} templating (B) provides minimal evidence for formation of selective Mg^{2+} binding geometries and is similar to the results with no templated metal (A). Cross-linking still occurs through the thiol groups and maybe to a lesser extent when a metal is bound prohibiting some disulfide formation either due to Mg^{2+} - thiol binding or perhaps increased steric constraints. Templating for Ni^{2+} (C) produces similar results except no increases in Ni^{2+} capacities are observed after cross-linking. The colored amine-thiol complexes observed during the metal binding studies may tie up the thiol groups reducing some cross-linking, however, still eliminating many Cd^{2+} sites.

Overall, attempts to template using these short-peptides show that selectivity depressions and enhancements are primarily a result of eliminating thiols that may participate in metal binding, in addition to the metal bound during templating, inhibiting a small percentage of thiols to be oxidized to disulfides.

4.4. CONCLUSIONS

Short peptides (2 and 7 residues) immobilized onto TentaGel resin, like previously explored single residues and biohomopolymers, show selective metal binding based on the amino acids used as well as the order (viz., secondary structure). Unlike the longer biohomopolymers, these peptides show very high metal to residue ratios. Additionally, the high surface coverage and the ability to be immobilized onto a commercial resin (e.g., TentaGel) contribute to a good capacity, especially for the 7-mers. It is postulated that the smaller peptides do not change conformation as much as the larger biohomopolymers previously studied. Thus, most -- if not all -- residues participate in direct metal binding. Peptides immobilized onto TentaGel resin also appear to display good mass transport through the resin and preliminary data suggests the establishment of equilibrium in the column under the flow conditions used in this study although confirmation of this remains to be verified.

These studies also indicate the importance of characterizing preconcentration and remediation materials with multi-metal solutions along with single metals solutions when a one-to-one correlation of the metals to “sites” is uncertain. In short, simple use of determined stability or dissociation constants for the metals of interest may not be predictive of the binding performance when mixed metal solutions are encountered.

Perhaps most significantly, the results from the 7-mer peptides demonstrated that very measurable differences in metal capacities and selectivities could result from subtle positional changes of only a few residues.

4.5. LITERATURE CITED

1. Malachowski, L.; Stair, J. L.; Holcombe, J. A. *Pure and Applied Chemistry* **2004**, *76*, 777-787.
2. Rulíšek, L.; Vondrášek, J. *Journal of Inorganic Biochemistry* **1998**, *71*, 115-127.
3. Rulíšek, L.; Havlas, Z. *Journal of Physical Chemistry A* **2002**, *106*, 3855-3866.
4. Stillman, M. J.; Shaw, C. F.; Suzuki, K. T., Eds. *Metallothioneins, Synthesis, Structure and Properties of Metallothioneins, Phytochelatins, and Metal-Thiolate Complexes*; VCH: New York, 1992.
5. Elmahadi, H. A. M.; Greenway, G. M. *Journal of Analytical Atomic Spectrometry* **1993**, *8*, 1009-1014.
6. Howard, M.; Jurbergs, H. A.; Holcombe, J. A. *Journal of Analytical Atomic Spectrometry* **1999**, *14*, 1209-1214.
7. Howard, M.; Jurbergs, H. A.; Holcombe, J. A. *Analytical Chemistry* **1998**, *70*, 1604-1609.
8. Jurbergs, H. A.; Holcombe, J. A. *Analytical Chemistry* **1997**, *69*, 1893-1898.
9. Gutierrez, E.; Miller, T. C.; Gonzalez-Redondo, J. R.; Holcombe, J. A. *Environmental Science and Technology* **1999**, *33*, 1664-1670.
10. Malachowski, L.; Holcombe, J. A. *Analytica Chimica Acta* **2004**, *517*, 187-193.
11. Malachowski, L.; Holcombe, J. A. *Analytica Chimica Acta* **2003**, *495*, 151-163.
12. Miller, T. C.; Kwak, E.-S.; Howard, M.; Vanden Bout, D. A.; Holcombe, J. A. *Analytical Chemistry* **2001**, *73*, 4087-4095.
13. Johnson, A. M.; Holcombe, J. A. *Analytical Chemistry* **2005**, *77*, 30-35.
14. Hagemeyer, A.; Jandeleit, B.; Jiu, Y.; Poojary, D. M.; Turner, H. W.; Volpe, A. F.; Weinberg, H. W. *Applied Catalysis A* **2001**, *221*, 23-43.

15. Wennemers, H. *Combinatorial Chemistry and High Throughput Screening* **2001**, 4, 273-285.
16. Reetz, M. T. In *Comprehensive Coordination Chemistry II*; McCleverty, J. A., Meyer, T. J., Eds.; Elsevier Ltd.: Oxford, 2004; Vol. 9, pp 509-548.
17. Francis, M. B.; Jamison, T. F.; Jacobsen, E. N. *Current Opinion in Chemical Biology* **1998**, 2, 422-428.
18. Shibata, N.; Baldwin, J. E.; Wood, M. E. *Bioorganic and Medicinal Chemistry Letters* **1997**, 7, 413-416.
19. Ye, Y.; Liu, M.; Kao, J.; Marshall, G. R. *Biopolymers* **2003**, 71, 489-515.
20. Atherton, E.; Sheppard, R. C. *Solid Phase Peptide Synthesis-a Practical Approach*; IRL Press: Oxford, 1989.
21. Merrifield, R. B. *Journal of the American Chemical Society* **1963**, 85, 2149-2154.
22. Cotton, F. A.; Wilkinson, G. *Advanced Inorganic Chemistry-a Comprehensive Text*, 3rd ed.; Wiley Eastern Limited: New Delhi, 1972.
23. Pearson, R. G. *Journal of the American Chemical Society* **1963**, 85, 3533-3539.
24. Masoom, M.; Townshend, A. *Analytical Chemistry* **1984**, 166, 111-118.
25. Sarin, V. K.; Kent, S. B. H.; Tam, J. P.; Merrifield, R. B. *Analytical Biochemistry* **1981**, 117, 147-157.
26. Cernik, M.; Borkovec, M.; Westall, J. C. *Environmental science & technology* **1995**, 29, 413-425.
27. *Perkin-Elmer User Manual 904244: Procise 49x Clc Protein Sequence System*, 1996.
28. Albericio, F.; Pons, M.; Pedroso, E.; Giralt, E. *Journal of Organic Chemistry* **1989**, 54, 360-366.

29. Büttner, K.; Zahn, H.; Fischer, W. H., *Proc. Am. Pept. Symp. 10th*, Aachen, Fed. Rep. Ger., 1988 1987; ESCOM Sci.; 210-211.
30. Gough, G. R.; Brunden, M. J.; Gilham, P. T. *Tetrahedron Letters* **1981**, 22, 4177-4180.
31. Köster, H.; Stumpe, A.; Wolter, A. *Tetrahedron Letters* **1983**, 24, 747-750.
32. Bard, A. J.; Faulkner, L. R. *Electrochemical Methods: Fundamentals and Applications*, Second ed.; John Wiley & Sons, Inc.: New York, 2001.
33. McAlpine, S. R.; Schreiber, S. L. *Chemistry- A European Journal* **1999**, 5, 3528-3532.
34. Miller, T. C.; Holcombe, J. A. *Journal of Hazardous Materials* **2001**, 83, 219-236.
35. Elefterov, A. I.; Kolpachnikova, M. G.; Nesterenko, P. N.; Shpigun, O. A. *Journal of Chromatography A* **1997**, 769, 179-188.
36. Vinodkumar, G. S.; Mathew, B. *Chemistry- A European Journal* **1998**, 34, 1185-1190.
37. George, B.; Mathew, B. *Journal of Macromolecular Science Pure and Applied Chemistry* **2001**, A38, 429-449.
38. Sugii, A.; Ogawa, N.; Katayama, I.; Hida, T. *Talanta* **1982**, 29, 263-266.
39. Miller, T. C.; Holcombe, J. A. *Analytica Chimica Acta* **2002**, 455, 233-244.
40. Neville, R. G. *Journal of the American Chemical Society* **1957**, 79, 518-519.
41. Neville, R. G.; Gorin, G. *Journal of the American Chemical Society* **1956**, 78, 4891-4893.
42. Schubert, M. *Journal of the American Chemical Society* **1931**, 53, 3851-3861.
43. Michaelis, L.; Guzman Barron, E. S. *Journal of Biological Chemistry* **1929**, 83, 191-210.

44. Arnold, A. P.; Jackson, W. G. *Inorganic Chemistry* **1990**, 29, 3618-3620.
45. Ritchie, S. M. C.; Kissick, K. E.; Bachas, L. G.; Sikdar, S. K.; Parikh, C.; Bhattacharyya, D. *Environmental Science and Technology* **2001**, 35, 3252-3258.
46. Hancock, R. D.; Martell, A. E. *Chemical Reviews* **1989**, 89, 1875-1914.
47. Torchinskii, Y. M. *Sulfhydryl and Disulfide Groups of Proteins*; Consultants Bureau: New York, 1974.
48. Voet, D.; Voet, J. G. *Biochemistry*, 2nd ed.; John Wiley & Sons, Inc.: New York, 1995.
49. Howard, M. E., The University of Texas at Austin, Austin, 1999.

Chapter 5: Metal Binding Characterization and Conformational Studies Using Raman Microscopy of Resin Bound Polyaspartic Acid

5.1. INTRODUCTION

Designing materials for metal remediation and preconcentration based on naturally occurring metal binding proteins has growing interest due to their inherent selectivity, strong binding, ease of synthesis with a variety of acid building blocks, and environmental innocuity.¹⁻⁴ Naturally occurring intercellular metalloproteins often lose metal selectivity when taken out of the pristine cellular environment due to their dependence on specific non-covalent interactions.⁵ One simplifying approach is through the use of immobilized synthetic biohomopolymers ($n = 30-70$). These materials often provide the needed selectivity based on the amino acid side chain moiety with easy on-demand release and reusability.¹

Specifically, these biohomopolymers can be attached to porous supports for use as ion-exchange media where metal cation binding often occurs under neutral conditions with the peptide chain conforming to a specific binding orientation in the presence of a complexing metal. Although conditional stability constants for these systems have been shown to reach $K \geq 10^{12}$,⁶ metal release can occur rapidly with the addition of acid.^{7,8} These materials are also effective in seawater matrixes^{7,9} and resistant to mild oxidizing conditions, increased temperatures, and some enzyme degradation¹⁰.

It has been suggested that these biohomopolymers reach a conformational free energy minimum during metal binding and not all residues are involved in metal binding.^{11,12} For example, previous studies of polyaspartic acid ($n = 50$), immobilized onto controlled pore glass (CPG), reported that one Ni^{2+} was bound per 160 aspartic acid residues due to the coiled nature of the peptide during metal binding.¹³ However, a shorter peptide ($n = 7$) composed primarily of Asp immobilized on CPG yielded a metal

per residue ratio of 1:6.⁸ In the same study, this number was lowered to 1:3 when PLAsp (n = 7) chain was synthesized on a polymeric resin, TentaGel.⁸ This large increase in aspartic acid residues per metal ion for these short peptides was thought to occur because of increased interchain metal-peptide interactions and/or reduced coiling of the peptide that make more residues available for metal coordination.

The peptide position and structure not only influences metal binding, but also influences metal release of PLAsp and other immobilized biohomopolymers. It has been speculated that the ease of metal release by acid not only occurs through metal displacement by H⁺, but also through conformational changes as a result of increased hydrophobicity that perturbs the overall binding geometry.^{7,12,14} The most direct evidence to date involved monitoring the height of peptides immobilized on a flat glass substrate using atomic force microscopy (AFM).¹² These authors interpreted height change under different solution conditions to changes in conformation of the peptide.

While the AFM data was supportive of the proposed mechanisms, it would be useful to obtain more direct, spectroscopic evidence of the tertiary structure of these immobilized peptides. It has been shown that Raman spectroscopy can provide spectral features that are assignable to structures such as α -helices, β -sheets, β -turns, and random chains.¹⁵

In the current study, the relationship between peptide length and peptide secondary structure during metal binding to and release from PLAsp on a polymeric resin, TentaGel, was evaluated. PLAsp composed of chain lengths 6, 20 and 30 was synthesized, and four different metal cations (Mg²⁺, Co²⁺, Cd²⁺ and Ni²⁺) were used for characterization. Metal binding capacities, conditional stability constants and metal release behavior were determined using a flow injection system with a packed microcolumn and either flame atomic absorption spectrophotometry (FAAS) or

inductively coupled plasma mass spectrometry (ICP-MS) detection. Additionally, Raman microscopy was used to monitor changes in the peptides' secondary structure by viewing single TentaGel resin beads containing immobilized PLAsp. Spectra from beads in metal-free buffer, beads exposed to metals and beads exposed to acidic solution were collected and compared.

5.2. METHODS AND MATERIALS

5.2.1. Chemicals

All chemicals were reagent grade unless noted, and deionized distilled water was used to prepare solutions. All glassware was soaked overnight in 4 mol L⁻¹ HNO₃ prior to use. Peptide synthesis reagents NovaSyn TG (TentaGel) resin (170 mesh; 0.24 mmol/g) and NovaSyn TGR (TentaGel) resin modified with the Rink linker (170 mesh; 0.25 mmol/g), aspartic acid (Fmoc-Asp(t-butyl ester (OtBu))-OH), 2-(1H-Benzotriazole-1-yl)-1,1,3,3-tetramethyluronium tetrafluoroborate, and 1-hydroxybenzotriazole (98%) were used as received from Novabiochem. Tacky Dot slides were purchased from SPI supplies (2388). Stock solutions of 1000 µg mL⁻¹ Cd²⁺ and Ni²⁺ (Acros) atomic absorption standards in 4% HNO₃ were used to prepare the loading solutions for the various metal binding experiments. For Co²⁺ and Mg²⁺ (J.T. Baker), the loading solutions were prepared from standardized solutions of the reagent grade nitrate salt in 1% (v/v) HNO₃ and 1% (v/v) HCl. A 0.2 mol L⁻¹ (N-[hydroxyethyl]piperazine-N'-[2-ethanesulfonic acid]) (HEPES) (Aldrich) buffer was prepared and purified by passing the buffer through a 100-200 mesh Chelex 100 (Bio-Rad) ion exchange column. Other reagents used included nitric acid (Sigma); trifluoroacetic acid (TFA) (99%),

triethylsilane (99%) (Acros); methanol, dichloromethane (DCM), N-methylmorpholine (NMM) (Fisher); piperidine (99%) (Aldrich).

5.2.2. Peptide synthesis and characterization

All immobilized peptides were synthesized by Fmoc-solid phase peptide synthesis (SPPS) using a Ranin Symphony Quartet automated peptide synthesizer. Peptides were synthesized on TentaGel resin consisting of 94% TentaGel TG and 6% TentaGel TGR (which contains a cleavable Rink linker). For all peptides synthesized, each amino acid coupling reaction was performed twice. TentaGel is an ideal resin for both peptide synthesis and continuous flow studies because it swells minimally in various solvents, yet has good transport through its cross-linked interior.

At the end of each synthesis, the resin was rinsed with methanol and DCM. The protecting groups on each amino acid were then cleaved using 0.5 mL of triethylsilane and 0.5 mL of DI water in 20 mL TFA. The filtrate was collected using suction filtration and precipitated with cold ether. The peptides were rinsed and centrifuged and then dissolved in 5 mL of DI water, froze with liquid N₂ and lyophilized. The 6% of cleavable peptide was analyzed for purity using mass spectrometry. The filtered resin was rinsed with methanol and DCM; then dried (3 h) using a speed vac concentrator (Savant) connected to a cold trap (Heto) (-115°C) that was held under vacuum.

5.2.3. Atomic absorption and metal binding experiments

A Varian FAAS (model AA-875) with an acetylene/air flame was used to characterize the metal-binding peptides. Hollow cathode lamps were operated at the manufacturer recommended currents. Wavelengths for Co, Ni, Cd and Mg were 240.7, 232.0, 228.8 and 285.2 nm, respectively, and were used in conjunction with a monochromator bandpass of 0.2 nm for Co and Ni, and 0.5 nm for Cd and Mg.

Solution was pumped through the system to the FAAS using an eight-roller peristaltic pump (Manostat Carter 4/8 cassette pump); 0.76 mm i.d. PTFE tubing and connectors, and columns (3 mm x 25 mm fitted with 100 μ m PTFE frits) (Omnifit). A Kel-F tee was placed after the column and immediately in front of the nebulizer to minimize the noise level by providing air compensation for the “solution starved” nebulizer. Approximately 0.01 g of dry resin was packed into the columns, filling approximately 20% of the column. The remaining dead space was loosely packed with glass wool. The glass wool had no discernable metal binding capacity for the metals used in this study.

The analysis system above was utilized in the metal binding studies after a 15 min warm-up of pumps, tubing and lamps. Before binding experiments were performed, the columns were conditioned by passing 20 mL of 0.1 mol L⁻¹ HNO₃ followed by 4 mL of 0.02 mol L⁻¹ HEPES buffer (pH 7.0). Metal solutions were then passed through the columns and monitored by FAAS. A 20 μ g mL⁻¹ solution of a particular metal (Ni²⁺, Cd²⁺, Co²⁺ or Mg²⁺) in 0.02 mol L⁻¹ HEPES buffer (pH 7.0) was passed through each column at 2 mL min⁻¹ (or a linear velocity of 11 ± 2 cm s⁻¹) until breakthrough was reached (i.e., when the FAAS absorbance signal became constant and indicated that the effluent concentration had reached the influent concentration). After breakthrough, HEPES buffer was passed through the columns at 1 mL min⁻¹ for ~1 min to remove metal-containing solution from the column dead volume and line tubing. A small volume of buffer was used to inhibit the removal of metal bound to weak sites. A 0.1 mol L⁻¹ HNO₃ solution was then passed through the column at 2 mL min⁻¹ to strip the metal from the column. The solution was collected in a volumetric flask for subsequent “strip analysis” via FAAS. Acidified standards, which were not retained by the column, were

passed through the system to construct a calibration curve. Capacity values for the single metal studies were determined using strip data and verified with the breakthrough data.

Transient Ni^{2+} strip profiles were also examined. Columns were loaded with 20 mL of a $0.50 \mu\text{g mL}^{-1}$ Ni^{2+} solution, exposed to one dead volume of HEPES buffer to remove excess metal solution, and then stripped with 0.1 mol L^{-1} of nitric acid into the FAAS. These experiments were carried out using a flow rate of 1 mL min^{-1} to minimize the impact of mass transport and better reflect differences in equilibrium-governed rates of release.

5.2.4. Determination of conditional stability constants

A GBC Scientific (Hampshire, IL) Optimass 8000 inductively coupled plasma orthogonal acceleration time-of-flight mass spectrometer (ICP-TOFMS) was used to rerun the initial baseline region ($0\text{--}5 \mu\text{g mL}^{-1}$) of each breakthrough curve to improve the detection limits in this region and better define the stronger binding sites. Breakthrough curve data was collected at 2.0 Hz for the atomic absorption measurements and 0.25 Hz for the ICP-MS. Duplicate data sets were averaged and the final data set combined the ICP-MS data from $0\text{--}5 \mu\text{g mL}^{-1}$ with the AA data from $5\text{--}20 \mu\text{g mL}^{-1}$. The binding isotherms were created from this final breakthrough curve data. Regularized regression analysis was used to determine conditional stability constants. The QUASI program¹⁶ was used to perform calculations on the binding isotherms created from the single metal breakthrough curves. The atomic absorption breakthrough curve data were smoothed using Savitzky-Golay least squares smoothing routine with a 50 point window (Origin). The QUASI parameters used were reported previously.⁸

5.2.5. Raman microscopy and peptide conformational studies

Measurements were made with an InVia Reflex Raman Microscope (Renishaw) using a 785 nm high power diode laser (Renishaw) with a 50× microscope objective (N.A. = 0.75) and a CCD detector. The instrument was calibrated using an internal silicon standard (521 cm^{-1}). Each spectrum was obtained using a dynamic scan for 5 accumulations at 30 s each at 50% laser intensity (115 mW). In the case of bound Ni^{2+} , 15 accumulations were collected using a static scan at 30 s each with a laser intensity of 10% (23 mW) due to absorption at 785 nm by the Ni^{2+} -peptide complex.

Resin beads prepared for Raman analysis were packed into microcolumns and exposed to one of three conditions: $0.1\text{ mol L}^{-1}\text{ HNO}_3$, $0.02\text{ mol L}^{-1}\text{ HEPES}$ buffer (pH 7.0), or $20\text{ }\mu\text{g mL}^{-1}$ of metal (Ni^{2+} , Cd^{2+} , Co^{2+} or Mg^{2+}) in $0.02\text{ mol L}^{-1}\text{ HEPES}$ buffer (pH 7.0). After exposure, the wet beads were placed onto both silicon wafers and glass microscope slides. The silicon wafer allowed minimal spectral interference above 1000 cm^{-1} and the glass microscope slide allowed minimal spectral interference below 1000 cm^{-1} . All Raman experiments were completed in duplicate and a new bead was used for each analysis ensuring minimal solvent evaporation and thermal degradation from the laser. Additional experiments were done to monitor the Raman spectrum at 1, 2, 3, 4, and 5 accumulations which ensured minimal change in the resin-peptide environment caused by laser exposure during data collection. No pronounced spectral differences from bead-to-bead were also observed. All Raman spectra were baseline corrected and normalized to a peak inherent to the resin (621 cm^{-1} or 1183 cm^{-1}) using Origin7. The TentaGel spectrum was then subtracted from each TentaGel + peptide spectrum, except the amide I region, to isolate the peptide spectrum.

Beads from each peptide bead set were shaken onto a Tackydots slide and exposed to one of three conditions for 24 hrs: $0.1\text{ mol L}^{-1}\text{ HNO}_3$, $0.02\text{ mol L}^{-1}\text{ HEPES}$ buffer (pH

7.0), or 20 $\mu\text{g mL}^{-1}$ of metal (Ni^{2+} , Cd^{2+} , Co^{2+} or Mg^{2+}) in 0.02 mol L^{-1} HEPES buffer (pH 7.0). Bead images from the Raman microscope were saved and the bead diameters were measured.

5.3. RESULTS AND DISCUSSION

5.3.1. Peptide sequences examined

For this study, PLAsp was examined since it is one of the more widely used biohomopolymers for metals remediation. The target chains lengths synthesized included a short-peptide ($n = 6$), a mid-range peptide ($n = 20$) that could form more easily structures such as α -helix, and a longer peptide similar to those available from major manufacturers ($n = 50$). The 6% TentaGel TGR resin used in each peptide synthesis allowed for the peptide on those beads to be cleaved and used for characterization via electrospray ionization mass spectrometry. The mass spectrum of the 6-mer peptide showed close to 100% of the peptide was of the six residue form. The mass spectrum of the 20-mer peptide showed that the peptide was 40% 20-mer, 40% 19-mer, and 20% 18-mer assuming minimal changes in the ionization efficiency. Multiple attempts were made to characterize the 50-mer via ESI-Q-MS and MALDI-TOF-MS, but were unsuccessful possibly due to the highly acidic nature of the peptide which was also a problem during the 20-mer characterization. As an alternative, the Raman peak area of the amide I band under neutral conditions was used to estimate the length of the longer peptide. Since each peptide spectra produced similar peaks in each peptide backbone region, we assumed the confirmation (i.e., composition of secondary structure) was similar for each peptide. The peak areas of the 6-mer and 20-mer were used for calibration and resulted in a roughly estimated peptide length for the longer peptide of

approximately 30 residues per chain, however this likely incorporates a distribution of varying peptide lengths. The longer peptide was significantly shorter than the target peptide, which is not surprising since long peptides are often more of a challenge to synthesize, especially those with bulky and charged functional groups. A second attempt to synthesize the 50-mer peptide yielded similar results.

5.3.2. Metal binding studies

The Mg^{2+} , Co^{2+} , Cd^{2+} , and Ni^{2+} metal capacities were determined for PLAsp of chain lengths 6, 20, and 30 (Table 5.1.). The metal binding trends for each peptide were $\text{Ni}^{2+} \geq \text{Co}^{2+} \geq \text{Cd}^{2+} \geq \text{Mg}^{2+}$ for $\text{T}_{\text{D}6}$, $\text{Ni}^{2+} > \text{Cd}^{2+} > \text{Co}^{2+} > \text{Mg}^{2+}$ for $\text{T}_{\text{D}20}$, and $\text{Cd}^{2+} > \text{Ni}^{2+} \geq \text{Co}^{2+} \geq \text{Mg}^{2+}$ for $\text{T}_{\text{D}30}$. However, the difference in the extremes in capacities for the test metals was always <27% of the average capacities for $\text{T}_{\text{D}6}$, $\text{T}_{\text{D}20}$, and $\text{T}_{\text{D}30}$. The variation is consistent with that seen in other studies of PLAsp immobilized to solid supports, however, the capacity values are much greater due to the increased peptide loading density of TentaGel.^{8,10,13,17} The metal binding capacities of $\text{T}_{\text{D}6}$ were similar to those seen in previous studies⁸ for $\text{T}_{\text{GD}6}$ with some variation perhaps due to the different resin batches used.

Table 5.1. Metal binding capacities of Mg^{2+} , Co^{2+} , Cd^{2+} , and Ni^{2+} to PLAsp on TentaGel resin.^a

Metal	$\text{T}_{\text{D}6}$ ($\mu\text{moles/g}$ of resin)	$\text{T}_{\text{D}20}$ ($\mu\text{moles/g}$ of resin)	$\text{T}_{\text{D}30\text{b}}$ ($\mu\text{moles/g}$ of resin)
Mg^{2+}	530 ± 20	1650 ± 60	3090 ± 20
Co^{2+}	560 ± 30	1820 ± 70	3300 ± 200
Cd^{2+}	550 ± 10	1960 ± 10	3710 ± 60
Ni^{2+}	590 ± 20	2160 ± 70	3400 ± 80

^a All measurements were made in triplicate. Metal solutions ($20 \mu\text{g mL}^{-1}$ Ni^{2+} , Co^{2+} , Cd^{2+} , or Mg^{2+} at pH 7) were passed through the column at 2 mL min^{-1} . T=TentaGel resin, D=aspartic acid.

^b Although this peptide was synthesized to a be PLAsp ($n = 50$), Raman microscopy peak measurements indicated that the synthesis was incomplete resulting in PLAsp ($n \sim 30$).

As noted above, all three peptides showed little selectivity between the metals tested. This is not surprising since each metal was tested separately (i.e., in the absence of other competing metals). Although the metal binding capacities are of the same magnitude for a particular PLAsp chain length, the binding strengths between metals may be very different. The overall selectivity of these materials often depends on the multi-metal mixture used for the experiment. This was demonstrated previously by comparing the selectivity of PLAsp using single metal solutions and multi-metal solutions.^{8,9,13} For this study, however, it was important to look only at single metal solutions to isolate the interactions of the peptide with each metal of interest.

Due to rapid binding of the peptide and good mass transfer within the resin,⁸ the progression of Ni^{2+} and Co^{2+} binding to the peptide was evident as a green or pink band moved slowly down the column during FI loading. Peptides immobilized to CPG, on the other hand, exhibit slower increases in capacity due to mass transfer limitations.⁶ Metal to residue ratios were calculated for T_{D6} , T_{D20} , and T_{D30} and resulted in one metal per 2-3 aspartic acid residues for all four metals tested indicating that most aspartic acid residues participate in metal binding. According to Ritchie et al., 2-3 residues per metal may indicate a primarily ion-exchange metal sorption mechanism.¹⁴

It was surprising, however, that the longer peptides, T_{D20} and T_{D30} , had high metal-to-residue ratios. Unlike shorter peptides, it was previously hypothesized that longer peptides are able to form complex tertiary structures rendering a large percent of binding residues inaccessible for metal binding.^{11,12} Previous studies of PLAsp ($n = 50$ - 80) immobilized onto CPG showed that one Ni^{2+} cation was bound for every 160 aspartic acid residues¹³, while studies with polycysteine (PLCys) on CPG showed that one Cd^{2+} cation was bound per every 20 cysteine residues.⁶ Atomic force microscopy (AFM) studies of PLCys immobilized on glass slides provided more evidence on the

conformational changes of longer peptides during metal binding and release.¹² The use of TentaGel as a resin for peptide synthesis and ion-exchange support seems to influence the peptide binding to yield its own unique properties. This may be due to the peptide density, in addition to the spatial positioning of each peptide within the lightly cross-linked resin structure. This may limit the peptide's mobility and ability to form complex tertiary and secondary structures within the resin matrix. High metal per residue binding, however, has been seen on other types of supports. For example, Johnson and Holcombe reported the binding of one Cd^{2+} per four cysteine residues for PLCys immobilized to a glassy carbon disc electrode¹⁸. Bhattacharyya and coworkers observed even greater binding on the order of 2 metals per residue for PLAsp and PLGlu immobilized on porous membranes where they attribute this high binding to counterion condensation, caused by a superposition of electric field charges present on closely packed and extended polyelectrolytes.^{9,11,14,19}

The resin with longer PLAsp chains, T_{D20} and T_{D30} , exhibited shrinkage when the pH was lowered, due to the larger peptide mass and conformational changes of the peptide. When exposed to acid for metal extraction, the resin material shrunk by about 6% of the packed column length for T_{D20} , and about 15% for T_{D30} as measured from microscope images taken using the Raman microscope. The resin returned to its original volume when exposed to a neutral buffer. T_{D6} does not show these physical characteristics possibly due to the smaller mass of peptide attached to the resin.

The ability of the peptide immobilized resin to release metals in the presence in acid was determined using Ni^{2+} . Only 10 μg of Ni^{2+} was loaded onto each column to ensure binding to primarily the strong sites of each immobilized peptide. Acid was then introduced into the column to strip off the metal and the absorption signal from the column effluent was monitored. The peak base width at 90% area of the stripped peak

was approximately 25 s (ca. 0.4 mL) for T_{D6} and T_{D20} and 35 s (ca. 0.6 mL) for T_{D30} . Interestingly, Ni^{2+} release from T_{D30} took 10 s longer than release from the other peptides. The longer release time is perhaps related to slower metal diffusion out of the beads with a greater peptide density.

5.3.3. Determination of conditional stability constants

Although the binding capacity of each peptide immobilized resin was similar between metals, it was of interest to compare the binding strengths. Conditional stability constants were determined for all three immobilized peptides and all four metals (Table 5.2.). Interestingly, the shortest peptide, T_{D6} , possessed larger stability constants for all four metals tested compared to the longer peptides. The strongest binding sites of T_{D6} ($\log K$ 7.0) were for Ni^{2+} and Cd^{2+} . The slightly longer peptide, T_{D20} , showed a large decrease in all the metal stability constants compared with T_{D6} . The lengthening of the peptide from 20 to 30 residues resulted in subtle changes in the stability constants and site distribution.

Large stability constants for the smaller peptide may be due to fewer steric effects within the resin matrix allowing each peptide chain to conform in a manner that is very favorable for metal binding with minimal peptide aggregation. With longer peptides, the chains may become aggregated and sterically confined to a conformation which does not produce the strongest metal-peptide interactions. Although the longer chains of PLAsp do not lose binding capacity due to length, they do have weaker binding for the metals tested. Compared to the immobilization on porous glass^{6,7,13,17} and carbon²⁰, longer chain peptides have higher capacity, but lack some of the stronger binding sites ($\log K \geq 8$) on TentaGel resin.

Table 5.2. Conditional stability constants^a and total number of sites (μmole/g of resin) of T_{D6}, T_{D20}, and T_{D30} with four metals.

Peptide	Mg ²⁺		Ni ²⁺		Co ²⁺		Cd ²⁺	
	<u>Log K</u>	<u>Sites</u>	<u>Log K</u>	<u>Sites</u>	<u>Log K</u>	<u>Sites</u>	<u>Log K</u>	<u>Sites</u>
T _{D6}	3.4	20	3.1	300	3.6	500	4.3	230
	4.0	190	4.8	260	6.6	360	7.0	360
	6.0	330	7.0	340				
T _{D20}	2.8	770	3.2	1200	2.5	1300	3.2	1200
	4.7	1400	5.1	1600	4.7	1700	5.1	1600
T _{D30} ^b	4.1	3400	3.0	2200	3.4	2400	3.3	2500
			4.7	2700	4.9	2200	4.9	2200

^aValues were calculated from binding isotherms using the QUASI program.

^bAlthough this peptide was synthesized to a be PLAsp (n = 50), Raman microscopy peak area measurements indicated that the synthesis was incomplete resulting in PLAsp (n = 30).

5.3.4. Peptide conformational studies using Raman Microscopy

Raman microscopy was used to look at secondary structure changes of each peptide on TentaGel resin. The utility of Raman spectroscopy for monitoring the peptide structure of resin bound peptides has been previously demonstrated by Nielson and coworkers for examining the synthesis problems of polyalanine ($n = 1-10$).^{21,22} Depending on the peptide environment (i.e., hydrogen bonding and rotational angles ϕ and ψ), Raman bands will shift, thus allowing determination of protein secondary structures such as α -helices, β -sheets, and random chains.^{23,24} The three regions typically monitored are the amide I (ca. 1640-1680 cm^{-1}), amide II (ca. 1225-1300 cm^{-1}), and C-C (ca. 880-1000 cm^{-1}) band, all of which pertain to the peptide backbone.^{25,26} Raman spectroscopy is particularly useful for observing peptides in aqueous environments as water is a very weak Raman scatterer and does not typically interfere with peptide bands.

The Raman spectra of TentaGel resin both dry and swollen is shown in Figure 5.1. Distinct changes in the spectra were observed between a dry bead from the manufacturer and a bead allowed to swell in either organic or aqueous solution. Once swollen, the conformation of the polymeric material changes and does not revert to the original form either by drying under N_2 or by speed vac drying with a cold trap. These spectral differences are similar to that seen by Nielson and coworkers between TentaGel and TentaGel + HMPA linker.²² The differences seen in their spectra may be primarily due to swelling of the resin in solution and less to the addition of HMPA.

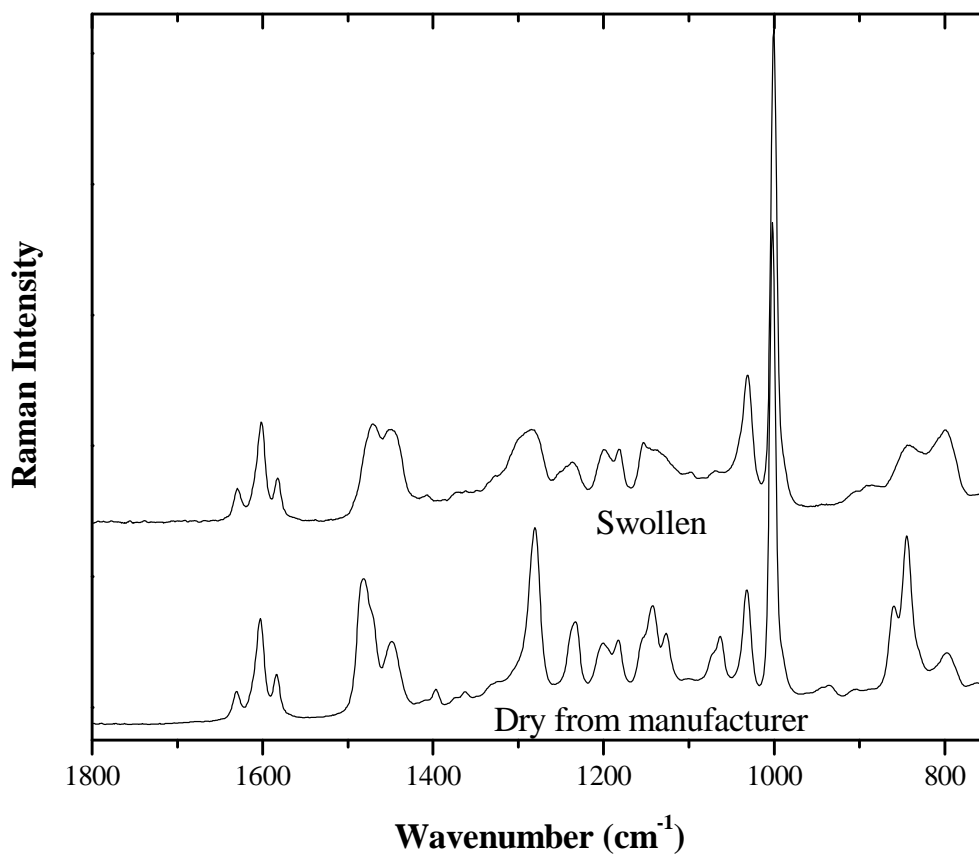


Figure 5.1. Raman Spectra of dry TentaGel resin from manufacturer (bottom) and after solvent exposure (top). Two spectra of each sample type were collected and each spectrum was collected on a new bead.

5.3.4.1. Amide I Region

Figure 5.2. shows the amide I region for each resin bound peptide under various conditions. The results from only Cd^{2+} are shown since Mg^{2+} , Co^{2+} , Ni^{2+} and Cd^{2+} showed similar Raman bands (i.e., secondary structure) in this region. Previous studies

by Yamoaka and Masujima using optical rotary dispersion (ORD) also observed no discernable changes between the secondary structure of a similar peptide, poly-L-glutamate, PLGlu, $n = 700$, with Ni^{2+} and Cd^{2+} .²⁷ Each spectrum in Figure 5.2. shows a broad peak spanning most of the amide I region ($1625\text{-}1715\text{ cm}^{-1}$) except under acidic conditions. A broad band peak at approximately 1680 cm^{-1} was seen for $\text{T}_{\text{D}20}$, $\text{T}_{\text{D}30}$ and $\text{T}_{\text{D}6}$. There were no noticeable differences between the peptides and the metal bound peptides at $\text{pH} = 7.0$.

These broad bands indicate various peptide secondary structures due to the wide distribution of the rotational angles ϕ and ψ .^{25,26} Similar broad bands have been observed for the ionized form of PLAsp in solution²⁸ and the solid-state form of Na-PLGlu²⁹. The spectrum of $\text{T}_{\text{D}6}$ resembled that of polyalanine ($n=2\&3$) immobilized on TentaGel resin, including also the shift downfield when the chain was lengthened²². The minimal structural changes may be responsible for the decreased metal binding strengths ($\log K \leq 7$) on these resins. Although amide I peak broadening and sharpening have been previously observed for PLGlu with salts of Ca^{2+} , Sr^{2+} , Ba^{2+} , and Na^+ ;²⁹ minimal differences were observed between Mg^{2+} , Co^{2+} , Ni^{2+} , and Cd^{2+} bound to resin immobilized PLAsp which may be a result of the resin environment.

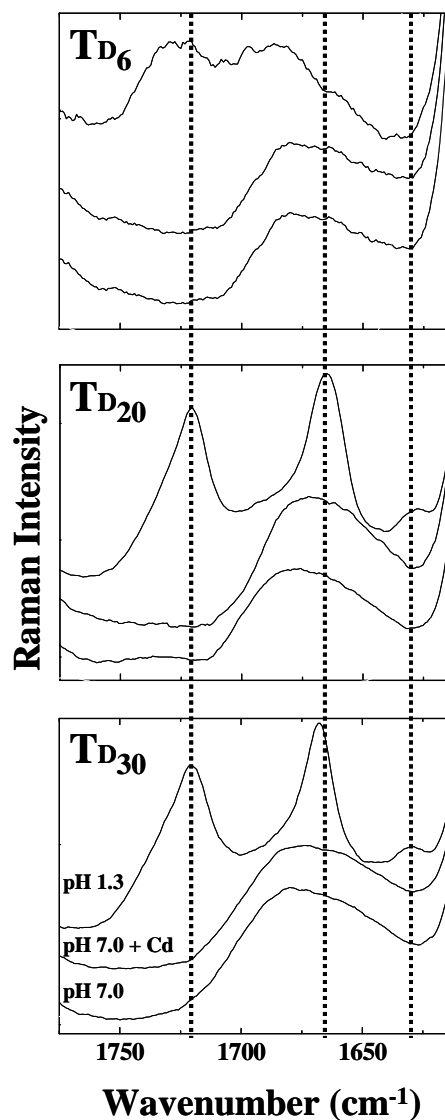


Figure 5.2. Raman spectra (amide I region) of PLAsp synthesized on TentaGel resin for T_{D6} , T_{D20} , and T_{D30} . The solution conditions in each set are pH 7 HEPES buffer (bottom spectrum), $20 \mu\text{g mL}^{-1}$ Cd in HEPES buffer (middle spectrum), and 0.1 mol L^{-1} HNO_3 (top spectrum). T_{D6} , T_{D20} , and T_{D30} have different intensity scales. The dotted line is positioned to assist in viewing the relative peak positions. The secondary structure locations from left to right ($1700 - 1600 \text{ cm}^{-1}$) are β -turns, β -sheets, random chain, and α -helices.

The most striking change in the amide I band is seen when the peptide is exposed to acid (i.e., metal release). The large peak at 1720 cm^{-1} for the acidic peptide identified the carboxylic acid of the side chain, confirming acidification of the peptide.³⁰ For T_{D20} and T_{D30} , the amide I band narrows and splits into two distinct bands. The more intense band at 1666 cm^{-1} is typically assigned to a β -sheet structure and the smaller band at 1630 cm^{-1} is typically assigned to an α -helix structure.^{25,26} Solution studies of PLAsp ($n = 120$) also showed bands at 1670 and 1638 cm^{-1} at pH 4.7 and were assigned to antiparallel β -sheet and α -helix structures; however, the α -helix was found to be the dominant form at pH 4.7.²⁸

In the case of T_{D20} and T_{D30} , the peptides preferentially reach a “free energy minimum” β -sheet structure due to fewer electrostatic repulsions when the carboxylate side groups are protonated. The antiparallel β -sheet structure, in particular, may be favored for these peptides. These results are in contrast various PLAsp solution studies^{28,31,32} and to AFM studies of PLCys ($n = 50$) immobilized on a glass slide,¹² Many studies of PLAsp in solution report helix/coil conformations to be dominant at lower pH's although some β -sheet structure may be present. In the PLCys study, it was suggested that the immobilized peptide was in a pseudo β -sheet/extended random coil structure at pH=7.0, changed to a random coil with the addition of metal, and changed once again to primarily α -helices upon acidification (i.e., metal release). In both this study and the PLCys study, however, metal release was shown to occur not only by proton displacement, but also from secondary structure changes that spoil the metal binding cavity. The choice of support media could ultimately decide which secondary structures are dominant and how metal is released. This may be a result of the peptide density and relative position of neighboring peptide chains on a particular support.

T_{D6} shows little variation under the different conditions retaining a primarily mixed conformation. It is interesting that T_{D6} does not form the same structure as T_{D20} and T_{D30} during acidification. A six residue peptide is limited to the formation of ca. one turn of an α -helix per chain, which may make this structure unfavorable. The formation of β -sheet structures may also be difficult for the shorter peptide if the adjacent chains are not in close enough proximity to form these more highly ordered structures.

5.3.4.2. Amide II Region

Typically, the use of one amide band to determine peptide/protein secondary structure can be unreliable as there are always exceptions and region overlap. Thus, it is important to look at the three distinct peptide backbone regions to verify the assignments made. Figure 5.3. shows the amide II region for each resin bound peptide. Only the results from Cd²⁺ are shown as all metals tested showed similar Raman bands in this region. Again, all peptides under neutral pH conditions with and without metal showed minimal differences with the broad peaks extending from 1230-1260 cm⁻¹ indicating the presence of multiple peptide conformations. In the case of the Co²⁺ bound form of T_{D20} and T_{D30}, two broad peaks start to appear at 1222 and 1260 cm⁻¹.

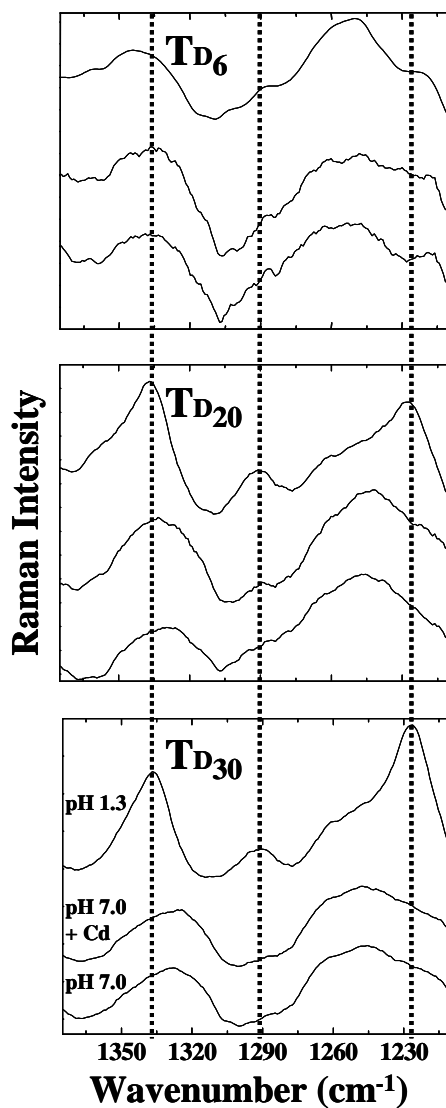


Figure 5.3. Raman spectra (amide II region) of PLAsp synthesized on TentaGel resin. (See caption from Figure 2) The secondary structure locations from left to right (1335 -1225 cm^{-1}) are β -turns, β -sheets, random chain, and α -helicies.

In acid, the amide II peaks became narrower, the 1247 cm^{-1} peak shifted to 1229 cm^{-1} and a small distinct peak at 1292 cm^{-1} emerged with $\text{T}_{\text{D}20}$ and $\text{T}_{\text{D}30}$. These changes indicate a conversion from a mixed conformation to predominantly β -sheets with some α -

helices, which agree with conclusion reached from assignments made for the amide I region in this study.

The region from 1354-1308 cm^{-1} has been assigned to side chain CH_2 twisting and wagging modes.^{28,33,34} Again, T_{D6} shows little variation under the different conditions, which suggests retention of a mixed conformation.

5.3.4.3. C-C Region

The last region monitored for secondary structure was the C-C backbone region (Figure 5.4.). In this region, there are also bands associated with the C-C bonds of the side chain moiety. These bands sometimes interfere with the C-C backbone bands and often make assignments in this region difficult.

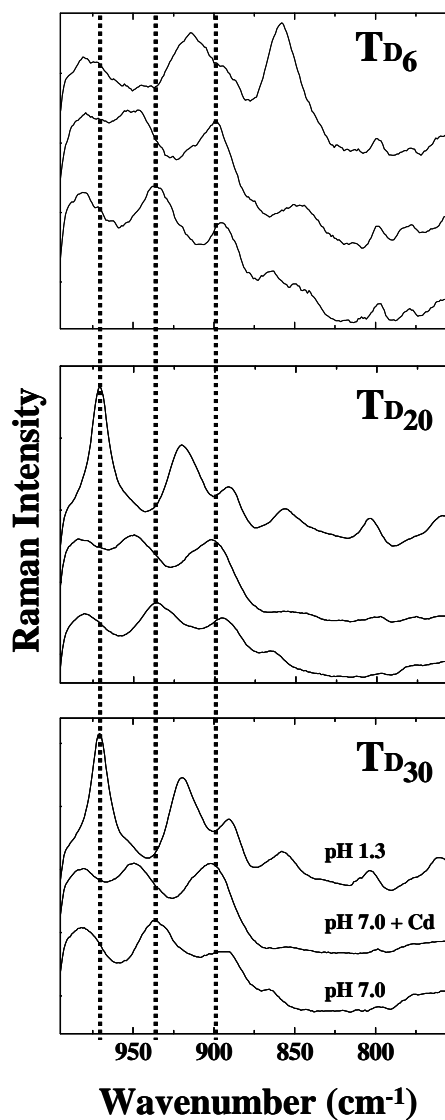


Figure 5.4. Raman spectra (C-C region) of PLAs synthesized on TentaGel resin. (See caption from Figure 2). The secondary structure locations from left to right (1000 -880 cm^{-1}) are β -turns, β -sheets, random chain, and α -helicies.

Peaks between 847 and 902 cm^{-1} for all spectra were assigned to the rocking mode for the side chain CH_2 groups as seen previously with PLGlu, PLAsp, and PLLys.^{28,33,34} Peaks at 982 cm^{-1} for the neutral peptides may indicate a small amount of random coil formation as seen in previous Raman studies with PLAsp²⁸ contributing to the mixed conformation as observed in the amide regions. Without metal, each peptide under neutral pH conditions had peaks at 982 and 936 cm^{-1} . For the Cd^{2+} bound peptide, the peak at 936 cm^{-1} shifted to 950 cm^{-1} . Earlier solution studies of PLGlu by Koenig and Frushour showed a peak shift from 930 to 950 cm^{-1} when the pH was changed gradually from 5 to 11 postulating that this band is particularly sensitive to the degree of ionization.³³ In this study, the same observations were made with metal introduction and, in particular, with the species of metal which will be discussed later in more detail.

Similarly, the peak at 950 cm^{-1} continues to shift toward 920 cm^{-1} as $\text{T}_{\text{D}20}$ and $\text{T}_{\text{D}30}$ are acidified. Although this shift is more extreme than that observed by Koenig and Frushour, the conditions used in this study are more acidic, viz., pH = 1.3. The peak at 920 cm^{-1} under acidic conditions was assigned to the backbone C-C α -helix band, consistent with assignments made in the literature for PLAsp and PLGlu.^{29,33} Also observed was a sharp peak at 970 cm^{-1} for acidic $\text{T}_{\text{D}20}$ and $\text{T}_{\text{D}30}$ which was similar to a peak seen at 965 cm^{-1} for the antiparallel β -sheet conformation of PLGlu and absent for the parallel β -sheet conformation.²⁹ These assignments agree with those made for the amide I and II regions. The peaks associated with the acid form of $\text{T}_{\text{D}6}$ again indicated that this peptide does not undergo significant changes in secondary structures when metal is released.

As mentioned earlier, the peptide C-C band was sensitive to the metal species bound. This may be related to the degree of ionization of the side chain as seen in other studies.^{28,33} Figure 5.5. shows $\text{T}_{\text{D}30}$ under different conditions including complexing to all

four metals. In this region, peak shifts due to the metal were identical for T_{D6} , T_{D20} and T_{D30} .

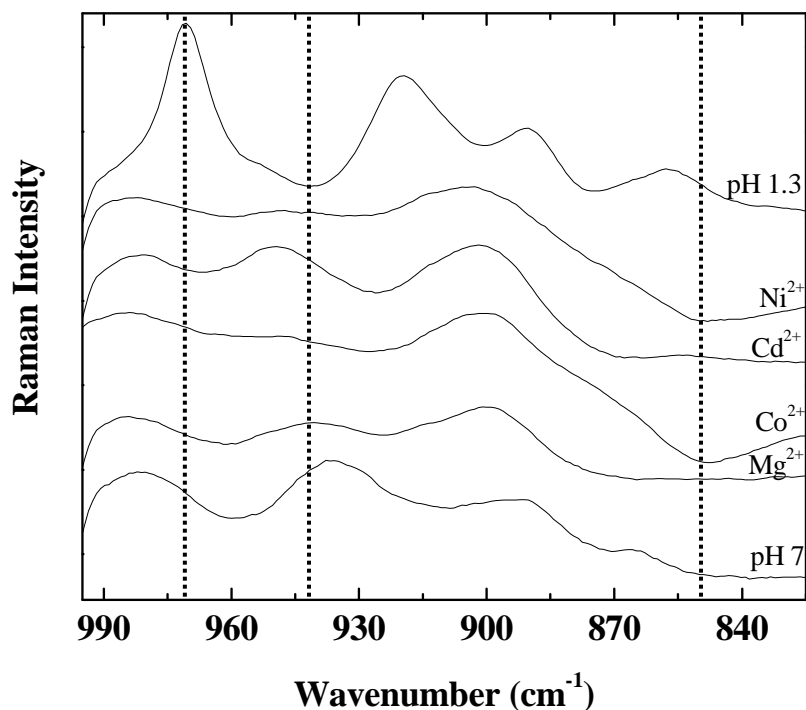


Figure 5.5. Raman spectra (C-C region) of T_{D30} after exposure to $0.1 \text{ mol L}^{-1} \text{ HNO}_3$, $20 \text{ } \mu\text{g mL}^{-1} \text{ Ni}^{2+}$, Cd^{2+} , Co^{2+} , or Mg^{2+} in HEPES, and pH 7 HEPES buffer. The TentaGel resin spectrum was subtracted from each spectrum. Two spectra of each sample type were collected and each spectrum was collected on a new bead. In this figure, the spectra Ni^{2+} , Cd^{2+} , Co^{2+} , and Mg^{2+} bound to the peptide is identical to that seen for T_{D6} and T_{D20} .

Depending on the identity of the metal bound, the region between 950 and 935 cm^{-1} changes. The peak shifts from 950 for Cd^{2+} bound peptide to 942 cm^{-1} when Mg^{2+} is bound and loses intensity when Ni^{2+} and Co^{2+} are bound. The figure also shows a slight negative dip for Ni^{2+} and Co^{2+} at 850 cm^{-1} where the TentaGel resin intensity

decreased. These metals may be interacting with the resin when bound to the peptide. Interestingly, the resin itself has been shown to have negligible binding to these particular metals.⁸ Previous studies with 8-hydroxyquinoline (8HQ)³⁵ and the cation exchanger Dowex 50W-X16,³⁶ also showed metal induced changes in the Raman spectrum of the chelating material and alluded to using Raman monitoring of the metal complex for remediation applications. The Raman specificity of different metals bound to PLAsp in the C-C region could also allow for the identification of metal binding species and/or *in situ* monitoring of these materials during metal clean-up.

5.4. CONCLUSIONS

This study demonstrates how the metal binding and release characteristics of an immobilized peptide, such as PLAsp, can be altered with judicious choice of chain length and support material. In contrast to rigid support materials, the confined space within the resin along with the spatial distribution of attachment groups allow for most residues to participate in metal binding regardless of peptide length, resulting in relatively high metal capacities. However, the dense packing of the longer peptide chains within the resin voids may decrease their mobility and result in an overall loss of strong binding sites when synthesized on these supports. In addition, metal release is slower and likely a result of the increased packing density slowing metal diffusion out of the resin. The use of larger sized resins, yet with similar loading capacities, may increase the binding strength and release times of these longer peptide chains.

Raman microscopy probing of individual resin beads appears to be a useful tool to evaluate the peptide secondary structures during metal binding and release. Addition of metal to each fully ionized peptide did not influence the peptide secondary structure. Raman shifts as a result of acidification (i.e., metal release) of the longer peptides ($n = 20$

& 30) occurred via two processes, proton displacement and a secondary structure change to β -sheets and α -helices, which spoiled the metal binding cavity. Interestingly, these structural changes were not observed for the shorter peptide ($n = 6$) on TentaGel resin which may indicate increased mobility and less steric restraint for this peptide.

5.5. LITERATURE CITED

1. Malachowski, L.; Stair, J. L.; Holcombe, J. A. *Pure and Applied Chemistry* **2004**, *76*, 777-787.
2. Wildgoose, G. G.; Leventis, H. C.; Davies, I. J.; Crossley, A.; Lawrence, N. S.; Jiang, L.; Jones, T. G. J.; Compton, R. G. *Journal of Materials Chemistry* **2005**, *15*, 2375-2382.
3. Sayed, S. A.; Saleh, S. M.; Hasan, E. E. *Mansoura Science Bulletin, A: Chemistry* **2005**, *32*, 1-19.
4. Huang, C.-C.; Su, C.-C.; Hsieh, J.-L.; Tseng, C.-P.; Lin, P.-J.; Chang, J.-S. *Enzyme and Microbial Technology* **2003**, *33*, 379-385.
5. Anderson, B. R. Dissertation, Univ. of Texas, Austin, 1994.
6. Jurbergs, H. A.; Holcombe, J. A. *Analytical Chemistry* **1997**, *69*, 1893-1898.
7. Howard, M.; Jurbergs, H. A.; Holcombe, J. A. *Journal of Analytical Atomic Spectrometry* **1999**, *14*, 1209-1214.
8. Stair, J. L.; Holcombe, J. A. *Microchemical Journal* **2005**, *81*, 69-80.
9. Ritchie, S. M. C.; Kissick, K. E.; Bachas, L. G.; Sikdar, S. K.; Parikh, C.; Bhattacharyya, D. *Environ. Sci. Technol.* **2001**, *35*, 3252-3258.
10. Miller, T. C.; Holcombe, J. A. *Journal of hazardous materials* **2001**, *83*, 219-236.
11. Bhattacharyya, D.; Hestekin, J. A.; Brushaber, P.; Cullen, L.; Bachas, L. G.; Sikdar, S. K. *Journal of Membrane Science* **1998**, *141*, 121-135.
12. Miller, T. C.; Kwak, E.-S.; Howard, M.; Vanden Bout, D. A.; Holcombe, J. A. *Analytical Chemistry* **2001**, *73*, 4087-4095.
13. Malachowski, L.; Holcombe, J. A. *Analytica Chimica Acta* **2004**, *517*, 187-193.

14. Ritchie, S. M. C.; Bachas, L. G.; Olin, T.; Sikdar, S. K.; Bhattacharyya, D. *Langmuir* **1999**, *15*, 6346-6357.
15. Miyazawa, T. *Journal of Chemical Physics* **1960**, *32*, 1647-1652.
16. Cernik, M.; Borkovec, M.; Westall, J. C. *Environmental science & technology* **1995**, *29*, 413-425.
17. Gutierrez, E.; Miller, T. C.; Gonzalez-Redondo, J. R.; Holcombe, J. A. *Environmental Science and Technology* **1999**, *33*, 1664-1670.
18. Johnson, A. M.; Holcombe, J. A. *Analytical Chemistry* **2005**, *77*, 30-35.
19. Hestekin, J. A.; Bachas, L. G.; Bhattacharyya, D. *Industrial & Engineering Chemistry Research* **2001**, *40*, 2668-2678.
20. Miller, T. C.; Holcombe, J. A. *Analytica Chimica Acta* **2002**, *455*, 233-244.
21. Larsen, B. D.; Christensen, D. H.; Holm, A.; Zillmer, R.; Nielsen, O. F. *Journal of the American Chemical Society* **1993**, *115*, 6247-6253.
22. Ryttersgaard, J.; Larsen, B. D.; Holm, A.; Christensen, D. H.; Nielsen, O. F. *Spectrochimica Acta, Part A: Molecular and Biomolecular Spectroscopy* **1997**, *53A*, 91-98.
23. Lord, R. C.; Yu, N. T. *Journal of molecular biology* **1970**, *50*, 509-524.
24. Small, E. W.; Fanconi, B.; Peticolas, W. L. *Journal of Chemical Physics* **1970**, *52*, 4369-4379.
25. Tu, A. T. In *Spectroscopy of Biological Systems*; Clark, R. J. H., Hester, R. E., Eds.; Wiley: Chichester, 1986; Vol. 13, pp 47.
26. Twardowski, J.; Anzenbacher, P. *Raman and Ir Spectroscopy in Biology and Biochemistry*; Ellis Horwood Limited: England, 1994.

27. Yamaoka, K.; Masujima, T. *Polymer Journal (Tokyo, Japan)* **1979**, *11*, 889-893.
28. Lagant, P.; Vergoten, G.; Loucheux, C.; Fleury, G. *Polymer Journal (Tokyo, Japan)* **1979**, *11*, 345-351.
29. Fasman, G. D.; Itoh, K.; Liu, C. S.; Lord, R. C. *Biopolymers* **1978**, *17*, 1729-1746.
30. Lambert, J. B.; Shurvell, H. F.; Lightner, D. A.; Cooks, R. G. *Organic Structural Spectroscopy*; Prentice Hall: Upper Saddle River, 1998.
31. Tanaka, S.; Nakajima, A. *Polym. J.* **1970**, *1*, 505-517.
32. Saudek, V.; Štokrová; Schmidt, P. *Biopolymers* **1982**, *21*, 1011-1020.
33. Koenig, J. L.; Frushour, B. *Biopolymers* **1972**, *11*, 1871-1892.
34. Yu, T.-J.; Lippert, J. L.; Peticolas, W. L. *Biopolymers* **1973**, *12*, 2161-2176.
35. Uibel, R. H.; Harris, J. M. *Applied Spectroscopy* **2000**, *54*, 1868-1875.
36. Wang, H.; Mann, C. K.; Vickers, T. J. *Applied Spectroscopy* **1995**, *49*, 127-131.

Chapter 6: Quantitative Determination of Single Bead Metal Content from a Peptide Combinatorial Library Using ETV-ICP-MS

6.1. INTRODUCTION

The use of combinatorial libraries has allowed the evaluation of numerous variations to a chemical system in a shortened amount of time. Combinatorial approaches have been utilized in many fields including catalysis,^{1,2} chiral separations,³ drug discovery,^{4,5} and inorganic material synthesis.^{6,7} In all approaches, one challenge is finding suitable ways to screen thousands of beads to obtain the desired information.

One recent area of growth is the use of peptide combinatorial libraries for identifying selective metal chelators.⁸ In these libraries, one approach is to design or optimize the composition of a short, metal binding peptide based on information from a larger protein (such as a metallothionein⁹). One objective is to simplify the chelator without losing metal binding capacity or specificity, and in some instances perhaps even increasing selectivity. This is done using libraries where specific amino acid positions along the peptide chain can be varied to increase and tune metal binding capacity and specificity. There are many advantages to this approach,^{10,11} including the design flexibility provided by 26 naturally occurring amino acid building blocks as well as the ease of peptide library synthesis. Beads with the desired metal binding properties can then be sequenced using methods such as Edman degradation and mass spectrometry.

Screening beads from a combinatorial library for metal content has previously been achieved through colorimetric or fluorescent dyes complexing with the metal of interest^{12,13} or by observing color changes due to metal-peptide complexation itself^{14,15}. Although non-destructive, these approaches are largely qualitative and are usually limited to the analysis of one metal at a time. Non-destructive techniques are mandatory for later determination of peptide sequences. For metal remediation and reclamation, determining

how well a chelator selects for or discriminates against particular species is often important and obtained through examining the binding of multiple metals simultaneously. Energy-dispersive X-ray spectroscopy (EDS) on a scanning electron microscope (SEM) has been previously used for multi-elemental analysis on single beads; however, beads must be initially flattened and then coated with a conductive material before analysis.¹⁶ Recently, Havrilla and coworkers have used micro x-ray fluorescence (MXRF) for both bulk and selective metal screening of beads exposed to metal solutions.^{17,18} This approach involves minimal sample preparation, is non-destructive, and also capable of simultaneous multi-elemental screening of single beads. The relative metal composition is determined from point scans and/or elemental imaging on the surface of the bead. Although this technique provides relative metal content at particular points within the bead, absolute metal content is more difficult to obtain.¹⁷

In the current study, electrothermal vaporization inductively coupled plasma mass spectrometry (ETV-ICP-MS) is used for the simultaneous quantitative determination of several metals extracted into solution from a single bead for purposes of characterizing binding properties of the peptide immobilized on the bead. The ETV exhibits excellent sensitivity (e.g., sub-picogram or part per trillion detection limits) and is ideally suited for use with very small sample volumes ($\leq 10 \mu\text{L}$). The mass analyzer used was a time-of-flight (TOF) system. The TOF mass analyzer allows for multi-elemental analysis with no loss in analytical duty cycle as the number of monitored masses increases.¹⁹

6.2. MATERIALS AND METHODS

6.2.1. Chemicals

All chemicals were reagent grade unless otherwise noted, and deionized distilled water was used to prepare solutions. All glassware and plasticware were soaked overnight in 4 mol L⁻¹ HNO₃ prior to use. The synthesis procedure for polyaspartic acid (PLAsp; n = 20) was similar to that previously described²⁰ and characterization using mass spectrometry showed the peptide was composed of 40% 20 residue form, 40% 19 residue form, and 20% 18 residue. The combinatorial library (CPC Scientific) was composed of the sequence GXXGXXGXXGXX (X = cysteine, aspartic acid, or glutamic acid; G = glycine) and synthesized onto TentaGel Macrobeads (Rapp-Polymere MB 250 002) resin (60 mesh; 0.25 mmol g⁻¹). Microwell plates (96 wells; 300 µL) were purchased from Fisher Scientific (21-377-203), adhesive sheets used to cover the wells were purchased from Nunc (236366), and Tacky Dot slides were purchased from SPI supplies (2388). Stock solutions of 1000 µg mL⁻¹ Cd²⁺, Ni²⁺, and Eu²⁺ (Acros) and Pb²⁺, In²⁺, Cu²⁺, and Mn²⁺ (SCP Science) standards in 2 and 4% HNO₃ were used to prepare both the multi-metal binding solution and the multi-metal standards. For Mg²⁺, the metal solutions were prepared from a standardized solution of the reagent grade nitrate salt (J.T. Baker) in 1% (v/v) HNO₃ and 1% (v/v) HCl. A 0.2 mol L⁻¹ ammonium acetate (Aldrich) and 0.2 mol L⁻¹ (N-[Hydroxyethyl]piperazine-N'-[2-ethanesulfonic acid]) (HEPES) (Acros) buffer were prepared and purified by passing the buffer through a 100-200 mesh Chelex 100 (Bio-Rad) ion exchange column. These metals were selected to demonstrate the multi-metal capability of this technique. Previous studies have shown that many of these metals should preferentially bind while others have no affinity for the amino acids selected.²¹ Ar was used for the ICP and sweep gas (Praxair, Austin, TX). Other reagents

used included nitric acid (70%, redistilled 99.999%) (Sigma); and DL-1,4-dithiothreitol (99%) (DTT) (Acros).

6.2.2. Metal Binding and Extraction

Prior to metal binding, the combinatorial library beads were exposed to 0.02 mol L⁻¹ DTT in 0.02 mol L⁻¹ of HEPES buffer (pH 8.0) in order to reduce disulfide bonds that may have formed between cysteine groups. The DTT solution was deaerated with N₂ prior to use and the reaction was allowed to proceed under constant mixing for 1 h. For both bead sets, approximately 50 beads were added to 20 mL of a deaerated multi-metal solution composed of 20 µg mL⁻¹ Mg²⁺, Mn²⁺, Ni²⁺, Cu²⁺, Cd²⁺, Eu²⁺, and Pb²⁺ in 0.02 mol L⁻¹ ammonium acetate buffer (pH 7.0). The reaction solution was allowed to react under constant mixing for 2 h. The beads were suction filtered (no rinse) and dried under N₂(g) overnight. The beads were then shaken onto a Tacky Dot slide for stereoscope measurements. Using microtweezers, individual beads were selected randomly from the Tacky Dot slide and placed into individual wells containing 100 ng µL⁻¹ In in 250 µL of 0.1 mol L⁻¹ of nitric acid. Indium was used as an internal standard in the ETV-ICP-MS to correct for solvent evaporation as well as autosampler variation. The acid solution from wells exposed only to the microtweezers which were placed in the sticky substance of the Tacky Dot slide was used for blank measurements. Once all the beads were placed into the wells, the wells were covered with a sealing adhesive sheet. The beads were soaked in acid for 2 h with 15 min on/off sonication cycling. After 2 h, 100 µL of the metal extract was transferred from the well into autosampler cups for elemental analysis. Multi-metal standards were prepared with 100 ng µL⁻¹ In in 250 µL of 0.1 mol L⁻¹ of nitric acid. For oxygen ashing experiments, the standards were rerun under the new ETV parameters (described under ETV-ICP-MS). After removing the nitric acid solution,

water (150 μ L) was added to each well containing a bead and each bead was pipetted up with \sim 100 μ L of water and deposited into the ETV for elemental analysis.

6.2.3. Stereoscope measurements

An Olympus (SZX12) Stereoscope was used to obtain images of the beads arrayed on a Tacky Dot slide. Slide sections were labeled for easy identification of the bead regions. Immediately after a bead image was saved, an image of a stage micrometer (1 mm long with and subdivided into 10 μ m increments) was taken at the same magnification. These images were used to determine the diameter of each bead prior to acid extraction for adjusting the metal capacities with respect to the bead volume.

6.2.4. ETV-ICP-MS

Measurements were carried out on a Optimass 8000 inductively coupled plasma orthogonal acceleration time-of-flight mass spectrometer (GBC Scientific; Hampshire, IL). Operating parameters for the ICP-MS are described in Table 6.1. Calibration was performed with the ETV prior to bead analysis using standard solutions containing the ions of interest. Calibrations were retaken before oxygen ashing experiments to account for changes in sensitivity due to the altered ETV parameters.

Table 6.1. ICP Operating Parameters

Sample Gas Flow	1.15 L min ⁻¹
Plasma Gas Flow	10.0 L min ⁻¹
Auxiliary Gas Flow	0.90 L min ⁻¹
RF Generator Forward Power	700 W
Torch Position (x)	8.0 mm
Torch Position (y)	0.3 mm
Torch Position (z)	-0.2 mm
Skimmer Potential	-1,000 V
Extraction Lens	-1,400 V
Pushout Plate	510 V
Pushout Grid	-540 V
Reflectron	580 V
Detector	3,200 V
Analytes (primary isotopes used)	²⁴ Mg, ⁵⁵ Mn, ⁵⁸ Ni, ⁶³ Cu, ¹¹⁴ Cd, ²⁰⁸ Pb, ¹⁵³ Eu
Confirmation isotope (where applicable)	²⁵ Mg, ⁶⁰ Ni, ⁶⁵ Cu, ¹¹² Cd, ²⁰⁶ Pb, ¹⁵¹ Eu

The ICP-MS was coupled to the ETV, a modified electrothermal atomizer and autosampler (Varian model GTA-95 ; Walnut Creek, CA) that has been previously described.²². Each sample was measured in triplicate using 10 µL injections. Pyrolytically coated graphite tubes were used as the vaporizer (Varian, part no.

6310001200). A valve system was utilized to separate the ETV from the ICP when material was not being vaporized (i.e., during drying and ashing cycles). During these steps, the instrument's sample gas flow was diverted directly into the torch. During analyte vaporization, the valves were toggled so Ar gas flow was directed through the graphite tube to sweep analyte into the mass spectrometer. During this cycle, the dosing hole of the graphite furnace was plugged by means of a pneumatically-activated graphite-tipped plunger. This also triggered data collection in the Optimass 8000. Analyte was carried to the ICP torch by 1 m of 6 mm i.d. Tygon[®] tubing. The ETV heating program is described in Table 6.2.

Table 6.2. ETV heating program

Step	Temperature (°C)	Ramp Time (s)	Hold Time (s)	Dosing Hole Closed
Dry	100	5	10	No
Char	300	20	20	No
Pause	50	3	15	Yes
Vaporize	2,800	3	5	Yes *
Cool	50	14	0	Yes *
Clean	2,800	1.3	3	No
Cool	50	14	0	No

* Denotes mass spectrometry data collection.

For oxygen ashing studies, the drying step was increased to 60 s to accommodate the increased sample volume of 100 µL. During the oxygen ash step, air was used in place of Ar, passing through the furnace at a rate of approximately 1.2 mL/min and the ash temperature was set to 800 °C (viz., dull red furnace appearance looking through dosing hole) for 20 s. After ashing, the furnace was cooled to room temperature with air still flowing through the furnace. After a 10 s Ar flush, the ETV was heated to a vaporization temperature of 2,800 °C and the signal collected.

6.3. RESULTS AND DISCUSSION

6.3.1. Metal determination from beads with immobilized PLAsp

In order to determine the precision of the ETV-ICP-MS method, beads containing the same peptide sequence were analyzed. The bead set used for this study was immobilized PLAsp ($n = 20$) which was reacted with a multi-metal solution for 2 h as described earlier. Depending on the peptide sequence and resin material used for the analysis, careful determination of reaction times must be considered for equilibrium conditions to be met. Based on the diffusion of large dye molecules through TentaGel,^{23,24} metal diffusion through TentaGel beads should occur in 15 min, and earlier studies suggested rapid metal-peptide binding kinetics²⁰. After metal exposure and drying, a light image of the beads was taken using a stereoscope. All beads were medium blue in color after metal binding indicating that each bead possessed the PLAsp and some complexed metal(s). A set of 9 beads was taken from the slide after the diameters were measured (Figure 6.1.). The beads ranged in size from 85 to 105 μm (± 2 μm).

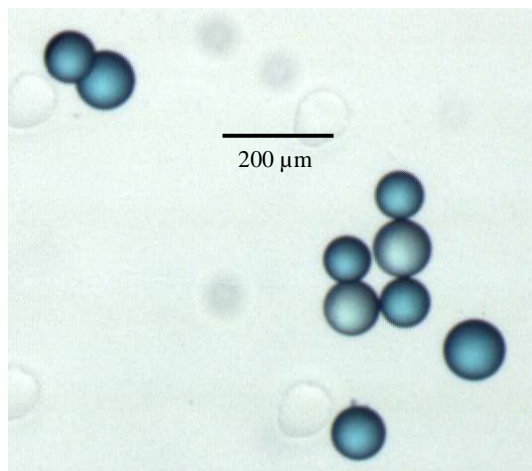


Figure 6.1. Stereoscope image of PLAsp-Tentagel beads after metal complexation.

The concentration of metal in the extract solution from each bead is shown in Figure 6.2. along with the bead volumes calculated from the bead diameters. Well #5 mistakenly contained two beads ($d = 90$ and $98, \pm 2 \mu\text{m}$), and thus the overall concentration is close to double that of the values in the other seven wells.

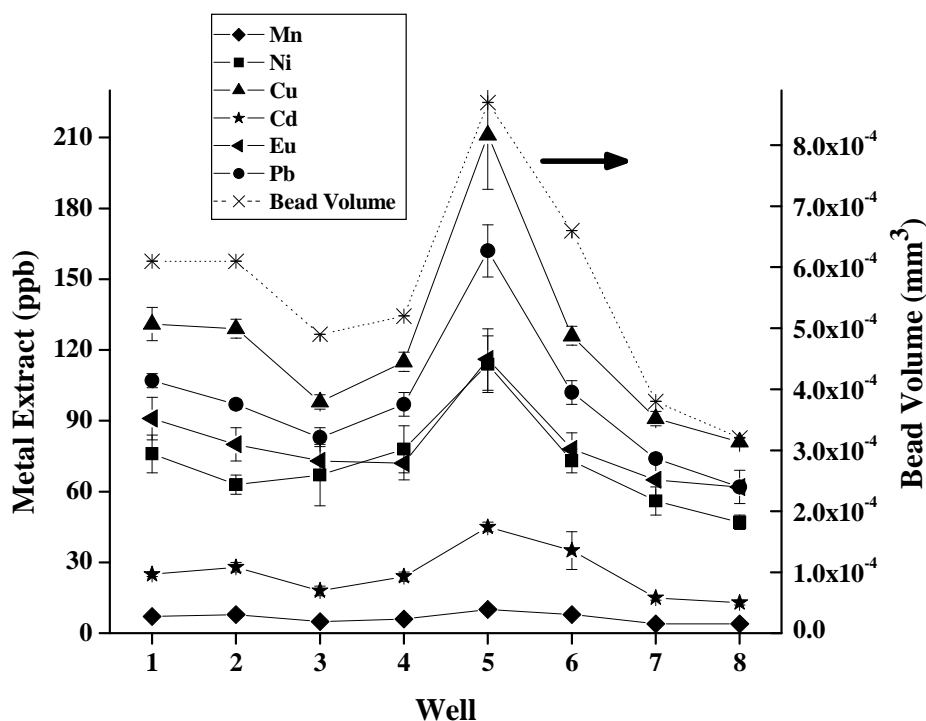


Figure 6.2. Concentration of metal extracted from single TentaGel-PLAsp beads and calculated bead volumes (right axis). The error bars represent $\pm 1 \sigma$ ($n = 3$) based on error propagated using the analysis error of the sample, blank, and calibration solutions. (Two beads were present in Well #5.)

The figure shows bead extract concentrations as low as 4 ng mL^{-1} for Mn^{2+} and as high as 130 ng mL^{-1} for Cu^{2+} , excluding well #5; Mg values were omitted from this

figure because they were not significantly detectable above the blank levels. Acid introduced into wells containing no bead were used as controls and showed metal signals near the detection limits, indicating that metal contamination from the microwell plate, well cover adhesive and tweezers was negligible. A small amount of Ni was observed, possibly from the tweezers, but was only slightly above the limit of detection. The bead-to-bead variation in the average metal content was relatively consistent (also see Table 6.3.), but there was an obvious binding selectivity for certain metals. As might be expected, much of the metal concentration variation in Figure 6.2. follows that of the bead size.

Table 6.3. Bead-to-bead variation in metal extract before and after adjusting for bead volume.^a Poly-L-aspartate (n=20) was immobilized on the beads.

Element	Mn ²⁺	Ni ²⁺	Cu ²⁺	Cd ²⁺	Pb ²⁺	Eu ²⁺
Metal Extracted (bead-to-bead RSD ^a)	29%	17%	18%	34%	18%	13%
Metal Extracted/ Bead Volume (bead-to-bead RSD ^a)	9%	14%	10%	13%	9%	16%

^a %RSD values were calculated from the average extract concentrations from seven beads. The metal extract from Well #5 was not included due to the presence of two beads giving a larger overall concentration.

Due to the variations in bead diameter, the metal extract values from Figure 6.2. were divided by the volume of the respective beads to calculate metal capacities. The standard deviation in the bead diameters was 7% ($n = 35$), which resulted in a 21% RSD in the volumes. When the metal capacities for each bead are normalized by the individual bead volume, a reduction in the bead-to-bead variation (9-16% RSD) is observed. (Figure 6.3. and Table 6.3.)

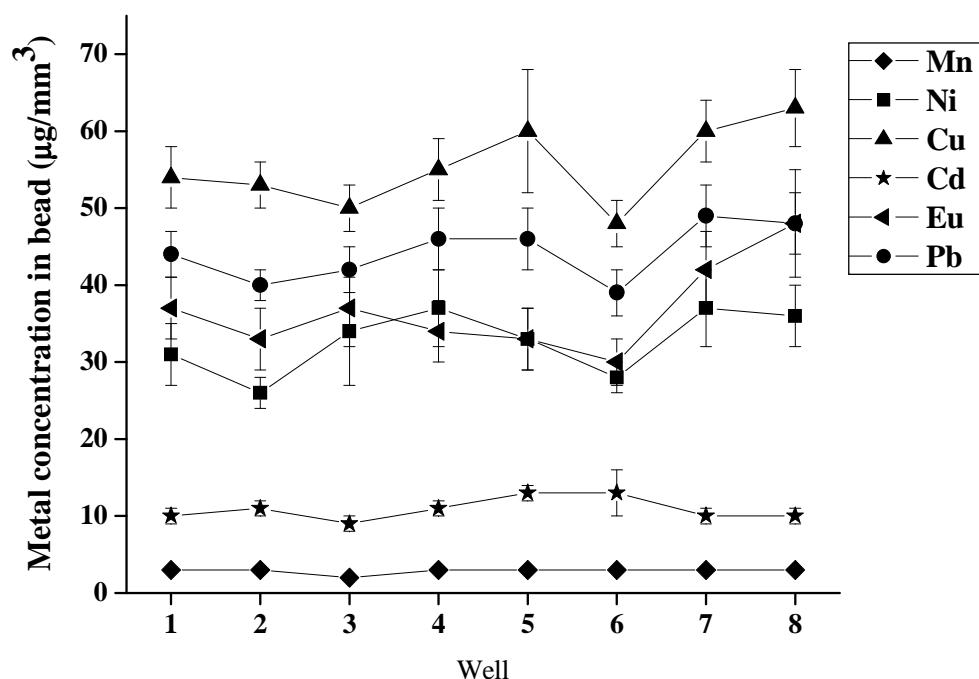


Figure 6.3. Single bead metal extract concentrations of TentaGel-PLAsp normalized to the individual bead volumes. The error bars represent $\pm 1 \sigma$ ($n = 3$) based on error propagated using the analysis error of the sample, blank, and calibration solutions. (Two beads were present in Well #5.)

The more refractory nature of Ni and Eu may account for the somewhat poorer precision between beads for these particular metals even after volume adjustment. The remaining error between capacity values is likely the result of measurement uncertainties in the determination of individual bead capacities.

An attempt was made to identify the possible sources of uncertainty when determining the volume corrected metal capacity of a single bead. The sources of indeterminate errors (i.e., precision) were: analysis error, variation in bead-to-bead binding site density, and error in measuring the bead diameter. The “analysis error” included contributions from the bead extract measurement, blank measurement, and calibration curve slope error; and excluded particle diameter measurement and bead-to-bead variations in active site density. An internal standard was used to minimize errors caused by evaporation and sample introduction into the ETV. After volume normalization of the bead set, the relative precision in the capacity (i.e., $\mu\text{g}/\text{mm}^3$) can be represented by Eq. 6.1.

$$RSD_{\text{capacity}} = \sqrt{RSD_{\text{analysis}}^2 + RSD_{\text{site density}}^2 + 9RSD_{\text{micrometer}}^2} \quad (6.1.)$$

It should be noted that propagating the measurement error of the radius (or diameter) to the bead volume yields a volume uncertainty of $3 \cdot RSD_{\text{micrometer}}$. Error propagation in Eq. 6.1. requires summing the squares of the relative error, hence $9 RSD_{\text{micrometer}}^2$. Variations in the site density cannot be measured directly; however, Eq. 6.1. can be used to determine if the $RSD_{\text{site density}}$ is significant relative to the other RSDs since they are known. Using $2 \mu\text{m}$ as σ for the micrometer stage error for a $98 \mu\text{m}$ bead yields 6.1% for $3 \cdot RSD_{\text{micrometer}}$. Using pooled data for each element, RSD_{analysis} was determined to be Mn (3%), Ni (11%), Cu (4%), Cd (12%), Pb (4%) and Eu (10%). Finally, the RSD_{capacity} was arrived at from the experimental data for Mn (7%), Ni (13%), Cu (7%), Cd (14%), Pb (7%) and Eu (12%). Using these data, it is obvious that major

uncertainties in site density are not required to account for the observed deviations in capacity measurements. Additionally, it can be deduced that analysis precision dominates the uncertainty in the Ni, Cd, and Eu capacities and that analysis and particle diameter imprecision contribute significantly to the uncertainty in the Mn, Cu, and Pb capacities for these beads. The F-test (95% CI) confirmed this conclusion, i.e., only small error contributions arise from errors in determining the bead diameters and negligible contribution comes from binding site density variations. Since no significant error was caused by variation in bead-to-bead differences in site density, all of the beads observed had nearly the same density of active sites. This observation is in agreement with a previous study using confocal Raman microscopy,²⁴ but in disagreement with diffusion studies of Rhodamine 6G through TentaGel²³.

To determine the amount of metal extracted by the acid soaking procedure, a selection from the PLAsp beads whose acid extract had been previously analyzed were separately analyzed directly in the ETV. In this study, total consumption of the beads was used to ensure that metal was extracted from the beads with acid. Total bead consumption is not necessary if peptide sequencing is desired. After inserting the bead and a small amount of solution into the ETV, the resin material was removed by O₂ ashing in the ETV at about 900°C, and the remaining metal was then vaporized and determined via ICP-MS. Total metal exposure was calculated by combining the metal amount extracted from the bead with the metal amount remaining on the bead to calculate the total metal on the bead after multi-metal exposure. The results for wells 1-4 and 6-7 showed approximately 97, 99, 100, 98, 100, and 100% of Mn, Ni, Cu, Cd, Eu and Pb were released upon acid exposure, which indicates quantitative release of the metals bound to this particular peptide.

6.3.2. Metal determination from the combinatorial library beads

A combinatorial peptide library was then used as an example for determination of selective metal binding peptides by this method. In order to minimize analysis error by increasing the signal magnitude, TentaGel Macrobeads were used for the combinatorial library. They were twice the diameter (i.e., 8 times the volume) of those used with the PLAsp but otherwise had the same nominal specification. Measurements of 35 beads showed an average diameter of $251\ \mu\text{m} \pm 5.4\%$ (i.e., $\pm 16\%$ in volume). After exposing the beads to a mixed metal solution, the library beads were noticeably different in color, ranging from dark red to light blue (Figure 6.4.).

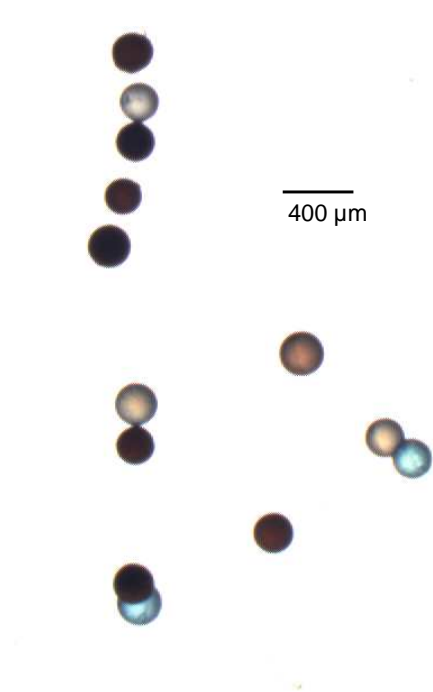


Figure 6.4. Stereoscope image of the peptide library beads after metal complexation.

Figure 6.5. shows the resulting volume-normalized capacities determined for the small set of peptide library beads. Mg values for wells B, C, E, and J were omitted from this figure because they were not significantly detectable above the blank levels. As expected, there are distinct differences in capacities for each element as well as in the relative capacities of one element to another for each bead. For example, beads from wells A and I had the highest capacity for Mg; beads from wells A and F had the highest capacities for Ni; beads from wells D and G had the highest capacities for Cu, Pb, and Eu; and beads from wells G and I had the highest capacities for Mn and Cd. Similarly, if one were in search of a bead that provided good Pb binding capacity with maximum rejection of Ni, bead G from this small set of the library would be the optimal choice.

Since these beads were also measured with the stage micrometer and were manufactured in a similar manner (i.e., similar variation in bead composition), the remaining error after bead volume adjustment can be ascribed primarily to analysis error since the relative error from the particle diameter uncertainty is smaller for these larger beads. In addition, the precision in these calculated capacities was slightly improved as a result of the higher concentrations extracted from the larger beads as a result of improved measurement precision and less error in measuring the bead diameter: Mg (10%), Mn (3%), Ni (5%), Cu (5%), Cd (6%), Pb (9%) and Eu (7%). In cases where measuring individual beads diameters would be difficult and/or excessively time consuming, larger bead sizes provide a means to decrease the overall concentration uncertainty from bead-to-bead by decreasing the relative analysis error. Obviously, bead sets with better monodispersity could also be used to increase precision if the diameters of individual beads were not measured.

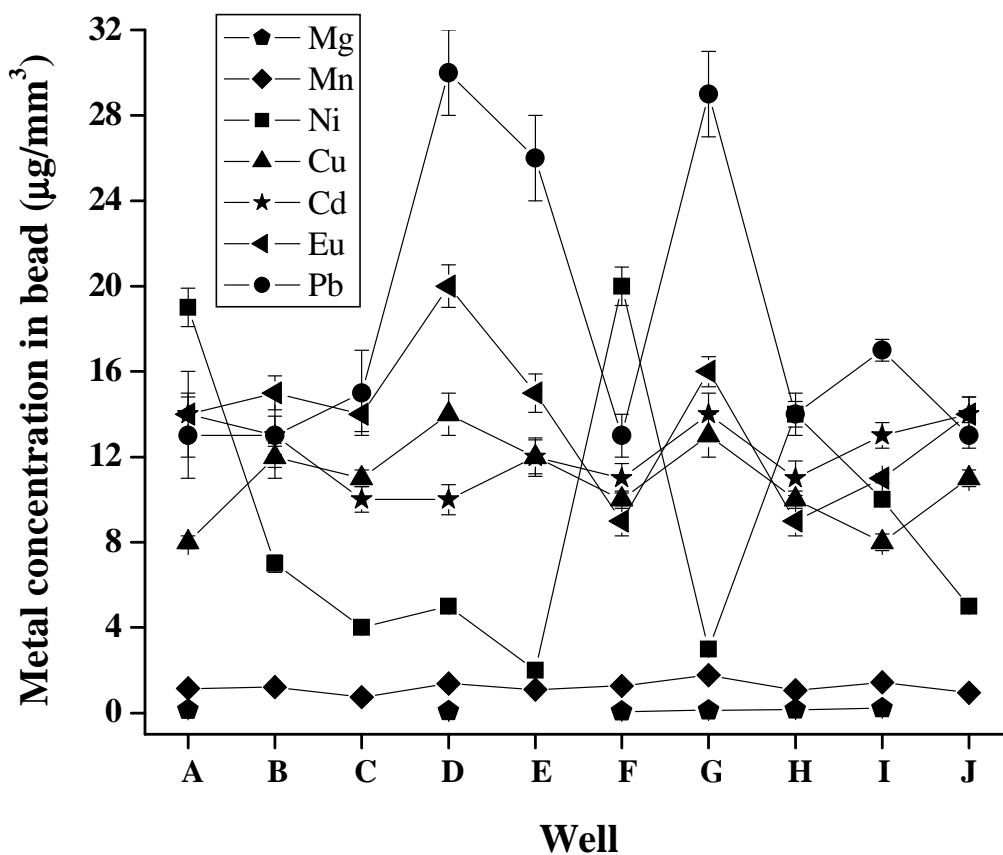


Figure 6.5. Single bead metal extract concentrations of the peptide combinatorial library normalized to the individual bead volumes. The error bars represent $\pm 1 \sigma$ (n = 3) based on error propagated using the analysis error of the sample, blank, and calibration solutions. Mg concentration in well B, C, E, and J were negligible. ($<0.6 \mu\text{g}/\text{mm}^3$)

A sample of 5 library beads were also analyzed directly using ETV after they had been soaked and rinsed in HNO_3 to see if the acid extraction was complete. While the beads released Mn, Cd, Eu, and Pb with 99-100% efficiency and Mg with 95-100% efficiency; Cu^{2+} showed a more varied retention (75, 100, 90, and 91, and 97% metal extracted). Since each of these particular beads likely had a unique peptide sequence, it

is not unexpected that strong binding sites on any given bead may not release the metal using this particular stripping solution. The beads were not sequenced in this study since the scope of the work was intended only to demonstrate the viability of using ETV-ICP-MS as a metal screening technique using a small bead set. While 95+% extraction is probably adequate for screening purposes, perhaps one might be concerned with <80% efficiency depending on the level of screening being sought. Clearly, total consumption of the bead via oxygen ashing and ETV-ICP-MS is not the answer if the peptide sequence is to be determined. It was only used in this study to illustrate that most metal is released by acid extraction. If the peptide is intended to be used as a reusable chelating media for metal remediation, one could argue that sites that cannot be reclaimed do not effectively “exist” and thus should not be counted in the binding capacity of the material. In these cases, beads with inadequate release should be preferentially selected against if the target metal concentration in the extract was low, regardless of how much metal was actually bound to the bead.

6.4. CONCLUSIONS

With the exception of metals that are bound tightly to the peptide, acid stripping of the metals in a single bead into a small volume is demonstrated to be a viable quantitative analytical approach when using determination by ETV-ICP-MS. Precisions of better than $\pm 10\%$ were achieved for all metals when the larger polymer beads were employed. While acid was used in this study, other reclamation (stripping) solutions could be employed, such as a competitive chelator like EDTA. Obviously, the use of different extraction solutions may also yield additional information on the relative strength of binding sites and other characteristics of the peptide sequence. The high sensitivity and low volume requirements of the ETV allow for single beads to be easily

analyzed, and the TOF allows for unlimited m/z monitoring analysis with no sensitivity loss for multielemental analysis since there is no loss in the mass analyzer duty cycle. Though the method presented here could be performed on other types of mass spectrometers (i.e. quadrupoles), the large number of isotopes observed might result in duty cycle related losses in sensitivity. For this study, the PLAsp beads and library beads had 21% and 17% variation in the volumes, respectively. This bead-to-bead variability associated with the metal extracted can be corrected for by normalization to the bead volume with the remaining error primarily ascribed to analysis error and for the smaller beads to the particle measurement error. Such volume correction may not be necessary, depending on the monodispersity of the bead set and the acceptable precision limit set by the analyst for the screen. Interestingly, this study does show that bead-to-bead site density variability was not a major contributor to the uncertainty in the overall capacity values for the Tentagel bead sets used.

The 2-3 min analysis time needed for each sample per replicate presently makes this technique suited for quantitative analysis of selected beads after an initial bulk screening method. Use of this approach for rapid, quantitative screening may be viable with automation of bead manipulation and an increase in throughput for the ETV-ICP-MS, such as has been suggested by work with a multiplexed ETV system^{25,26} where >100 analyses/h were reported.

6.5. LITERATURE CITED

1. Breit, B. *Angewandte Chemie, International Edition* **2005**, 44, 6816-6825.
2. Qi, S.; Yang, B.; Zhuo, Y. *Xiandai Huagong* **2003**, 23, 58-60.
3. Bluhm, L.; Huang, J.; Li, T. *Analytical and Bioanalytical Chemistry* **2005**, 382, 592-598.
4. Kellam, B. *Smith and Williams' Introduction to the Principles of Drug Design and Action (4th Edition)* **2006**, 355-376.
5. Weber, L. *QSAR & Combinatorial Science* **2005**, 24, 809-823.
6. Koinuma, H.; Takeuchi, I. *Nature Materials* **2004**, 3, 429-438.
7. Woo, S. I.; Kim, K. W.; Cho, H. Y.; Oh, K. S.; Jeon, M. K.; Tarte, N. H.; Kim, T. S.; Mahmood, A. *QSAR & Combinatorial Science* **2005**, 24, 138-154.
8. Francis, M. B.; Jamison, T. F.; Jacobsen, E. N. *Current Opinion in Chemical Biology* **1998**, 2, 422-428.
9. Stillman, M. J.; Shaw, C. F., III; Suzuki, K. T.; Editors *Metallothioneins: Synthesis, Structure and Properties of Metallothioneins, Phytochelatins and Metal-Thiolate Complexes*, 1992.
10. Atherton, E.; Sheppard, R. C. *Solid Phase Peptide Synthesis: A Practical Approach*, 1989.
11. Merrifield, R. B. *Journal of the American Chemical Society* **1963**, 85, 2149-2154.
12. Francis, M. B.; Finney, N. S.; Jacobsen, E. N. *Journal of the American Chemical Society* **1996**, 118, 8983-8984.
13. Franz, K. J.; Nitz, M.; Imperiali, B. *ChemBioChem* **2003**, 4, 265-271.
14. Shibata, N.; Baldwin, J. E.; Wood, M. E. *Bioorganic & Medicinal Chemistry Letters* **1997**, 7, 413-416.

15. Pirrung, M. C.; Park, K.; Tumey, L. N. *Journal of Combinatorial Chemistry* **2002**, 4, 329-344.
16. Neilly, J. P.; Hochlowski, J. E. *Applied Spectroscopy* **1999**, 53, 74-81.
17. Miller, T. C.; Mann, G.; Havrilla, G. J.; Wells, C. A.; Warner, B. P.; Baker, R. T. *Journal of Combinatorial Chemistry* **2003**, 5, 245-252.
18. Minogue, E. M.; Havrilla, G. J.; Taylor, T. P.; Burrell, A. K.; Warner, B. P. *Proceedings of SPIE-The International Society for Optical Engineering* **2005**, 5699, 526-530.
19. Vazquez Pelaez, M.; Costa-Fernandez, J. M.; Sanz-Medel, A. *Journal of Analytical Atomic Spectrometry* **2002**, 17, 950-957.
20. Stair, J. L.; Holcombe, J. A. *Microchemical Journal* **2005**, 81, 69-80.
21. Malachowski, L.; Stair, J. L.; Holcombe, J. A. *Pure and Applied Chemistry* **2004**, 76, 777-787.
22. Langer, D.; Holcombe, J. A. *Analytical Chemistry* **1999**, 71, 582-588.
23. Taniguchi, M. M.; Farrer, R. A.; Fourkas, J. T. *Journal of Combinatorial Chemistry* **2005**, 7, 54-57.
24. Kress, J.; Zanaletti, R.; Rose, A.; Frey, J. G.; Brocklesby, W. S.; Ladlow, M.; Bradley, M. *Journal of Combinatorial Chemistry* **2003**, 5, 28-32.
25. Venable, J. D.; Detwiler, M.; Holcombe, J. A. *Spectrochimica Acta, Part B: Atomic Spectroscopy* **2001**, 56B, 1697-1706.
26. Kreschollek, T.; Holcombe, J. A., 32nd meeting of the Federation of Analytical Chemistry & Spectroscopy Societies (FACSS), Quebec City, Canada, October 9-13 2005; 204.

Chapter 7: Conclusions and Future Work

7.1. CONCLUSIONS

The synthesis and use of custom peptides for metal remediation and preconcentration has been demonstrated. Previously, simple biohomopolymers were easily attached to porous supports such as beads or membranes to create a novel ion-exchange media. These systems showed strong metal binding due to an “effective” wrapping of the peptide around the metal introduced, creating a defined binding cavity. Metals are also easily released from these peptides using dilute acid which not only protonates the metal binding side chain groups, but also causes spoiling of the metal binding cavity which assists in release of the metal from the peptide. Judicious choice of the repeating amino acid unit does provide some selectivity flexibility. For example, aspartic acid with the side group carboxylate functionality tends to preferentially bind “hard acid” metals such as Cu^{2+} and Ni^{2+} , while cysteine residues with the thiol functionality tends to bind “soft acid” metals such as Cd^{2+} and Pb^{2+} . Enhancing selectivity could be made by, again, mimicking natural metal binding proteins by creating defined peptide structures (i.e., metal binding cavities) using covalent linkages as a substitute for weaker intermolecular forces; and through careful choice of amino acid sequence.

Cross-linking was initially used to improve the selectivity gains of biohomopolymers and copolymers. Most of the reactions were done “on-line” using a column and peristaltic pump. In this way, the selective binding material could be easily created and custom made for any metal using one type of peptide/cross-linking chemistry. The use of a flow through system also increases mass transport through porous supports compared to typical batch tumbling and thus decreases the amount of

chemicals needed for the desired reaction. Cross-linking was done in aqueous solutions to keep the peptide in the same environment as when metal binding takes place. This prevented likely shrinking of the peptide to the support surface which may have occurred with organic solvents due to an increased hydrophobic environment. A majority of cross-linking was done using EDC to cross-link the peptide directly or to create cross-links via a bifunctional linker both through the formation of amide bonds. Cross-linking of strategically positioned disulfides and photocrosslinking with arylazide groups were also used. The difficulty with using these methods is the need for the metal to remain bound to the peptide with minimal change in the preferential binding cavity during cross-linking. Aqueous cross-linking, especially with EDC, was a challenge due to the pH requirements of the cross-linkers and the groups cross-linked in addition to the need to avoid low pH's that would release the bound metal. Overall, cross-linking was confirmed through the gradual decrease in metal capacities that were determined at various stages. These capacity decreases were not accompanied by increases in metal binding selectivity for the target metal.

Successful approaches for templating metal species by other groups have resulted in very rigid structures that were “locked” into place via bulk polymerization which relied on the construction of the polymer support to assist in placement and position of the metal binding functional groups. Our attempts to create binding cavities via single polymer chains with minimal interchain interactions may still have a large degree of flexibility. The immobilization of peptides and polymers on controlled pore glass (CPG) typically resulted in coverages of about 10%. This could inhibit the construction of a rigid cross-linked peptide structure if the structure only relied on intrachain cross-linking.

A second approach used to increase the metal selectivity of immobilized peptide materials was through altering the peptide sequence. This entailed experimenting with

the amino acids used and their position in the overall peptide chain. Solid phase peptide synthesis (SPPS) was used to build the desired sequences. Direct synthesis onto controlled pore glass (CPG) resulted in sequences that were of less than 90% purity. In order to compare composite peptides, the purity should be fairly high which is easy to accomplish with shorter chain peptides. A polymer resin designed for use as both batch and “on-line” continuous SPPS was used to synthesize the peptides via batch synthesis and the resulting material was then packed into microcolumns to study the metal binding characteristics.

The use of a polymeric resin for the support material did yield numerous differences compared to similar peptides on more rigid porous supports. Due to the large loading capacities of these resins compared to those seen on porous glass and carbon, the metal binding capacities were two orders of magnitude larger. The higher loading capacities perhaps increased the interchain interactions between peptides, resulting in a larger number of residues participating in metal binding. A larger percentage of residues participating in metal binding indicated that the shorter peptides are not undergoing the tertiary structure changes that were evident with the longer peptide chains on the more rigid supports. In addition, equilibrium conditions were reached quite rapidly due to fast metal-peptide kinetics plus minimal mass transport limitations through the lightly cross-linked polymeric support media. Rigid glass and carbon supports can have mass transport limitations due to defined solution paths. Displacement of trapped air is also difficult to remove which limits mass transport to active peptide groups. Interestingly, these short peptides showed selectivity changes with the changing of only one amino acid position showing that amino acid placement can also be very important in immobilized short-chain peptides.

Raman microscopy was then used to determine the tertiary structure changes of a commonly used biohomopolymer, polyaspartic acid (PLAsp). PLAsp was synthesized onto TentaGel resin of chain lengths 6, 20, and 50. Synthesis of a 50-mer PLAsp was difficult and repeated synthesis resulted in only a 30-mer PLAsp. This may have been a result of the difficulty of synthesizing longer peptides with bulky side chains onto smaller 90 μm resins. All peptide chains bound one metal per 2-3 residues for each metal tested (i.e., Mg^{2+} , Co^{2+} , Cd^{2+} , and Ni^{2+}). This was in contrast to the longer peptides immobilized onto carbon and glass supports in which a larger percentage of residues were not available for metal binding due to the coiled tertiary structure. This was also evident from the Raman spectra. Each PLAsp chain length had the same overall secondary structure when under neutral pH conditions, and no change was observed when metal was added and all binding sites were filled to capacity. This lack of secondary structure change may be due to the concentrated environment of the TentaGel resin with peptide chains enabling more inter and intrachain interactions with less need to conform to a coiled structure. This lack of secondary structure change also explains the slight decrease in conditional stability constants compared with values determined for the longer peptides on more rigid supports. The longer peptides ($n = 20$ & 30) do show interesting secondary structure changes during metal release with acid. Upon protonation of the side chains, the longer peptides form primarily β -sheets and some α -helices. Polycysteine immobilized onto glass slides had been shown to release metals with acid by forming coiled conformations such as α -helices. Perhaps the choice of supporting material dictates the structure formed during metal release with acidic solutions. This conformational change during metal release assists in the rapid release of metal. The shorter 6-mer PLAsp chain did not show a distinct secondary structure change with acid.

One method which is recently being used to discover novel sequences for metal binding is through the use of combinatorial chemistry. Through split/pool synthesis, a peptide bead library can be created with each bead possessing a unique peptide sequence. Beads that successfully bind a particular metal of interest are often determined through colorimetric analysis for both metal catalysis and metal remediation purposes. Although this method is quick and cheap, it is, at best, semiquantitative and usually able to determine the presence of only a single metal species. If selective metal uptake is desired, it may be important to confirm that competing species, if bound, are bound in very small amounts. A species may bind a particular metal well, but it may be necessary to determine to what extent in comparison to other metals before bulk synthesis is attempted.

To this end, electrothermal vaporization inductively coupled plasma mass spectrometry (ETV-ICP-MS) was used to determine the metal content of individual beads belonging to a peptide library. This was done by placing individual beads into individual wells containing acid to strip off the metal with subsequent analysis of the metal concentration in each well. Coupling of the ETV for sample introduction to the ICP-MS allows for very small sample volumes to be analyzed. Since each bead was approximately 90-250 μm , a 100 μL acid solution was used to extract the metal from an individual bead which resulted in metal concentrations from 1-1000 ppb. By using an ICP-MS, the concentrations of metals in the extract solution can be determined simultaneously. The capacity values were normalized for the variation in the bead volumes which decreased variability to +20% in some cases. Although there were remaining error contributions from bead-to-bead site density differences, they were small compared to those from the propagated analysis error and in some cases error contributions from the micrometer. Capacity precision was reduced to $\leq 10\%$ when the

larger beads (250 μm) were employed. Beads were also oxygen ashed in the ETV furnace to determine the metal that was not extracted during treatment with acid and showed that 98-100% of metal was extracted in most cases. At present, this method could not be easily used to analyze an entire peptide library. It would be most useful for the detailed analysis of beads that were selected through a more semiquantitative rapid screening method. It is likely, however, through the use of a multi-ETV and an automated bead preparation system; this method could be used to analyze full peptide combinatorial libraries.

7.2. FUTURE WORK

7.2.1. Templating

Various attempts to template in our laboratory were made through cross-linking long peptide chains together at various positions. This approach does not afford rigidity in the structure and the metal binding cavity cannot be sustained. Other approaches that have been more successful have done so by “locking” a small metal complex and its support material into place through polymerization. In this way, the polymerization of the support material provides extra rigidity to the metal complex.

An approach using monolithic columns may be a unique way to create these types of materials. Small or larger peptides with metal bound could be incorporated into the reaction mixture pre-polymerization. The reaction conditions can be tailored to create the desired pore sizes. In addition to less back pressure from these materials, there are fewer difficulties due to column packing, and the shrinking and swelling of resins.

As a result of the studies done using TentaGel resin and composite peptides, this seems like a viable route for creating very specific rigid structures. Peptides of longer

than six residues containing various amino acids could be cross-linked via disulfide linkages through strategically positioning cysteine residues among other metal binding residues. This was attempted using 6-mer residues which provided some selectivity based on the masking of the thiol groups, however, less on the formation of actual cavities. Longer peptides with increasing intrachain interactions, as shown in the Raman microscopy studies, may provide the needed 3D interactions to effectively “lock” a binding conformation into place.

7.2.2. Peptide Combinatorial Libraries For Selective Metal Binders

Preliminary work determined that resins such as TentaGel are excellent resins both for the synthesis of peptides and for use as ion-exchange support material. Further studies into the short-chain metal binding libraries could be advanced through modeling peptide libraries to a greater extent on biological metal binding proteins. A rough peptide structure can be used to create libraries with specific amino acids substituted at various positions. These peptides could be created with the formation of particular structures such as α -helices or β -sheets in mind. Confirmation of these structures could be easily determined using Raman microscopy or further investigation using solid state NMR.

In addition, the screening of these materials could be enhanced by automating bead sample preparation and by the further development of the multi-ETV system. For bead batches that have a narrow size distribution, volume corrections would not be necessary and each metal sample could be reduced to a single aliquot in the ETV. This could also greatly reduce analysis time. Extra analysis could be done by constructing a flow through system for individual bead analysis. In this way, single beads could be characterized for metal binding strength in addition to metal binding capacities.

7.2.3. Multicolumn Analysis Using Automated System

The analysis of data from breakthrough curves provides useful information on the binding character of an immobilized chelator. However, the larger capacity of the solid phase synthetic resins such as TentaGel increases the analysis time an order of magnitude in some cases. One way to reduce that time spent characterizing one column is to test multiple columns simultaneously. The frequency of data collection for these materials can be reduced since the overall breakthrough analysis time is much greater. An automated system could be constructed that would rotate a number of columns so the same fraction of the overall time was spent on each individual column with no significant loss in the definition of the breakthrough curve shape. This would be useful not only for atomic absorption measurements, but also in conjunction with the ICP-MS. The ICP-MS not only provides greater sensitivity for the determination of large binding constants, but is also useful for monitoring many metals simultaneously and, thus, the characterization of multi-metal solutions. To this end, fast analysis of multi-metal binding behavior would allow for a more detailed analysis of this behavior.

Vita

Jacqueline Leslie Stair was born in Dover, Delaware on March 1, 1977, the daughter of Robin Ann Stair and Scott Bradley Stair. After completing her work at Charlotte High School, Charlotte, Michigan, in 1995, she entered Michigan State University in East Lansing, Michigan. She received the degree of Bachelor of Science from Michigan State University in May 2000. During the next year she was employed as a research assistant at Michigan State University. In August 2001 she entered the Graduate School of The University of Texas.

Permanent address: 5433 Samels Rd, Williamsburg, MI 49690

This dissertation was typed by the author.